Silsesquioxane Hybrid Nano-Building Blocks for Extreme Ultra-violet Photoresists

A Thesis

Presented in Partial Fulfillment of the Requirements for the

Degree of Master of Science

with a

Major in Chemical Engineering

in the

College of Graduate Studies

University of Idaho

by

Brandon T. Hardie

Major Professor: Mark Roll, Ph.D.

Committee Members: Wudneh Admassu, Ph.D.; David N. McIlroy, Ph.D.

Department Administrator: D. Eric Aston, Ph.D.

August 2015

Authorization to Submit Thesis

This thesis of Brandon Hardie, submitted for the degree of Master of Science with a Major in Chemical Engineering and titled "Silsesquioxane Hybrid Nano-Building Blocks for Extreme Ultra-violet Photoresists," has been reviewed in final form. Permission, as indicated by the signatures and dates below, is now granted to submit final copies to the College of Graduate Studies for approval.

Major Professor: _____ Date: _____

Mark Roll, Ph.D.

Committee Members: _____ Date: _____

Wudneh Admassu, Ph.D.

_____ Date: _____

David N. McIlroy, Ph.D.

Department Administrator: _____ Date: _____

D. Eric Aston, Ph.D.

Abstract

The development and characterization of silsesquioxane (SSQ) hybrid nano-building blocks (NBBs) shows potential for the future improvement in patterning for semiconductor devices using Extreme Ultra-Violet Lithography (EUVL, λ~13.5nm). The versatility of SSQ macromolecules—organic functionality with a thermally stable inorganic core—is very desirable for application to EUV materials.

Syntheses for both octamer and decamer SSQ structures have been completed for this Semiconductor Research Corporation-funded project. In addition, the given materials have been applied to vital processing steps such as spin coating and electron-beam lithography to determine the SSQ's viability as a photoresist. E-beam contrast curve data was determined and compared to an SU-8 resist standard to show both capabilities and limitations of various SSQ structures. Future work utilizing EUV facilities at NIST and other industry partners may be used to determine characteristics such as off-gassing, contrast, sensitivity, and optimum etch parameters.

Acknowledgments

I would like to thank the following:

Semiconductor Research Corporation for the funding of Task 2439.001.

Dr. Mark Roll for his incredible guidance and support throughout the duration of my Master's degree and this research project.

Dr. Wudneh Admassu for his advising since I was an undergraduate and being a part of my thesis committee.

Dr. David McIlroy for his introduction to using ellipsometry and being a part of my thesis committee.

Dr. Tom Williams for allowing us to work extensively with the scanning electron microscope and X-ray diffractometer.

Dr. Christine Berven for her presentation on Nanolithography and fabrication as we stepped into the realm of E-beam lithography.

Joshah Jennings from the WSU cleanroom for providing valuable wafer samples and spin coating tips.

Jeff Fischer (for his work on the POM side of this project) and Natalie Kirch for their support both in and out of the lab.

Table of Contents

List of Figures

List of Tables

Chapter 1: Introduction

Background

Closely followed by those in the semiconductor industry, Moore's Law continues to push ahead with the scaling down of feature sizes within semiconductor devices. In short, Moore's Law essentially states that the number of transistors that may fit onto a given chip should double roughly every two years as feature sizes continue to shrink [1]. A few different methods of keeping up with the ever-increasing transistor load include both techniques used today (immersion, optics manipulation at 193nm) and those proposed for the future of the industry (EUV, 3-D device architectures). A few factors can be taken into account when determining minimum feature sizes including: wavelength of patterning light (λ), proportionality constant (k), and numerical aperture (NA). These variables can be used within a very simple equation (1.1) to define the relation between feature sizes (R), optics, and source wavelength [2, 3]:

$$R = \frac{k\lambda}{NA} \tag{1.1}$$

Through the introduction of high refractive index liquids in lens technology and careful monitoring of sensitivity in the imaging process, k and NA values can be modified to further shrink feature sizes. In the current lithography node, optimal values for k and NA were reported as 0.2 and 1.35, respectively [4]. The issue here is that these are either very generous values (0.25 is the theoretical limit for k) or improving these values can come at a potentially high cost. This ultimately shows that source light wavelength eventually becomes the limiting factor for small feature sizes. Varying lithography techniques which may enhance k and/or NA values include high index immersion lithography (NA modifier) and double patterning lithography (k modifier). These techniques push the limits of deep UV lithography (λ=193nm), thus causing the expanding gap between feature size and lithography wavelength as shown in Figure 1.1. Reducing wavelength, 157nm lithography was heavily researched, but ultimately fell short on time due to its issues with the absorption within lens materials. As wavelengths become smaller and photon energies larger,

absorption becomes more of an issue that requires more time to develop solutions. This drives the need to drop to an even smaller wavelength node to warrant improvements in a more desirable and timely manner, which brings Extreme Ultra-violet lithography (EUVL) into the big picture.

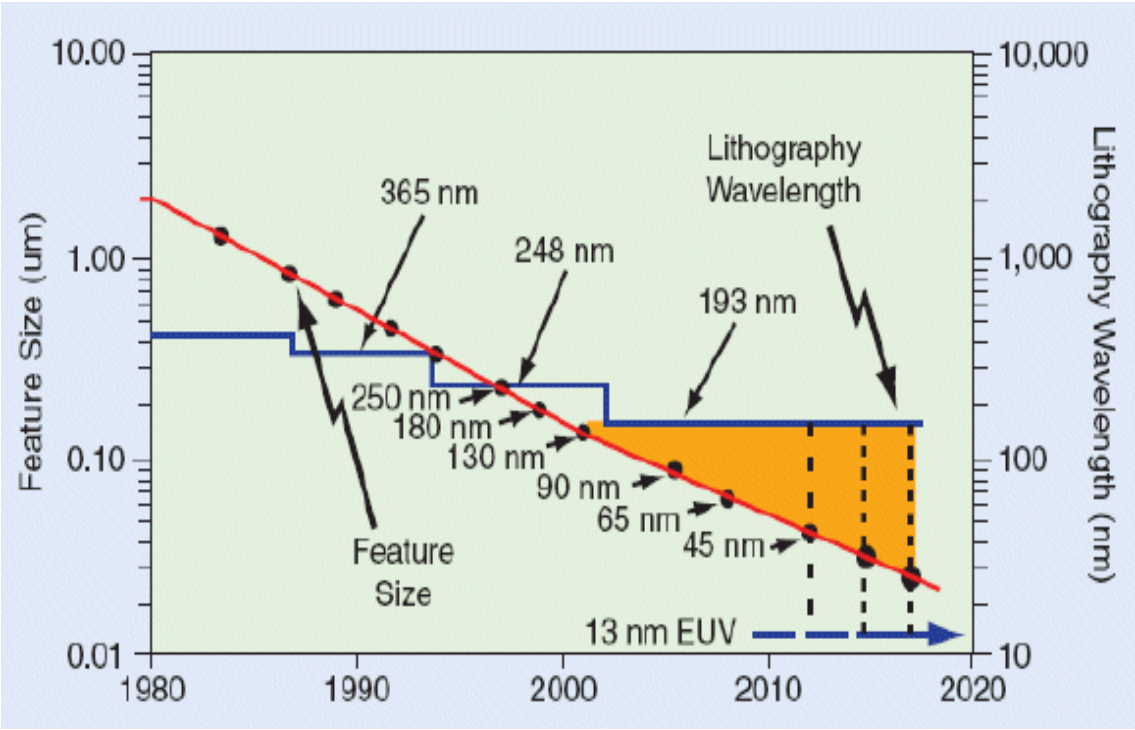

Figure 1.1. Moore's Law feature size and wavelength progressions [5].

To touch up on the fundamentals, lithography—in microelectronics fabrication terms—is the writing of micro or nanostructures through use of a photon beam or an electron beam. At its very basic, a photoresist is deposited onto a substrate (typically an Si wafer) via spin coating, physical/chemical vapor deposition, or thermal spray deposition [6]. In systems that are not direct-write litho (E-beam), a photomask is often used to effectively shield portions of the resist from exposure. Photomasks today are most commonly comprised of an opaque metal (impervious/reflective of photons) on top of a glass substrate (transparent to photons). These masks are also valuable in that they allow rapid duplication of a particular pattern when large quantities are to be reproduced. A photoresist may have either positive or negative sensitivity. In a positive resist, the exposed portion is weakened and

subsequently washed away during the development stage. For a negative resist, strengthening of the exposed portion will occur, often as a result of cross-linking within the resist. For this instance, any unexposed regions will be washed away during the development period. Figure 1.2 depicts a very general patterning and development method for both positive and negative photoresists with the use of a mask. It is in this very briefly described process that micro/nano-electronic devices that drive today's technology are developed and mass produced on a large scale and continue to be improved upon.

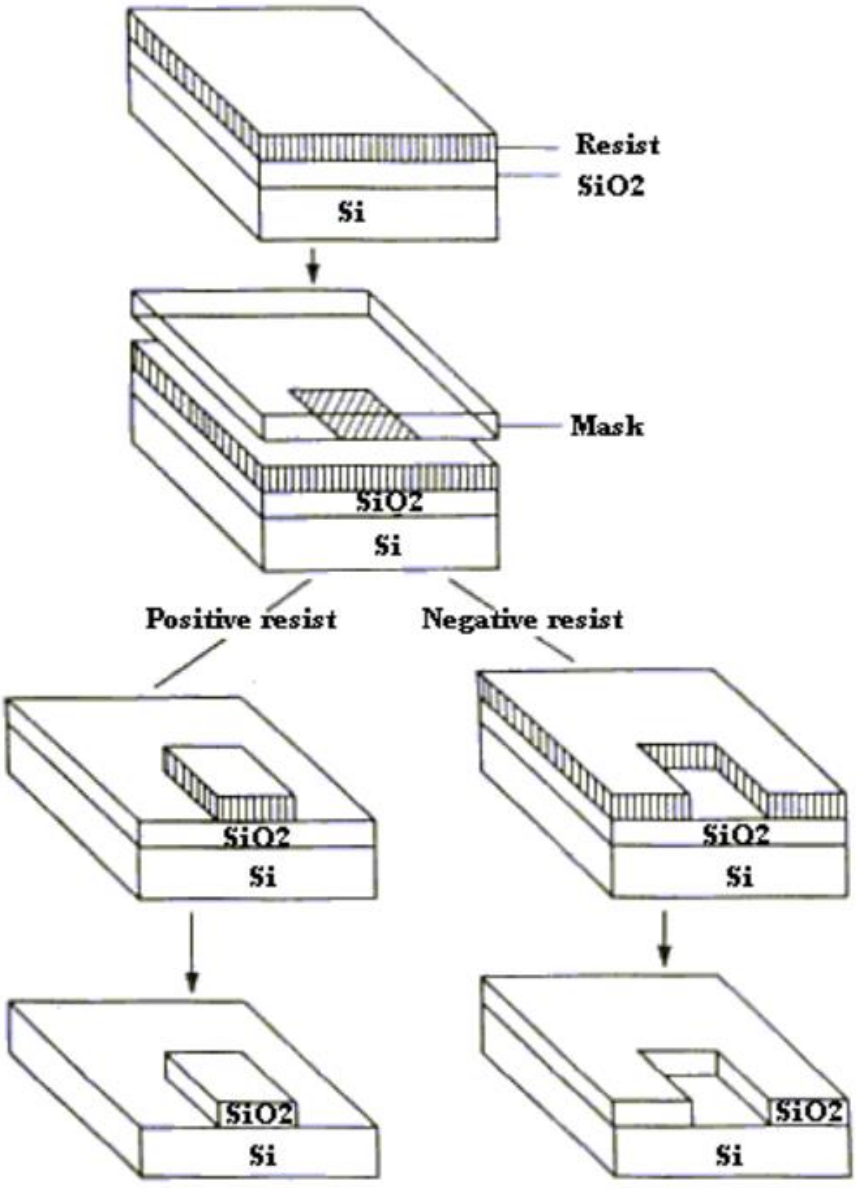

Figure 1.2. Exposure and development of positive and negative photoresists [7].

Operating at a wavelength of about 13.5nm and photon energy of ~92eV, EUVL potentially offers a natural progression of optical lithography [8], leading to a more fast-paced development than the likes of current immersion and double patterning technologies. EUVL has shown its potential as a successor to 193nm immersion technology through experimentation [9], though a few hurdles remain before implementing this technology on a full scale within the industry.

In a short list, some of the main issues encountered with EUVL today include: powerful light sources, photoresist properties/suitability, and mask technology/optics [2, 10]. The research within this thesis deals in particular with the synthesis of suitable EUV photoresists, though all issues in confronting EUVL are in need of brief discussion. Power sources for EUV light remain a major challenge that significantly limits high volume production desired in industry. Additionally, at increasingly small scales, photomask defects become more abundant and more difficult to detect. Photoresist performance, however, is slowly pushing EUVL technology forward. Specific characteristics often studied with resists include sensitivity, resolution, line edge roughness (LER), etch resistance, off-gassing during exposure, and swelling during development. High sensitivity in these resists is sought out in part to alleviate the struggles faced with EUV power sources and throughput.

Due to the high absorption of EUV photons (even in a “clean air” environment), these lithography tools must be operated within a vacuum environment. Because of this, contamination of the optics becomes a risk. In this very low pressure environment, free molecular flow of the hydrocarbon contamination from EUV-induced resist debris is a likely event which can lead to undesirable carbon growth on optics. [11, 12].

Depending on the characteristics of a photoresist, swelling and/or pattern collapse can occur during development in liquid organic solvents due to evaporative surface tension as seen in Figure 1.3. Supercritical CO_2 has been looked at as a method to improve upon these issues [13]. While individually assessing and improving upon each of these as a standalone issue for EUVL resists may appear simple, satisfying all of the issues simultaneously remains the core objective.

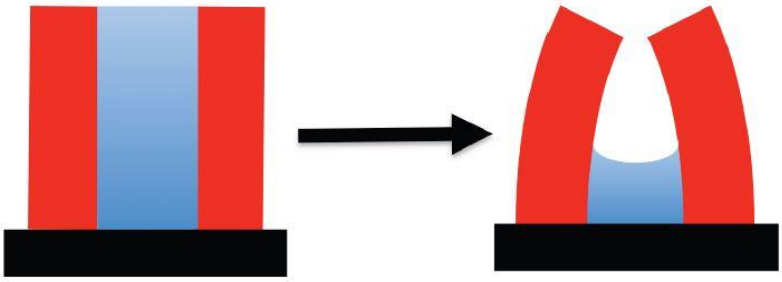

Figure 1.3. Pattern collapse via evaporative surface tension.

Silsesquioxane Hybrid Nano-Building Blocks

In lithography, chemically amplified resists (CARs) have attained incredible success as wavelengths have continued to be pushed to smaller levels [14]. As stated by the name itself, these resists are more sensitive to exposure due to their photo-acid generating attributes. Once exposed, photo-acids are released from these resists during the post-exposure baking. The acids deprotect functional groups in exposed portions (or unexposed for negative resists) of the resist, meaning the polymer becomes more soluble in developer and thus, a more sensitive or "chemically amplified" resist is formed [15]. Because these acids are acting as catalysts, they are capable of regeneration and reuse [16]. This has been especially useful as smaller wavelengths bring about greater absorption and longer exposure times.

However, when stepping down further to EUV-type wavelengths, acid diffusion can go from negligible at higher wavelengths to a significant limiter in resolution and line edge roughness at the 13.5nm node [17]. To give a quick idea of the scope of this issue, ITRS reported an acid diffusion length of 9.7nm for a PBP methacrylate resin, a seemingly undesirable value when considering sub-20nm lithography [18]. It is because of this issue, among others, that the push for novel materials for use with EUVL has become one of the greater challenges moving forward in the semiconductor industry.

One proposed EUV resist material is based on hybrid nano-building blocks (NBBs), which couples an inorganic metal oxide core with ligands of organic functionality. The goal of hybrid materials are not only to overcome certain limits of common resist materials, but to also potentially enhance organic/inorganic properties given the interaction of the two [19]. Specific to this research, silsesquioxanes (SSQ) were synthesized and characterized as a photoresist material. Also known as Polyhedral Oligomer Silsesquioxanes (POSS), these macromolecules are silicate cages composed of double n-ring structures. Figure 1.4 gives an example of a double 4-ring structure, also referred to as an octameric structure. Attached on each corner of this structure, through synthesis methods discussed later, are various chemically stable organic functional groups.

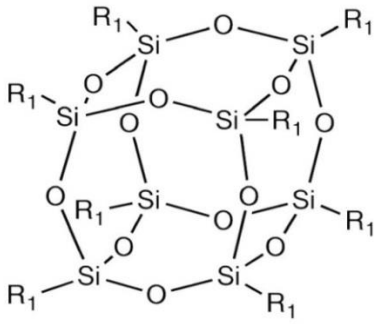

Figure 1.4. Octameric silsesquioxane standard structure; R_1=organic functional group.

Containing the strong –Si-O-Si- bonds well known in silicate chemistry, this high electron density inorganic core provides high thermal stability, etch resistance, and EUV absorption desired in semiconductor technology [20]. A common issue encountered by EUVL is photon shot noise and photoelectron diffusion, an unsuitable attribute previously discussed for the CARs used today. By using non-photoacid generating chemistry, off-gassing during exposure is expected to be significantly minimized or even entirely negligible. Not only does this solve the issue with optics contamination, but it is also anticipated to greatly improve line edge roughness and overall resolution of the film features. The functional corner groups studied in these resists included both vinyl (current) and benzocyclobutenyl (future work), both of which have been shown to polymerize under e-beam, X-ray, and deep UV light. In fact,

octavinyl silsesquioxane, an octameric SSQ macromolecule with very similar corner groups as studied here, was shown to act as a crosslinking negative photoresist under these three lithographies with relatively high sensitivity and cross-linking [21]. Through the utilization of up to 8 polymerizable groups per macromolecule, these NBBs are expected to display excellent sensitivity when exposed to EUVL.

On top of the advantages discussed above, it was initially proposed that these silsesquioxane resists could act as "pixelated" photoresists. This particular concept has been studied with CARs and describes the resists as having uniformly sized pixels in a well-defined heterogeneous film [22, 23].

Pixelated photoresists have shown potential especially in bulky clusters or polymer chains, in which a "self-contained" reaction may take place for individual pixels during pattering [16]. At roughly $1nm^3$ in volume with a cubane structure (for the octamer POSS), the currently studied NBBs have potential to act as a strong candidate for pixelated resists. POSS macromolecules in particular appear to fit the bulky cluster model, utilizing self-assembly to reinforce the idea of a uniformly packed resist [16].

Though POSS macromolecules already are expected to improve LER as non-photoacid generating resists, pixelation further adds to the appeal by being the principal controller in LER. By utilizing pixel size as the limiting factor in resolution, a high contrast can be achieved with hybrid NBBs. Figure 1.5 shows a simple schematic of how the patterning and development of a pixelated photoresist would ideally progress. In this image, emphasis is placed on the well-defined line edge as unexposed "pixels" are developed off of the negative photoresist.

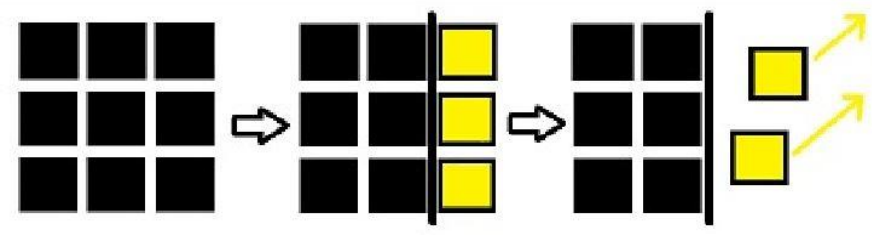

Figure 1.5. Patterning and development of a positive pixelated photoresist.

While the literature pertaining to both SSQ/POSS synthesis and lithography is large and continues to grow, in the EUVL regime, their use is relatively limited outside of the hydridosilsesquioxane family (hydrogen silsesquioxane or HSQ [24-26]). HSQ is a well-known negative tone e-beam resist recognized for its very high resolution at small feature sizes. Its properties as both an e-beam and EUV resist are further discussed in Chapter 4.

It is hypothesized that these novel hybrid materials may address the challenges encountered with developing suitable photoresists for EUVL. Once again, this appears achievable through the versatility of a stable inorganic core combined with a high degree of crosslinking from functional corner groups.

The initial goal of this research was to first synthesize and characterize these novel hybrid POSS materials. Following this, spin coating parameters were to be developed, leading into electron beam lithography as a general proxy to EUVL. The success of these preliminary goals could then ultimately be applied to EUVL for characterization including sensitivity, contrast, off-gassing, and optimum etch parameters.

Chapter 2: Experimental

Analytical Equipment

Products obtained were characterized via ^{1}H NMR (Proton NMR) on a Bruker Avance 300 MHz Spectrometer. All samples used $CDCl_3$ (Cambridge Isotope Laboratories, inc.) as an NMR solvent. ^{1}H spectra were obtained at 300 MHz. SpinWorks 3 software was used to analyze NMR peak and integration data. ^{1}H NMR data was calibrated based on $CDCl_3$ peaks reported in literature [27]. Additional characterization was done using powder X-ray diffraction on a Siemens Model D5000 (theta-theta goniometer) with Cu k-alpha (1.54 angstroms) radiation wavelength. Scanning was done from 2-80° (2-theta scale) at a step of 0.02° per second (approximately 1 hour total). EVA software was used to collect XRD data.

Silicon wafers for spin coating were cleaned using a Jelight Model 42 UVO-Cleaner. Wafers were spin coated using a Laurell Technologies WS-650 Series Spin Processor (Figure 2.1).

Figure 2.1. Laurell Technologies spin coater setup.

Coated wafers were exposed under electron beam lithography using a Zeiss Supra 35 VP FEG Scanning Electron Microscope (Figure 2.2). Zeiss SmartSEM software was used for resist exposures and imaging. A standard beam aperture of 30µm was used. Photoresist

exposures were done at an accelerating voltage of 20keV. Viewing of the resist films and exposures was done at an accelerating voltage of 5keV. Beam currents were measured using a Faraday cup during exposure.

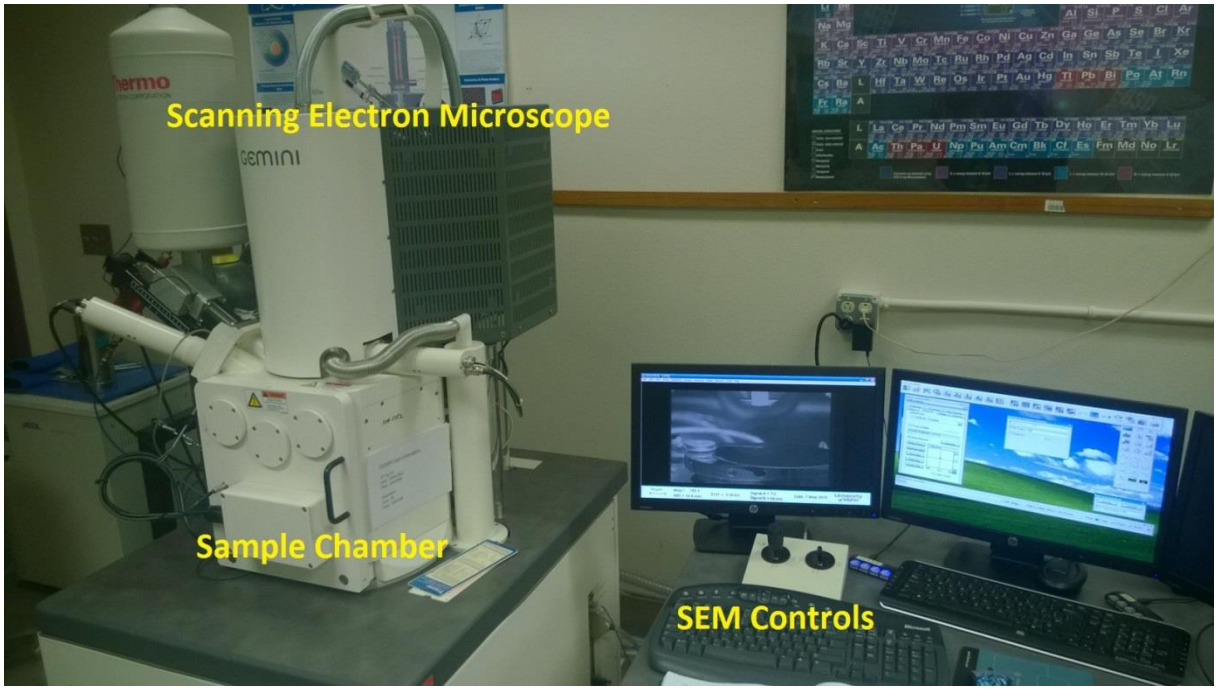

Figure 2.2. Zeiss SEM setup.

Synthesis: Octamer

Octaanion:

The synthesis of both octamer and decamer POSS products were typically a two part process. The first being the synthesis of a silicate cage anion, followed by silyation with varying chlorosilanes. The octaanion was synthesized using two different procedures [28, 29]. First, a batch reaction of 10mL (44.6mmol) tetraethyl orthosilicate (TEOS; Alfa Aesar) and 11mL choline hydroxide (45% wt. in H_2O; Acros Organics) was stirred for ~20 hours then allowed to settle [28]. An additional 10mL methanol was added to dissolve solids and create a homogeneous mixture prior to silyation. A second synthesis route to the octaanion was a batch reaction of 4.5mL (20.5mmol) TEOS with 3.624g tetramethylammonium hydroxide

pentahydrate (Alfa Aesar) dissolved in 8mL methanol and 1.8mL H_2O [29]. An additional 12mL methanol was added and the mixture was stirred for ~20 hours. Solution was concentrated via rotary evaporator until crystals appeared in solution. Crystals were cooled, filtered, and re-dissolved in methanol prior to silyation.

Trimethyl POSS:

For silyation of the first batch, a mixture of 22.2mL (175.6mmol) trimethyl-chlorosiane (TMCS; Acros Organics) and 19.5mL hexane was prepared. The octaanion/methanol solution was added dropwise to this mixture and allowed to stir for ~1 hour. The resulting mixture formed both an organic hexane phase and an acidic aqueous phase. The upper organic phase was obtained via separatory funnel and concentrated under rotary evaporator to give a white crystalline solid, which was washed using methanol. Further drying of the crystalline product was done under nitrogen. Silyation of the second anion batch was done using the same silyation procedures. An excess of 10mL (78.7mmol) TMCS and 9mL hexane solution was prepared. Octaanion/methanol solution was added dropwise to this mixture and stirred for ~1 hour. The resulting organic phase was obtained and concentrated under rotary evaporator. The resulting product was washed with methanol and further dried using nitrogen.

Through these methods, it was determined that the Hasegawa prep [28] was most suitable for octaanion synthesis and silyation. The remaining available choline hydroxide of 65.3mL was used to make a large batch of octaanion with 58.4mL (261.5mmol) TEOS. The large mixture was stirred for roughly 1 week. Rather than dissolving the solids in methanol as before, the solids were filtered off using acetonitrile. Prior to storage in cold temperatures, the solid was dried under nitrogen for ~2 hours at room temperature. This resulted in 58.88g of a gel-like white solid with the molecular formula of $[OSiO_{1.5}]_8[(CH_3)_3NCH_2CH_2OH]_8 \cdot 24H_2O$ [30], which was used later on in calculating yields for the various POSS products.

From this batch of octaanion, various POSS products were made using the same silyation procedure as above. First, a silyation method was tested using solid octaanion rather than

dissolving in methanol first. To a mixture of 10.8mL (83mmol) TMCS and 14.4mL hexane, was slowly added 5g (2.76mmol) of octaanion solid. This reaction was stirred for ~1 hour. Organic layer was obtained via separatory funnel and removed using rotary evaporation. Resulting white crystalline solid was washed with methanol and further dried under nitrogen to give 1.59g solid. This method of direct crystal addition resulted in poorer yields and was deemed inefficient in comparison to the step requiring the dissolving of the octaanion in methanol. Proton NMR and powder XRD were used to characterize the trimethyl POSS product.

Yield: 51.0% ("dry" crystal addition); ^{1}H NMR: 0.151 (s); Powder XRD major low angle peaks: 6.72, 8.14, 9.48, 9.86.

Vinyldimethyl POSS:

The first POSS product with functional organic attachments called for a silyation mixture of 6.18mL (43.9mmol) vinyldimethylchlorosilane (VDMCS; Gelest) in 5.43mL hexane. 2.52g (1.39mmol) of solid octaanion was dissolved in 2.5mL methanol and added dropwise to the hexane mixture. Reaction mixture was stirred for ~1 hour. Organic layer was separated and evaporated under rotary vacuum. Resulting crystals were washed using methanol and further dried under nitrogen at room temperature to give 1.10g product. Another larger batch of vinyldimethyl POSS was made for further studies in spin coating and e-beam lithography. 8.56g (4.73mmol) octaanion dissolved in 9mL methanol was added dropwise to a mixture of 21mL (152.1mmol) VDMCS and 18.4mL hexane. Reaction mixture was stirred for ~1 hour. Organic layer was obtained and evaporated under rotary vacuum. White crystalline product was washed in methanol and further dried under nitrogen to give 3.42g product. Proton NMR and powder XRD were used to characterize the vinyldimethyl POSS product.

Yield: 64.5% (Rxn 1), 59.0% (Rxn 2); ^{1}H NMR: 6.14 (t), 5.98 (d), 5.81 (d), 0.209 (s); Powder XRD major low angle peaks: 6.54, 7.84, 9.10, 9.46.

Dimethyl POSS

To a silyation mixture of 8.5mL dimethylchlorosilane (DMCS, Gelest) and 9mL hexane was added, dropwise, 5g (2.76mmol) of octaanion in 5mL methanol. The reaction mixture was stirred for ~1 hour. Organic layer was separated, placed under rotary evaporator, and a white crystalline product was obtained. Instead of washing the product with methanol as above, acetonitrile was used as the washing agent, per literature. Further drying of the product was done under nitrogen and resulted in 1.94g product. Proton NMR was used to characterize the dimethyl POSS product.

Yield: 69.0%; ^{1}H NMR: 4.73 (m), 0.259 (d); Powder XRD major low angle peaks: 8.00

Trivinyl POSS

1g (0.553mmol) octaanion was dissolved in chilled methanol. This solution was added dropwise to a chilled mixture of 2.6mL (16.6mmol) trivinylchlorosilane (TVCS, Gelest) and 3.5mL hexane. Reaction was stirred for ~45 minutes. Organic layer was removed and placed under rotary evaporator. The resulting product after vacuum removal of the solvent contained both a white crystalline solid and a clear viscous liquid. The white solid was cold-filtered from the liquid portion and further dried under nitrogen to give 0.306g product. The liquid product was set out overnight (~16 hours) to dry on a watch glass. This portion remained a viscous substance, thus, it was dissolved in acetone and set aside to dry in a separate vial. Over time, white crystals became present. Following characterization, it was determined that the “liquid” crystal product was of the same composition as the initial solid product. Proton NMR was used to characterize the trivinyl POSS product.

Yield: 39.1%; ^{1}H NMR: 6.08 (t), 5.90 (d), 5.84 (d).

Trimethyl/Vinyldimethyl POSS

A 50/50 molar mixture of trimethyl and vinyldimethyl corner groups was synthesized to form a random mixture of corner groups. 1g (0.553mmol) of octaanion dissolved in methanol was added dropwise to a silyation mixture containing 3.5mL (27.6mmol) TMCS, 3.8mL

(27.6mmol) VDMCS, and 9.7mL hexane. Both solutions were chilled prior to reaction. Reaction was stirred for ~1 hour. Following evaporation of the organic layer, washing, and drying of the white crystalline product, the solids were recrystallized using heated acetonitrile with vigorous mixing. Recrystallized product was measured to be 0.410g and was examined under microscope to determine any observable crystal structure differences. Proton NMR and powder XRD were used to characterize the trimethyl/vinyldimethyl mixed POSS product.

Yield: 63.0% (using averaged MW of products); ^{1}H NMR: 6.08 (t), 5.98 (d), 5.83 (d), 0.213 (s), 0.149 (s); Powder XRD major low angle peaks: 6.70, 8.02, 9.36, 9.78.

Vinyldimethyl/Trivinyl POSS

1.5g (0.829mmol) octaanion in methanol was added dropwise to a silyation mixture containing a mixture of 1.72mL (12.4mmol) VDMCS, 2.04mL (12.4mmol) TVCS, and 5mL hexane. Both solutions were chilled prior to reaction. Reaction was stirred for ~1 hour. Following organic layer separation and solvent removal via rotary evaporator, a product consisting of both a white crystalline solid and viscous clear liquid (similar to what was observed above for trivinyl POSS). Recrystallization of the entire product was done in acetonitrile. Solid products were obtained via filtration, while remaining liquid product/acetonitrile mixture was set aside to dry. Upon drying, liquid portion of the product was shown to be similar to the initial solid product from proton NMR characterization. Total overall solid product obtained in this manner was 0.486g. In addition to proton NMR, powder XRD was used to characterize the vinyldimethyl/trivinyl mixed POSS product.

Yield: 44.4%; ^{1}H NMR: 6.09 (m), 5.91 (m), 5.83 (m), 0.202 (t); Powder XRD major low angle peaks: 7.10, 8.00.

Trimethyl/Vinyldimethyl/Dimethyl/Trivinyl POSS

1g (0.553mmol) octaanion in methanol was added dropwise to a silyation mixture containing a primarily equimolar mixture of 0.6mL (4.73mmol) TMCS, 0.6mL (4.34mmol) VDMCS, 0.5mL (4.50mmol) DMCS, and 0.7mL (4.50mmol) TVCS, with 3mL hexane. Both mixtures were

chilled prior to reaction. Reaction was stirred for ~1 hour. Following organic layer separation and solvent removal via rotary evaporator, a white crystalline product was formed. Further drying of the product was achieved under nitrogen and resulted in 0.4290g product. Proton NMR and powder XRD were used to characterize the trimethyl/ vinyldimethyl/ dimethyl/ trivinyl mixed POSS product.

Yield: 64.8%; ^{1}H NMR: 6.10 (m), 5.93 (m), 5.88 (m), 4.73 (m), 0.248 (s), 0.217 (s), 0.153 (s); Powder XRD major low angle peaks: 6.64, 7.64, 7.92, 9.12, 9.98.

7-Octenyldimethyl POSS

1g (0.553mmol) octaanion in methanol was added dropwise to a silyation mixture of 4.5mL (16.6mmol) 7-octenyldimethylchlorosilane (ODMCS; Gelest) and 6mL hexane. Both mixtures were chilled prior to reaction. Reaction was stirred for ~1 hour. Following organic layer separation and solvent removal via rotary evaporator, a liquid was left behind. Following several hours of additional drying under nitrogen, a liquid product remained. An attempt to precipitate a solid from the product was done using ethanol. A sample of the product was dropped into ethanol to form a cloudy substance which dissolved back into the ethanol over time. Addition of water to this solution caused more cloudy precipitate to form. This mixture was place in a freezer in an attempt to collect the solid later. This precipitate simply went back into solution upon attempted solid extraction. Separately, 1mL of the 7-octenyldimethyl POSS liquid product was added to 50mL of a 50/50 (v/v) mixture of methanol and water. Addition of water to this mixture caused resulted in a more cloudy solution. This solution was filtered using glass fiber filters. No solid product was obtained by this method. The final attempt at obtaining a solid involved placing a test tube of the liquid POSS product in a dry ice/acetone bath. A white solid appeared during this process, but was only found to be frozen solvent.

5-Hexenyldimethyl POSS

1g (0.553mmol) octaanion in methanol was added dropwise to a silyation misture of 4mL (16.6mmol) 5-hexenyldimethylchlorosilane (HDMCS; Gelest) and 6mL hexane. Both mixtures

were chilled prior to reaction. Reaction was stirred for ~1 hour. Following organic layer separation and solvent removal via rotary evaporator, a liquid was left behind. Extensive drying under nitrogen further revealed a liquid product. A sample of the product was dropped into ethanol, leaving a cloudy mixture that re-dissolved back into the ethanol over time. A vial of this ethanol solution was placed in a freezer to see if any solid product could be collected. No solid product was collected in this fashion.

Vinyldimethyl/5-Hexenyldimethyl POSS mixtures

The following ratios seen are representative of each of the 8 corner groups for the octaanion (i.e. a "pure" POSS product would have a ratio of 8:0; an equimolar mixture of 2 chlorosilanes as 4:4). The varying mixtures were as follows: a 7:1 corner ratio (vinyldimethyl:5-hexenyldimethyl), 6:2, 5:3, and 4:4. 1g (0.553mmol) octaanion in chilled methanol was added to each respective silyating mixtures, which were also chilled. For the 7:1 mixture a silyating solution of 2mL (14.5mmol) VDMCS, 0.45mL (2.07mmol) HDMCS, and 3.25mL hexane was prepared. For the 6:2 mixture: 1.72mL (12.4mmol) VDMCS, 0.65mL (3.11mmol) HDMCS, and 3.25mL hexane. For the 5:3 mixture: 1.45mL (10.4mmol) VDMCS, 1.29mL (6.22mmol) HDMCS, and 3.6mL hexane. For the 4:4 mixture: 1.15mL (8.29mmol) VDMCS, 1.72mL (8.29mmol) HDMCS, and 3.81mL hexane. All resulting organic layers from each respective silyation reaction were concentrated under rotary evaporator and further dried under nitrogen. With increasing amounts of HDMCS reacted, it was evident that more liquid "product" was present. Recrystallization of each product was done with vigorous stirring in heated acetonitrile. Solid products that recrystallized in solution were filtered and collected for the 7:1 and 6:2 mixtures. For the 5:3 mixture, recrystallization did not initially result in solid products. Instead a liquid phase separation was evident between acetonitrile and the liquid "product." Following ~16 hours of cooling, crystals were obtained from the 5:3 acetonitrile solution. Solid product was obtained in this way through multiple filtrations. For the 4:4 mixture, a very small amount of solid product was obtained through multiple acetonitrile recrystallizations, cooling and filtrations. At this point, for each of the respective mixtures, a liquid product in acetonitrile remained. Since a liquid phase separation occurred

with acetonitrile and the liquid product, acetonitrile was pipetted off and replaced with butanol, where both solid and liquid components of the "product" were completely soluble. Following ~16 hours of cooling in a freezer, additional solid product was obtained from the 6:2, 5:3, and 4:4 mixtures (the 7:1 mixture was primarily a solid product already). Solid products obtained for each mixture were as follows: 0.347g (7:1), 0.279g (6:2), 0.203g (5:3), 0.0658g (4:4). Proton NMR was used to characterize the above vinyldimethyl/5-hexenyldimethyl solid products obtained from mixtures. Peak data closely resembles that of vinyldimethyl POSS for each mixture

Yield (calculated by vinyldimethyl POSS MW): 51.2% (7:1), 41.2% (6:2), 30.0% (5:3), 9.71% (4:4); ^{1}H NMR (7:1): 6.14 (t), 5.98 (d), 5.81 (d), 0.208 (s); ^{1}H NMR (6:2): 6.14 (t), 5.98 (d), 5.81 (d), 0.208 (s); ^{1}H NMR (5:3): 6.14 (t), 5.98 (d), 5.81 (d), 0.208 (s), 0.119 (s); ^{1}H NMR (4:4): 6.14 (t), 5.98 (d), 5.81 (d), 0.208 (s), 0.119 (s), 0.033 (s).

Tri-N-Propyl/Vinyldimethyl POSS

1.2g (0.663mmol) octaanion in methanol was added dropwise to an equimolar silyation mixture of 2.2mL (9.95mmol) tri-n-propylchlorosilane (TNPCS; Gelest), 1.40mL (9.95mmol) VDMCS, and 4.8mL hexane. Both mixtures were chilled prior to reaction. Reaction was stirred for ~1 hour. Following organic layer separation and rotary evaporation, a partially solid and liquid product was left behind. Rather than attempting further drying under nitrogen, a vacuum condenser apparatus was set up to pull off what was anticipated to be hexapropyl disiloxane. The product was heated in a roundbottom flask which was attached to a short condenser under vacuum. A small amount of liquid was pulled from the final product. Remaining product was dried under nitrogen before testing solubility of the product in various solvents. Tetrahydrofuran (THF) was used to dissolve the entirety of the product and placed in a diffusion cell. This consisted of the product in THF solution in a small vial, which was placed inside of a beaker containing water. After 3 days, any remaining liquid was pulled off and filtered through a pipette containing a Kimwipe. Liquid passing through the filter was placed in another diffusion cell.

Synthesis: Decamer

Decamer Anion:

Decamer POSS production involves two steps: synthesis of the silicate cage anion, followed by silyation of the decamer anion. Multiple products may be formed depending on varying concentrations and ratios of the initial reactants. 10 different batches were made with varying amounts of initial constituents and different silyation methods from multiple pieces of literature [31-34].

Batch #1: [Si] = 1.11; TBA/Si = 0.5

4.47mL TEOS (20.1mmol) was reacted in a batch mixture with 6.487mL tetrabutylammonium (TBA) hydroxide solution (40% wt. in H_2O; Alfa Aesar). 3.892mL dimethyl sulfoxide (DMSO) was added to the mixture. An additional 1.57mL each of water and DMSO to maintain an Si concentration of 1.11 in the overall solution. Mixture was allowed to stir for ~60 hours. Silyation reaction mixture consisted of 9.92mL (76.9mmol) TMCS and 8.71mL hexane. TBA mixture was added dropwise to the silyation mixture and allowed to mix for ~1 hour. Hexane was added to this reaction mixture until all solids were dissolved. Upper organic layer of the mixture was partially evaporated under rotary vacuum. Crystal product appearing after this partial solvent removal was collected via filtration at room temperature and labeled “first out of solution.” Hexane filtrate was placed in a freezer for ~16 hours. Crystals formed in chilled hexane solution were collected via “cold filtration” with chilled hexane and labeled “cold filtered solids.” In both filtrate flasks, a goopy polymer-like substance could be observed. Filtered products, room temperature and chilled, were placed in a desiccator to dry. Proton NMR and powder XRD were used to characterize the above products.

^{1}H NMR: 0.151 (s); Powder XRD major low angle peaks: 6.80, 8.19, 9.53, 9.84.

Batch #2: [Si] = 1.83; TBA/Si = 0.5

5.2mL TEOS (23.3mmol) was reacted in a batch mixture with 7.5mL TBA solution. No DMSO or additional water was added for further dilution. Solution was stirred for ~16 hours. TBA mixture was added dropwise to a silyation mixture containing 11.3mL (89.1mmol) TMCS and 15mL hexane. Reaction was allowed to mix for ~1 hour. Upper organic layer was placed under rotary evaporator to remove hexane. Upon solvent removal, very little product was obtained. Remaining solids in the flask primarily contained a polymer product. Small amount of crystalline product was separated from the polymer and obtained via filtration with cold hexane. Proton NMR and powder XRD were used to characterize the above products.

^{1}H NMR: 0.150 (s); Powder XRD major low angle peaks: 6.58, 8.10.

Batch #3: [Si] = 1.44; TBA/Si = 0.5

4.5mL TEOS (20.2mmol) was reacted in a batch mixture with 6.5mL TBA solution. Mixture was diluted with 3mL water to bring Si concentration of the overall solution to 1.44. Solution was stirred for ~16 hours, then placed in a freezer with the expectation that decamer anion solids would crash out of solution. Entire solution freezes, thus, a 50/50 mixture (v/v) of water and ethanol was added to promote crystallization of desired solids in cold temperature conditions. Under these conditions, a liquid and solid mixture was obtained. Liquid layer was removed and placed in a separate flask in the freezer. Liquid layer was added dropwise to a silyation mixture of 5mL (39.6mmol) TMCS and 6.6mL hexane (an estimate due to unknown Si content in liquid layer). Following rotary evaporation of the organic layer, no product was obtained. Remaining solid anion in freezer was measured at ~20g. Multiple silyation methods were used with this particular batch. The first silyation procedure [35], assuming a 60:40 molar mixture of octamer:decamer anions, called for a silyation mixture of 10.3mL (81.4mmol) TMCS in 51.5mL heptane and 20.6mL dimethylformamide (DMF). This mixture was chilled prior to reaction. 2g of Batch #3 solids were added via spatula to the silyation mixture over a 10-15 minute period. Following addition, mixture was allowed to stir for ~20 minutes and allowed to come to room

temperature. 100mL ice water was added to the mixture and allowed to stir an additional 15 minutes. Upper organic layer of the mixture was separated out and washed with water (2x). Washed organic layer was placed in freezer for ~60 hours. Rotary evaporation of this layer revealed a very small amount of product other than a polymer. Product was "cold-filtered" using hexane. Crystalline solids were separated from polymer. A second silyation procedure [36] called for two separate solutions. The first was a mixture of 35mL dimethoxypropane, 1.5mL 10M HCl, and 5mL hexamethyldisiloxane (HMDSO). 2.463g Batch #3 solids were added to this solution over a period of 10 minutes. An additional 10 minutes was allowed for the stirring of this reaction. Mixture was concentrated under rotary evaporator for ~10 minutes. To this concentrated solution was added a silyation mixture of 2.5mL (19.8mmol) TMCS, 10mL DMF, and 5mL HMDSO. This reaction mixture was allowed to stir for ~10 minutes. 10mL heptane and 20mL water were added to the mixture and stirred for an additional 5 minutes. Upper organic layer resulting from the reaction was separated out and stored in freezer conditions. For the third silyation method [36], the same procedure was used, substituting isopropanol for DMF. Both solutions were placed under rotary evaporator and very little amount of crystalline product was obtained in the presence of polymer products. Crystalline product was separated via cold hexane filtration. Remaining Batch #3 anion was estimated to be 15mL solution at [Si] = 0.5. This remaining anion solution was added to a silyation mixture of 4.5mL (35.6mmol) TMCS with 6mL hexane. All mixtures were chilled prior to reaction. Reaction was allowed to mix for ~1 hour. Upper organic phase in resulting mixture was concentrated under rotary evaporator. A small amount of crystalline product and polymer were obtained. Solids were rinsed in acetone to remove majority of polymer from crystalline product. Acetone/polymer layer was allowed to dry. Crystals formed in this polymer were washed and separated as above. Proton NMR was used to characterize the above products. Sufficient enough product was not obtained to run powder XRD analysis.

^{1}H NMR: 0.151 (s).

Batch #4: [Si] = 0.90; TBA/Si = 0.84

4.5mL TEOS (20.2mmol) was reacted in a batch mixture with 11mL TBA solution. Solution was stirred for ~16 hours. 20mL 50/50 (v/v) water and ethanol was added to the reacted mixture to promote anion crystallization under freezing temperatures. Under these conditions, a liquid and solid mixture was obtained. Liquid layer was removed and placed in a separate flask in the freezer. Liquid layer was added dropwise to a silyation mixture of 5mL (39.6mmol) TMCS and 6.6mL hexane (an estimate due to unknown Si content in liquid layer). Reaction was mixed for ~1 hour. In addition, a second silyation was run on a small sample of Batch #4 solids. 3.75g of solids was added via spatula to a silyation mixture of 5mL (39.5mmol) TMCS with 6.6mL hexane. Reaction was mixed for ~1 hour. Following organic layer solvent removal from both reactions, a very small amount of crystalline product was present with polymer product. Remaining anion solution was estimated to be ~25mL of [Si] = 0.4. This remaining solution was added to a silyation mixture of 6mL (47.5mmol) TMCS and 8mL hexane. All mixtures were chilled prior to reaction. Reaction was allowed to mix for ~1 hour. Upper organic phase in resulting mixture was concentrated under rotary evaporator. A small amount of crystalline product and polymer were obtained. Solids were rinsed in acetone to remove majority of polymer from crystalline product. Acetone/polymer layer was allowed to dry. Crystals formed in this polymer were washed and separated as above. Proton NMR was used to characterize the above products. Sufficient enough product was not obtained to run powder XRD analysis

^{1}H NMR: 0.151 (s).

Batch #5: [Si] = 0.64; TBA/Si = 0.70

4.91mL TEOS (22.1mmol) was reacted in a batch mixture with 11mL TBA solution. An additional 19.29mL water was added to reduce the concentration of TBA to 0.45M. Mixture was stirred at room temperature for ~6 hours. Solution was stored in a freezer for ~16 hours. Solution was allowed to melt and acetone was added to make a 50/50 (v/v) solution and test a new method of extracting the solids. Following ~16 hours in freezer conditions, acetone was removed via rotary evaporator. Remaining solution was placed back in a

freezer for ~16 hours. A greater amount of crystalline material had crashed out of solution at this point. A silyation mixture was prepared from 51.8mL (409mmol) TMCS, 104mL HMDSO, and 10.4mL isopropanol. Precipitate formed by the mixture of TMCS with isopropanol was removed prior to reaction. Anion solids were added via spatula to this mixture. Reaction was stirred for ~15 minutes. Organic layer was separated and placed under rotary evaporator to remove excess HMDSO and TMCS. Solution was re-dissolved in ~25mL HMDSO. 1g Amberlyst 15 ion exchange resin (Alfa Aesar) was added to this solution and stirred for ~16 hours. Amberlyst 15 was removed from solution via filtration. Filtrate was stored in the freezer. Crystalline and polymer product obtained in this manner was placed in a vial of ethanol for recrystallization. Upon heating up to boiling, remaining solids in this vial were filtered and collected as an octamer product. Remaining filtrate was allowed to cool in a freezer. Additional crystals crashed out of solution which could be washed with ethanol to separate from the polymer side product. Proton NMR and powder XRD were used to characterize the above products.

^{1}H NMR (octamer): 0.150 (s); ^{1}H NMR (decamer): 0.146 (s); Powder XRD major low angle peaks (octamer): 6.74, 8.14, 9.42, 9.82; Low angle peaks (decamer): 6.18, 6.44, 7.84, 8.00, 8.80, 9.56, 9.96.

Batch #6: [Si] = 0.64; TBA/Si = 0.70

1g (16.7mmol) solid silica gel (SiO_2; Sorbent Technologies) was added to 7.56mL TBA solution and 18.3mL water. Reaction was stirred for ~60 hours. Solution was stored in freezer. Acetone was added to the overall solution to create a 50/50 (v/v) mixture. Acetone was allowed to mix with overall solution then was removed via rotary evaporator. 11mL ethanol was added to make a 31% (v/v) solution with ethanol, a mixture just with a freezing point just under that of the provided freezer (-14°C; assuming an all water initial solution). Solid and liquid layer were formed after ~16 hours. Solid anion was added via spatula to a silyation mixture of 39.2mL (310mmol) TMCS, 78.6mL HMDSO, and 7.85mL isopropanol. Precipitate in this mixture was removed prior to reaction. Reaction was allowed to mix for ~15 minutes. Following organic layer separation and HMDSO and TMCS removal via rotary

evaporator, ~40mL HMDSO was used to re-dissolve the concentrated solution. 0.6g Amberlyst 15 was added to the mixture and allowed to mix for ~16 hours. Amberlyst 15 was removed from solution via filtration. Remaining solution was placed under rotary evaporator under a mixture of crystalline/ emulsion material remained. Products were placed in ethanol for recrystallization. Undissolved material after heating were filtered out and collected as octamer product. Remaining products can be re-dissolved to a clear solution by reheating ethanol. Upon cooling of the solution, decamer crystalline product could be obtained by washing in ethanol to remove majority of polymer side product.

Batch #7: [Si] = 1.00; TBA/Si = 0.70

1g (16.7mmol) solid silica gel was added to 7.56mL TBA solution and 9mL water. Reaction was stirred for ~60 hours. A small sample from this batch was placed in a test tube in a desiccator to draw water out of solution. Remaining solution was placed under nitrogen to determine what would result from complete drying of the solution. Both the desiccator and nitrogen dried samples formed a polymer like substance with very small amount of crystalline material. Both samples were re-dissolved in methanol and returned to the freezer. Roughly half the volume in solution was removed via rotary evaporator and solution was returned to the freezer.

Batch #8: [Si] = 1.66; TBA/Si = 0.70

1g (16.7mmol) solid silica gel was added in 0.25g increments to 7.56mL TBA solution to make a concentrated solution. An additional 3.5mL water was added to help the silica gel dissolve in solution and solution was slightly heated to increase solubility. Solution was allowed to come to ambient temperatures and was then placed in a salt-ice bath for ~1 hour. Any solution that remained as a viscous liquid was pulled off and stored in a separate vial under freezer conditions. 1mL acetone was added to this liquid layer and stored in the freezer. Solid layer was stored separately in the freezer. This crystal layer was silyated using a solution of 39.2mL (310mmol) TMCS, 78.6mL HMDSO, and 7.85mL isopropanol. A precipitate appeared to form upon mixing of TMCS with isopropanol; this was kept in the solution. Anion crystals were slowly added to this solution via spatula. Reaction was stirred

for ~15 minutes. Upper organic layer was collected and remaining HMDSO and TMCS was removed via rotary evaporator. The remaining solution was a cloudy mixture that was re-dissolved in ~15mL HMDSO. 0.5g Amberlyst 15 was added to the solution and stirred for ~16 hours. Amberlyst 15 was removed from the solution via filtration. Remaining solution was concentrated under rotary evaporator followed by nitrogen drying, leaving behind a cloudy emulsion. Ethanol was added to solution until clear and stored in the freezer. Roughly half of ethanol was removed via rotary evaporator until very small amounts of crystals appeared. Liquid layer was pipetted off and remaining crystals were dissolved in HMDSO and placed in a separate vial.

Batch #9: [Si] = 0.59; TBA/Si = 1.00

3.72mL (16.7mmol) TEOS was reacted in a batch mixture of 8.12mL TBA solution, 16.3mL water, and 1.34g tetrabutylammonium bromide (Alfa Aesar). Reaction was stirred for ~7 hours then placed into a freezer. Ethanol was added to make a 31% (v/v) mixture to induce crystal anion crashing out of solution. Solid anion was added via spatula to a silyation mixture of 39.2mL (310mmol) TMCS, 78.6mL HMDSO, and 7.85mL isopropanol. Precipitate in this mixture was removed prior to reaction. Reaction was mixed for ~15 minutes. Organic layer was concentrated under rotary evaporator. Remaining solution was re-dissolved in HMDSO and 0.6g Amberlyst 15 was added and stirred for ~16 hours. Amberlyst 15 was removed from solution via filtration. Remaining solution was placed under rotary evaporator to remove remaining solvents. Resulting crystalline/emulsion product was placed in a vial with ethanol for recrystallization. Undissolved solids after heating were collected as octamer product. Remaining solution was allowed to cool and decamer crystals were washed with ethanol to remove polymer side product.

Batch #10: [Si] = 0.63; TBA/Si = 0.75

2mL (9.17mmol) TEOS was reacted in a batch mixture of 4.5mL TBA solution and 8mL water. Reaction was stirred for ~6 hours. Ethanol was added to the mixture to create a 30% (v/v) solution to induce crystallization in freezer conditions. A reaction mixture of 21.6mL (170mmol) TMCS, 43.3mL HMDSO, and 4.32mL isopropanol was made for silyation. Anion

solution was placed in an ice bath containing acetone and dry ice. A reverse silyation was done by adding silyation mixture dropwise to a continuously stirred anion solution. Following complete addition of the silyation mixture, reaction was stirred and allowed to come to room temperature. Organic layer was separated and stored in a freezer for ~16 hours. Organic layer was concentrated under rotary evaporator and redissolved in ~30mL HMDSO. 0.4g Amberlyst 15 was added and mixture was stirred for ~16 hours. Amberlyst 15 was removed from solution via filtration. Remaining solution was placed under rotary evaporator to remove remaining solvents. Resulting crystalline/emulsion product was placed in a vial with ethanol for recrystallization. Undissolved solids after heating were collected as octamer product. Remaining solution was allowed to cool and decamer crystals were washed with ethanol to remove polymer side product.

Spin Coating

Spin coating samples were primarily made using propylene glycol monomethyl ether acetate (PGMEA) as a solvent. An additional solvent used included methylethyl ketone (MEK), typically for trimethyl decamer POSS products. Solutions were made on a basis of weight percent. Solid POSS product (as prepared above) was added to a vial of solvent and mixed until fully dissolved for all spin coating samples.

Silicon wafers (2” diameter; University Wafers) were initially cleaned via acetone rinse followed by 15 minutes under UVO cleaning. A second, better cleaning procedure consisted of a series of rinses—acetone, isopropanol, deionized water, acetone, isopropanol—followed by ~10 minutes under UVO cleaning. Some wafer surfaces were silyated prior to spin coating. These wafers were placed in a hexane bath with a few drops of TMCS and allowed to soak for ~30 minutes. Prior to loading wafer in spin coater, a jet of air was used to remove any dust from the wafer surface (non-cleanroom conditions). Wafers were loaded after this step then rinsed (2x) in solvent at high speed and acceleration to remove a majority of any remaining large particles on the wafer surface.

Solutions were applied to the wafer via syringe through a 0.2µm polypropylene filter. Roughly three quarters of the wafer surface area was to be coated for optimal coating of POSS products. For solutions of 2-5% wt. with PGMEA as a solvent, standard spin parameters were as follows: 100rpm for 10s, 150rpm (acceleration 3) for 30s, 400rpm (acc 6) for 60s, 600rpm (acc 2) for 3min. For PGMEA solutions at >1% wt., slow spin parameters were as follows: 80rpm for 1min, 120rpm (acc 10) for 3min, 150rpm (acc 10) for 15 min. For attempted thin resists at >1% wt. in PGMEA, fast spin parameters were as follows: 100rpm for 40s, 180rpm (acc 10) for 30s, 1500rpm (acc 10) for 4min. For solutions employing MEK as a solvent, spin parameters were as follows: 100rpm for 10s, 150rpm (acc 5) for 20s, 400rpm (acc 5) for 2min. For 5-hexenyldimethyl and 7-octenyldimethyl POSS liquid products (no solvent) spin parameters were as follows: 200rpm for 15s, 700rpm (acc 10) for 40s, 1000rpm (acc 10) for 5min, 3000rpm (acc 10) for 8min. In cleanroom conditions, SU-8 2010 E-beam resist (Microchem) was applied to wafers by pouring. Spin parameters were as follows: 100rpm for 10s, 3000rpm (acc 100) for 2min.

Following spin coating, a post application bake ("soft bake"; commonly used to remove any residual solvent) was typically not used. Rather, the wafer and resist were allowed to dry in ambient conditions. A 5% vinyldimethyl POSS resist and SU-8 2010 E-beam resist were exceptions. For the 5% vinyldimethyl POSS, wafer was placed on a hot plate at 45°C and slowly ramped up to 65°C for annealing of the resist. Further ramping to ~100°C and above caused sublimation of the resist. For the SU-8 2010, wafer a post application bake at 95°C for 3 minutes was done.

Lithography

Photoresist on Si wafers were exposed under E-beam using a scanning electron microscope (SEM). Prior to exposing the wafer surface, electron current was measured using a Faraday cup. Exposure area was controlled using reduced raster scanning. From these data, exposure doses were calculated with a given amount of time. Initial exposures were done at doses from 1000-3500 $\mu C/cm^2$ for 40µm x 40µm exposure areas. Subsequent exposures for

contrast curve development and sensitivity data called for exposure doses of 0.1-1000 $\mu C/cm^2$. Exposure areas were expanded to a range of 100µm x 100µm to 2000µm x 2000µm. Typical exposure procedures were as follows: set exposure area via reduced raster, blank beam, set stage/beam location, un-blank beam, expose resist for desired time, blank beam, repeat.

A post exposure bake was typically not used on POSS resists. For SU-8 2010 resists, both PEB and non-PEB methods were used. For the PEB SU-8 2010 resist, wafer was baked on a hot plate at 95°C for 3 minutes. Exposed POSS resist wafers were developed in a 20/80 (v/v) PGMEA/methanol mixture for ~1 minute followed by rinsing in methanol for ~10s. Exposed SU-8 2010 wafers were developed in PGMEA for ~1 minute followed by rinsing in PGMEA for ~10s. Wafers were cleaved either with a diamond scriber or by crack propagation along the wafer.

Exposures were imaged from a top down perspective. Cross-sectional imaging was done with an SEM stage tilt of 1°. For very thin, low % wt. films, stage tilt was set at 5° for cross-sectional imaging.

Chapter 3: Results and Discussion

Synthesis: Characterization

Many synthesis routes to developing the octameric POSS macromolecules (with trimethyl corner groups) have been studied with increasing success and applications over the years [28, 29]. Two relatively simple and time friendly steps include first synthesizing the silica cage anion, followed by a silyation reaction which allows placement of the corner groups onto the POSS cages. It should be noted that while the initial silica source may vary (silica gel, tetraalkoxysilane, etc.), tetraethylorthosilicate (TEOS) was the preferred silicate source throughout the majority of synthesis procedures. The first route to these products utilized the well-known rearrangement of TEOS in strong, quaternary ammonium base solutions to form the octameric, octaanionic silicate core as shown in Figure 3.1.

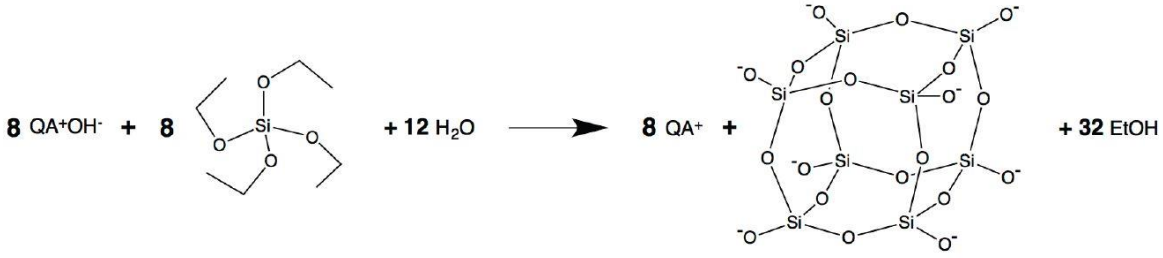

Figure 3.1. Synthesis of the SSQ octaanion.

The silyation reaction steps from octaanion to octamer product are as shown in Figure 3.2 below, where R may represent varying corner groups based on chlorosilane used (vinyldimethyl groups shown below).

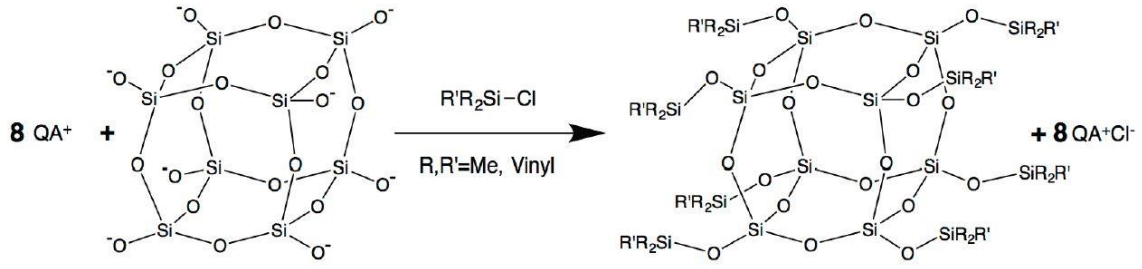

Figure 3.2. Silyation of octaanion to octamer product.

Trimethyl and dimethyl silyations were successfully run to obtain the same product from literature procedures and develop an understanding of the overall reaction. Additionally, they were used in mixed-silyation reactions. Other reactions were completed for the placement of useful functional groups on the octameric structures. For this project, vinyl functional groups were the primary desired functionality. A wide variety of chlorosilanes were employed in this procedure due to crystallinity issues with the photoresist film, an issue to be discussed later on regarding spin coating. The varying additional purposes of the corner groups studied ranged from tripling the amount of functional groups on each corner to using long chain groups and/or molar mixtures of multiple chlorosilanes in an effort to break up crystallinity. The different chlorosilanes used, their additional purpose, and mixtures based on corner ratios (8 groups total for octamer) are shown in Table 3.1.

Table 3.1. Octamer silyated corner groups.

Corner Group	**Additional Purpose**	**Additional Mixtures (corner group ratios)**
Trimethyl	Replicating Literature	4:4 w/ vinyldimethyl 2:2:2:2 w/ vinyldimethyl, dimethyl, trivinyl
Vinyldimethyl	Target Functional Group	4:4 w/ trimethyl 2:2:2:2 w/ trimethyl, dimethyl, trivinyl 4:4 w/ trivinyl (See 5-Hexenyldimethyl)
Dimethyl	Replicating literature	2:2:2:2 w/ trimethyl, vinyldimethyl, trivinyl
Trivinyl	Additional cross-linking groups	2:2:2:2 w/ trimethyl, vinyldimethyl, dimethyl 4:4 w/ vinyldimethyl
7-Octenyldimethyl	Long chains to reduce crystallinity	N/A
5-Hexenyldimethyl	Long chains to reduce crystallinity	1:7, 2:6, 3:5, 4:4 w/ vinyldimethyl
Tri-n-propyl	Long chains to reduce crystallinity	4:4 w/ vinyldimethyl

Each of the above corner groups, with the exclusion of tri-N-propyl, was run as both "pure" and mixed silyations. Yields for the solid octamer products were calculated based on the moles of silica octaanion (1809 g/mol; formula from Chapter 2) used. These yields and average molecular weights used (for mixed silyation products) are as reported in Table 3.2. Low yields were typically found in trivinyl and 5-hexenyldimethyl mixtures, as liquid products were not included in these calculations.

Table 3.2. Octamer POSS product yields.

Product	**Calculated Avg. MW [g/mol]**	**Yield %**
Trimethyl POSS	1129	51.0 ("dry" anion addition)
Vinyldimethyl POSS	1225	64.5 (Rxn 1); 59.0 (Rxn 2)
Dimethyl POSS	1017	69.0
Trivinyl POSS	1417	39.1
Trimethyl/Vinyldimethyl POSS	1177	63.0
Vinyldimethyl/Trivinyl POSS	1321	44.4
Trimethyl/Vinyldimethyl/ Dimethyl/Trivinyl POSS	1197	64.8
5-Hexenyldimethyl/Vinyldimethyl POSS mixtures	1225	51.2 (7:1); 41.2 (6:2); 30.0 (5:3); 9.71 (4:4)

For the trimethyl, vinyldimethyl, and dimethyl "pure" octamer, the final products were obtained as a white crystalline solid that could be recrystallized using acetonitrile. While it was discovered that such crystalline material wasn't suitable as a spin-coatable product, the ability to recrystallize does allow for a very pure product formation. Mixed silyation and/or long chain corner group reactions, as noted in the above table, were an attempt to break up the symmetric, crystalline order of the structure by randomizing corner group placement. Ideally, this would allow for the formation of a more amorphous product that would more readily form a thin, uniform layer that is suitable for spin coating optimization and various

forms of lithography. In ^{1}H NMR—using the trimethyl/ vinyldimethyl mixed silyation product for example—one would expect to see additional peaks in the mixed product that are not viewed in the "pure" product NMR. Figure 3.3 shows a stacked proton NMR with trimethyl, vinyldimethyl, and trimethyl/vinyldimethyl mixed POSS products.

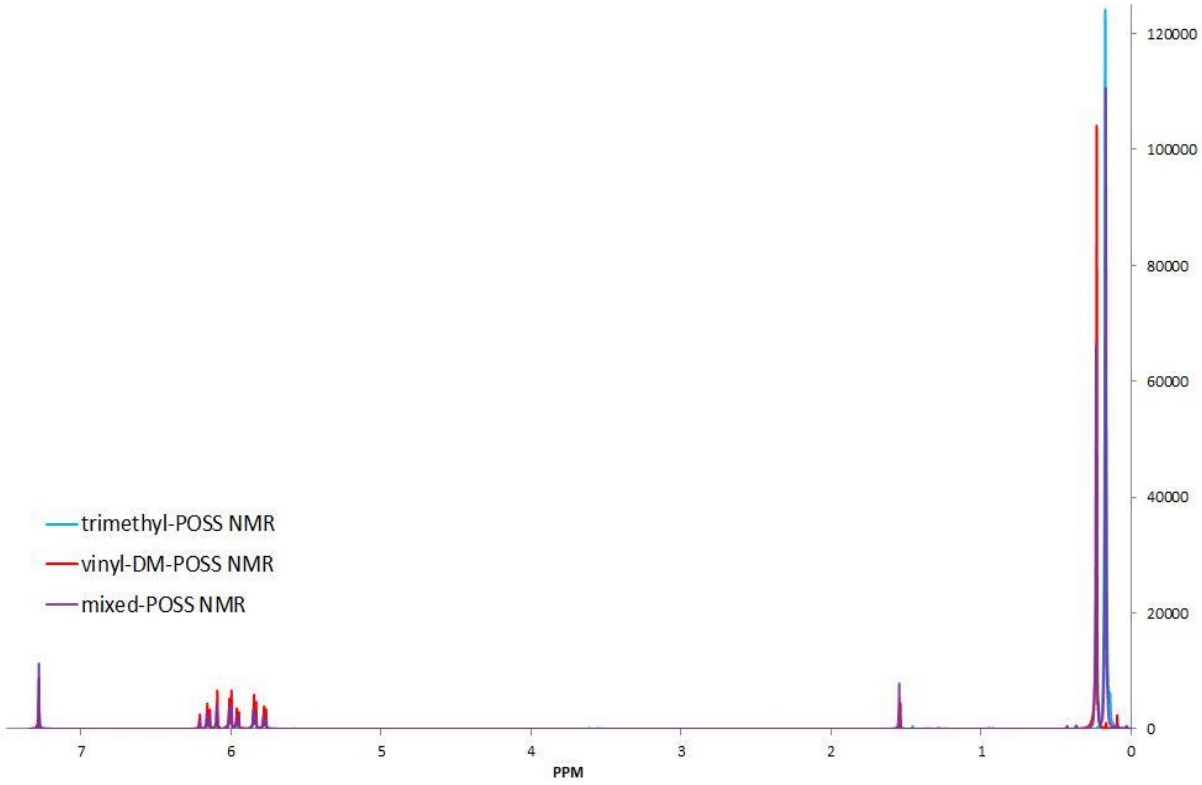

Figure 3.3. Stacked ^{1}H NMR plot of trimethyl, vinyldimethyl, and mixed POSS.

Against the concept described above, this plot appears to simply be a "stack" of pure POSS product peak data. Instead, one would expect the presence of more peaks/peak shifts representative of the varying proton environments caused by the random arrangement of corner groups on each macromolecule. An explanation regarding the "pure" appearance of the above mixed-POSS NMR peaks could be that the corner groups are too far from each other and the silicate cage itself to exhibit any sort of noticeable change in the peak data.

However, even if random, asymmetric ordering of the corner groups went unregistered on ^{1}H NMR, one would still expect a mixed-POSS product to show a less crystalline film than a "pure" octamer POSS product due to increased disorder in the material's structure. Similarly

with the vinyldimethyl/5-hexenyldimethyl mixtures, no physical difference between the "pure" and mixed POSS solid products was observed. Figure 3.4 shows a stacked ^{1}H NMR plot of all the vinyldimethyl/ 5-hexenyldimethyl mixtures. Once again, the appearance of "pure" product peaks stacked is exhibited, while anticipated peak shifts for differing proton environments are not. The only noticeable differences between each reaction mixture appear to be solvent peaks from butanol and acetonitrile, as more washing/filtering was used on samples with higher 5-hexenyldimethyl concentrations. Though, in addition to the singlet peak observed for pure vinyldimethyl POSS products (0.208-0.217 ppm), peaks at 0.119 and 0.033 ppm (Figure 3.4) began to form with increased 5-hexenyldimethyl silyation concentrations. Despite this change in the ^{1}H NMR data, the solid products appeared no less crystalline than pure vinyldimethyl POSS following drop tests in PGMEA on an Si wafer.

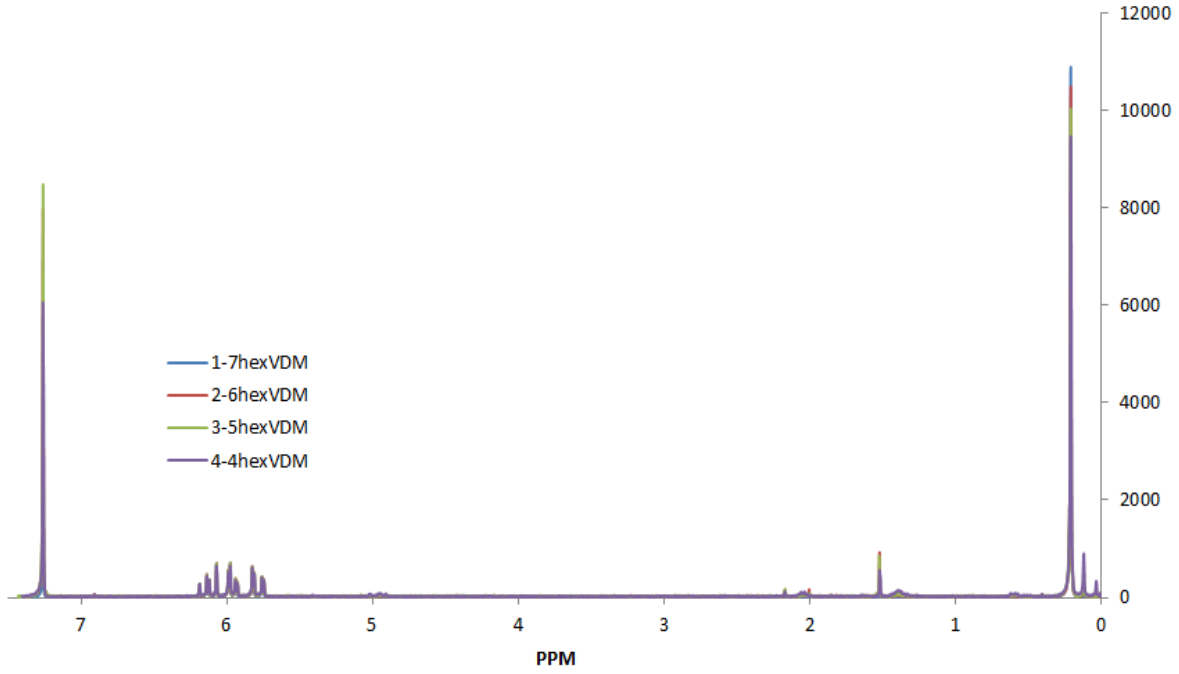

Figure 3.4. Stacked ^{1}H NMR plot of vinyldimethyl/5-hexenyldimethyl mixtures.

Due to the unexpected crystallinity of the octamer products, a second type of POSS geometry was additionally synthesized in an effort to reduce crystallinity issues experienced with octamer product photoresists—the decamer. Very similar to the octamer in structure, the decamer contains a silicate cage of 10 Si atoms (Figure 3.5). In comparison to octamer products, the decamer structure tends to be significantly more flexible in solution, thus, less

prone to crystallinity as a resist film [37]. This differing solubility in a spin coating solvent could lead to a more reasonable and uniform film surface. Unlike the octamer, decamer products unfortunately require much more complicated synthesis procedures [31-34] since multiple silicate products are formed. By varying the concentrations and ratios of the given precursors, a variety of products containing a range of 1-10 Si atoms and larger polymers are formed.

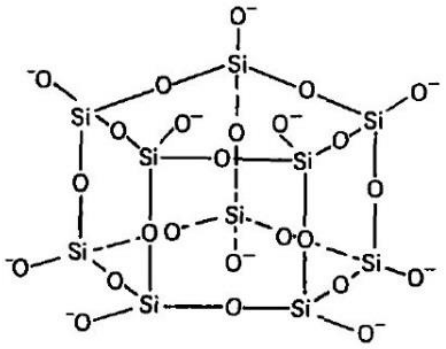

Figure 3.5. Decamer silica anion.

Multiple silicate sources were used for the formation of this product. While TEOS was determined to be the preferred precursor due to its ability to more quickly achieve a homogeneous solution, solid silica gel was also used with some success both experimentally and in literature. As noted above, several procedures from literature were utilized; some reactions were able to more closely replicate the literature while others presented much different results. Table 3.3 gives a summary of the different reactions run including: silicate source, Si concentration, reactants (TBA and Si) ratio, silyation method used, and literature procedures cited. The decamer anion in solution—following the TBA/silicate reaction—was a viscous mixture of highly basic solution containing very soluble anion crystals. Two different methods were employed to silyate the desired crystal material. One method was to slowly add anion solids from a chilled/frozen mixture to the silyating solution, the hypothesis being that undesired water in the solution would melt off from the crystals. To promote the formation of the anions crashing out of solution, ethanol was added to the system to create a water/ethanol mixture that would remain a liquid under freezing conditions while the crystals remained solid. These mixtures were typically ~31% ethanol

(v/v), assuming water represented the remainder of solution. However, because this method only required silyation of the solid portion in this mixture, loss of initial anion content to the liquid portion was probable. Because of this, final product yields were likely lowered. The second method was to add nearly the entire batch of anion solution, ignoring any side reactions with water and trimethylchlorosilane. This second method was also used as a "reverse silyation," where, instead of dropwise addition of the anion to a silyation mixture, the silyation mixture was added dropwise to the anion batch.

Table 3.3. Decamer anion/product synthesis methods used per solution.

Solution #	Silica Source	[Si]	TBA/Si Ratio	Silyation Method	Ref.
1	TEOS	1.11	0.50	Whole solution silyation; [28]	[31]
2	TEOS	1.83	0.50	Whole solution silyation; [28]	[31]
3	TEOS	1.44	0.50	Chilled crystal extraction; [28]; [35]; [36]	[31]
4	TEOS	0.90	0.84	Chilled crystal extraction; [28]	[32]
5	TEOS	0.64	0.70	Chilled crystal extraction; [33]	[33]
6	SiO_2	0.64	0.70	Chilled crystal extraction; [33]	[33]
7	SiO_2	1.00	0.70	Chilled crystal extraction; [33]	[33]
8	SiO_2	1.66	0.70	Chilled crystal extraction; [33]	[33]
9	TEOS	0.59	1.00	Chilled crystal extraction; [33]	[33]
10	TEOS	0.63	0.75	"Cryo" bath reverse silyation; [33]	[33]

Between each of the decamer reaction batches, there were some notable things to point out not mentioned in the chart. For batch #1 only, dimethyl sulfoxide (DMSO) was employed as an organic solvent to the initial mixture to potentially reduce the amount of polymer found in the final product. While this visually appeared to be the case, only an octamer product was obtained from solids. Batch #9 used tetrabutylammonium bromide in order to bring TBA:Si ratio to 1:1 without further addition of water from the TBA hydroxide solution. Because silyation reactions are exothermic, an increase in temperature can have a potential

to polymerize and form larger molecular weight silicate species such as the polymer often seen with the previous decamer reactions [38]. With this in mind, silyation for batch #10 was done in a "cryo" bath of dry ice in acetone. It was also completed using "reverse" silyation, or, adding the silyating mixture with TMCS to the anion instead of vice versa. Over time, the solid mass of anion was partially melted to allow surface reactions to occur.

Batches 1-4 used silyation procedures obtained from literature pertaining to octamer synthesis (still useful for any Si cage silyation), while batches 5-10 used a single literature source containing both the anion and POSS-product procedures. The decamer silyation procedure called for hexamethyldisiloxane (HMDSO) as the organic solvent and added an additional step of reacting with Amberlyst 15 overnight (~16 hours).

Product yields as initially reported by Hoebbel [32] were of mass percents of the various silicate products obtained. Product physical properties (crystalline, polymer, etc.), mass quantities and molar yields obtained are as reported in Table 3.4. Note that only batches 5, 6, 9, and 10 are reported, as these were the only reactions to yield any amount of measurable decamer. Yields were calculated based on the moles of Si, whether the source was TEOS or solid silica gel.

Table 3.4. Decamer/octamer yields from TBA/TEOS mixtures.

Batch #	**Initial Si [mmol]**	**Octamer Yield %**	**Decamer Yield %**
5	22.1	5.96	5.91
6	16.7	2.85	4.38
9	16.7	10.4	3.83
10	9.17	3.81	7.49

The very low yield of decamer product is a crucially limiting factor in further syntheses on a large scale. It should also be noted that the method of separation of the final products likely could use some improvement. Experimentally, it was shown that the octamer trimethyl POSS product was insoluble in ethanol at boiling temperatures, decamer trimethyl POSS was

primarily insoluble in ethanol at room temperature, and remaining polymer products were soluble in ethanol at room temperature. However, there is potential for the octamer product to have a small amount of solubility in boiling ethanol, leading to powder XRD peak shifts/impurities at higher angles as seen in Figure 3.7. Likewise, final polymer products obtained were not transparent as expected. This could potentially mean that, because of the decamer product's high solubility, these crystals are still "trapped" in the polymer phase and require an extended period of time to separate out.

As with the octamer products, proton NMR and powder XRD were used for characterization. Powder XRD was particularly useful in distinguishing between octamer and decamer products based on their crystalline cage structures. Where NMR only showed minimal peak shifts, powder XRD could be compared to single crystal structure data for both trimethyl octamer and decamer POSS products.

Powder XRD peak data from Batch #5—the first to result in a measurable amount of decamer product—was obtained for both the octamer and decamer and compared to standards as shown in Figures 3.6 and 3.7, respectively.

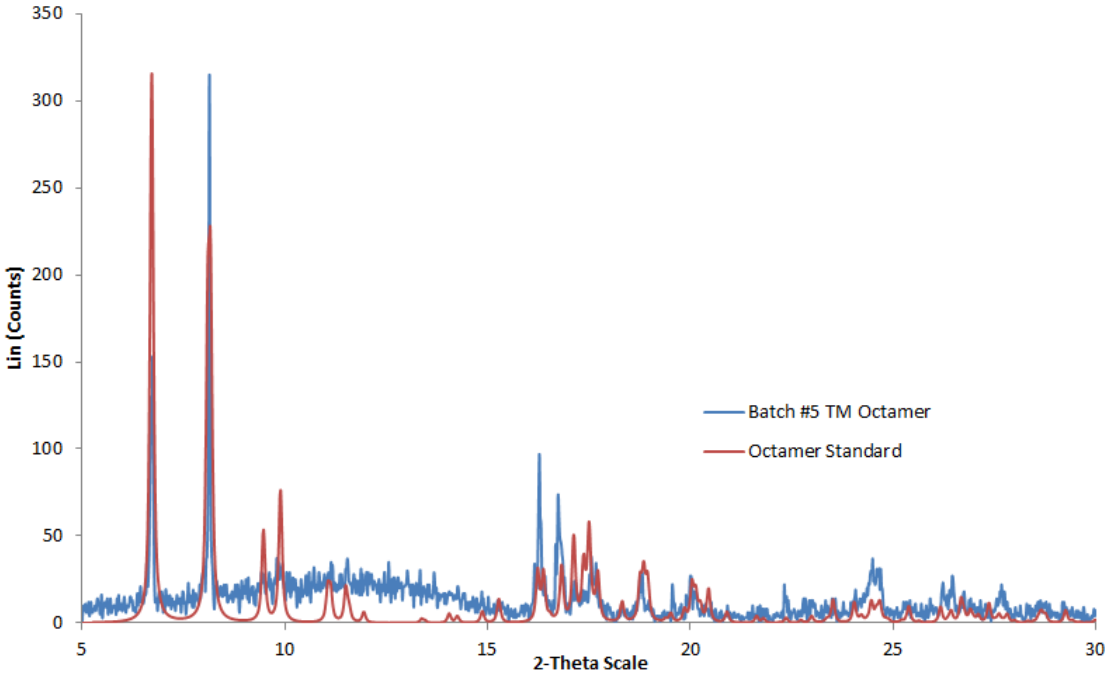

Figure 3.6. Batch #5 trimethyl octamer vs. standard.

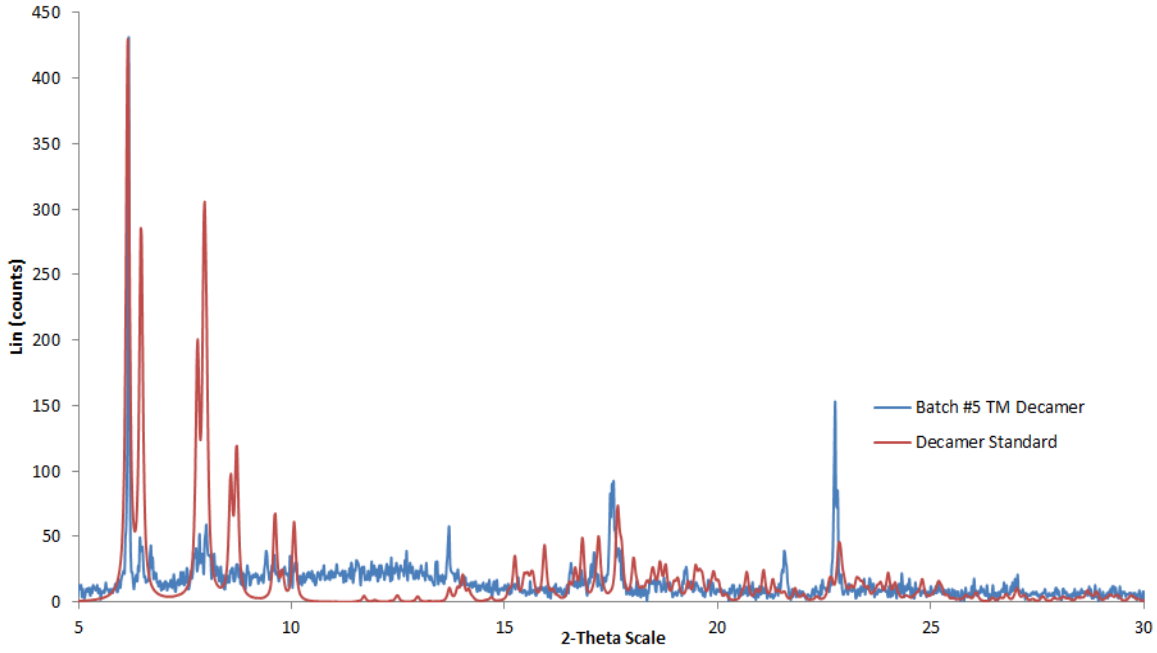

Figure 3.7. Batch #5 trimethyl decamer vs. standard.

Spin Coating

Prior to spin coating, new wafers were rinsed in acetone prior to UVO cleaning. It was later discovered, however, that acetone leaves a small residue. This called for the addition of deionized water and isopropyl alcohol in the rinsing process described in Chapter 2. A brief introduction to ellipsometry was done by investigating the surface of a rinsed and UVO cleaned wafer. Findings resulted in ~5nm SiO_2 film on the surface of the wafer. While this kind of surface was most common pertaining to this research, another method of altering the wafer surface was by silyation. At higher spin speeds, a majority of the POSS product solutions in PGMEA simply did not adhere to the wafer. By silyating the surface of a wafer, hydrophobic species are replaced and moisture removal can occur [39]. Despite these enhanced properties obtained from surface silyation, no difference in spin coating results was observed. Lastly, issues such as resist streaking ("comet" shapes on wafer, some examples of which can be found in Appendix C) were a common occurrence, as these spins were done without the use of a cleanroom environment. Causes of these defects could have

included anything from residual particles blocking the resist flow to rapid drying of portions of the resist.

The first trial runs for spin coating consisted of vinyldimethyl octamer products of 5, 10, and 15% wt. in PGMEA solvent. Following these runs, it was determined that any solution above 5% wt. would be too crystalline to be of value as a photoresist, especially with small feature sizes under EUV. It was also determined through these initial spins (2000rpm) that the issues with adhesion to the wafer in POSS products would require much slower spin speeds (< 1000rpm).

The initial response to solving the crystallinity issue was to mix the vinyldimethyl POSS with a well-known molecular glass resist: calixarenes. Calixarenes are a set of macrocyclic, organic compounds synthesized through the condensation of hyrdroxylated aromatics, such as resorcinol or pyrogallol with an aldehyde to form ring structures similar to that shown in Figure 3.8. Such compounds have been explored as molecular glass resists for EUVL [40]. From previous research, SMPI was made available for use in this research.

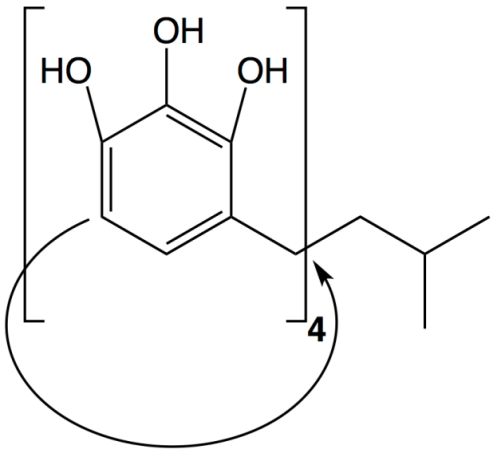

Figure 3.8. SMPI calixarene structure.

When spin coated, the SPMI by itself appeared as a transparent brown/blue film (depending on film thickness/spin speeds). Initial drop tests of 50/50 (by mass) SMPI/vinyldimethyl POSS in PGMEA (5% wt.) showed promising results regarding reduced crystallinity. This mixture was run at the standard spin speeds/settings as described in Chapter 2 for the

PGMEA solvent. The resulting film is as shown in Figure 3.9, as compared to a 5% wt. vinyldimethyl POSS wafer.

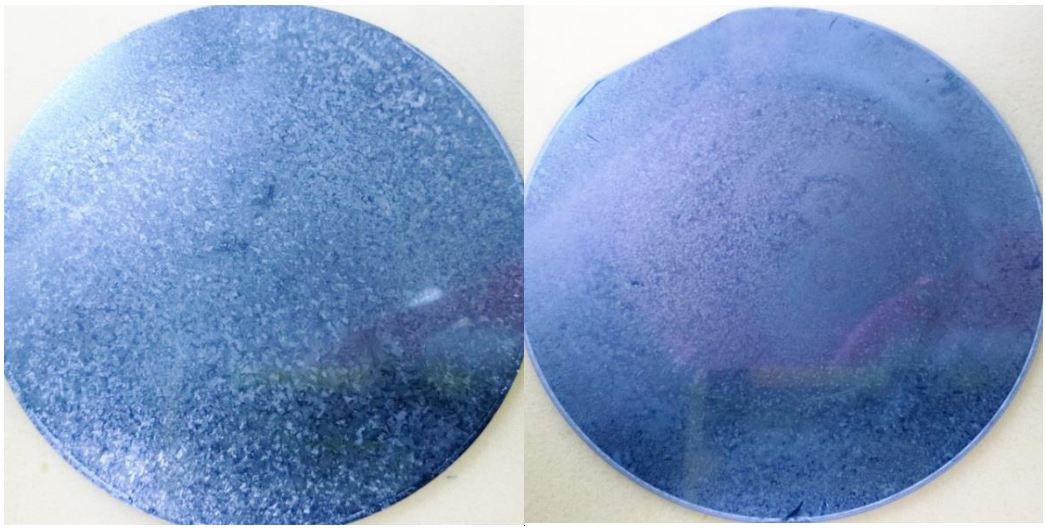

Figure 3.9. 5% wt. vinyldimethyl POSS resist (L) vs. 5% wt. vinyldimethyl/SMPI (R) resist.

While an improvement between the two above films was observed, crystalline features could still be seen in the SMPI mixture. Further magnification of these features is observed in the micrographs of Figure 3.10.

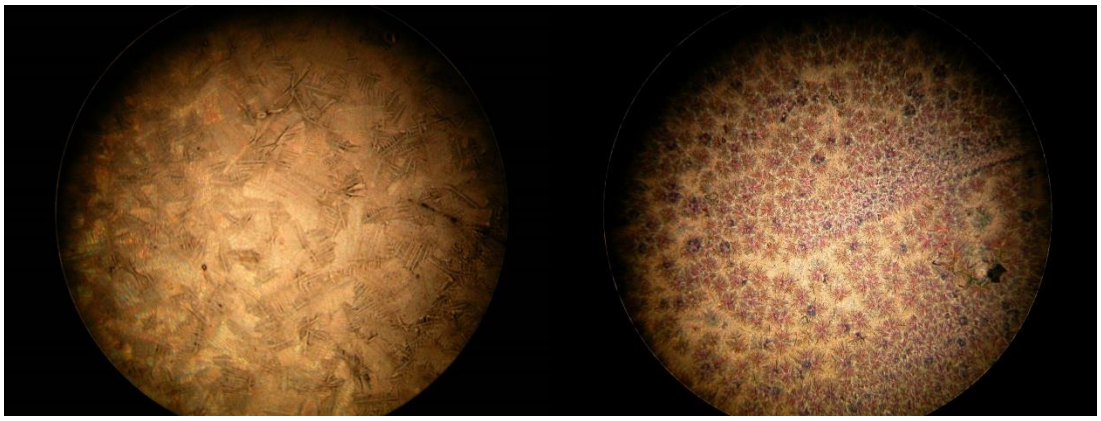

Figure 3.10. Micrographs of vinyldimethyl (L) and vinyldimethyl/SMPI (R) resists.

Following SMPI mixtures, mixed-silyation reactions were proposed as a means to break up crystallinity using asymmetry of corner groups. Unfortunately, the resulting crystalline product from these reactions acted in the same manner as their “pure” POSS counterparts.

Drop tests—where a single drop of solution is allowed to dry on a cleaned Si wafer—were introduced as a good means of determining how a POSS product would spin coat. This was particularly useful for mixed silyation products. As shown in Figure 3.11, the drop test not only showed crystallinity, but it also appeared to display a variety of features and sizes representative of the studied corner groups.

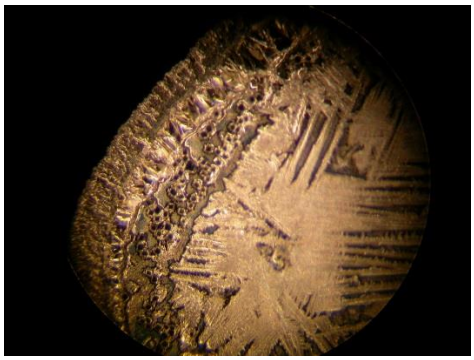

Figure 3.11. Trimethyl/vinyldimethyl/dimethyl/trivinyl mixed POSS drop test.

The next method taken was to try annealing the resist following spin coating. From 45-65°C, no changes occurred in the crystalline film. However, when ramping up the temperature from 65°C, the resist appeared to sublime rapidly as the wafer temperature approached 100°C. Figure 3.12 shows the progression observed during this process.

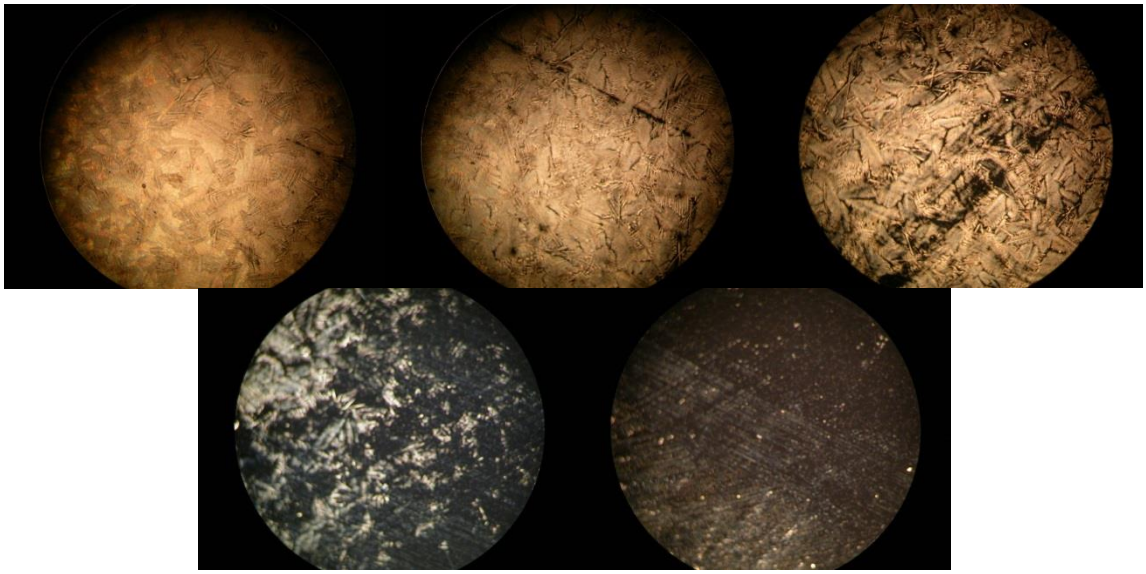

Figure 3.12. 5% wt. vinyldimethyl POSS sublimation progression.

The next proposal for reducing crystallinity was to gradually drop the weight percent and potentially use higher spin speeds at slower accelerations. It was observed that around ~1% wt. and below, films began to exhibit a blue color and smaller crystalline features. Smaller weight percent did show a reduction in crystalline feature size, though still present. Regarding the blue film portion of these resists (Figure 3.13), imaging under SEM was able to reveal the presence of crystallinity not visible under a normal light microscope. Higher spin speeds tended to show a more speckled, random blue film, while slow spin settings showed a more uniform blue film. When examined under a light microscope at an angle, higher spin speed films were visible as a faint blue layer.

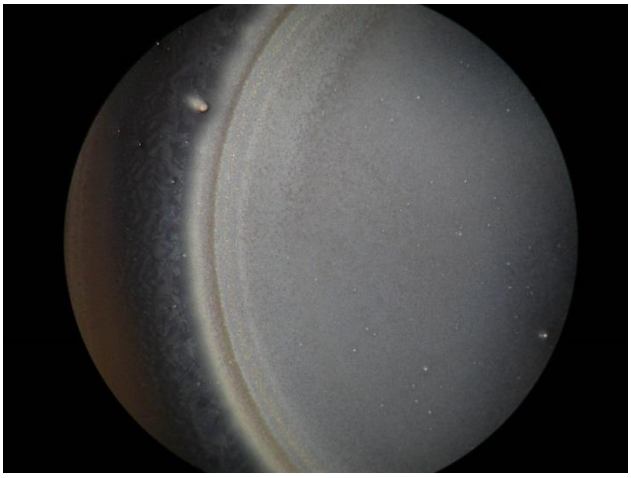

Figure 3.13. Film exhibited at very low weight percent and slow spin speeds.

The long-chain POSS products that resulted in a liquid product following silyation were also tested for spin coating. Even at very high speeds (3000rpm), pure 5-hexenyldimethyl POSS (no solvent) was found to be too oily as a resist, likely containing more disiloxane components than just a liquid POSS product. Additionally, the spin coated resist (unexposed to e-beam) was insoluble in the typical PGMEA developer solution and instead had to be physically scrubbed from the wafer using a Kimwipe and acetone rinse.

Simultaneously working with polyoxometalate (POM) cores appeared to show more promise as a spin-coatable product. By themselves, the POM core products were able to form a uniform, transparent orange or blue film (depending on spin speed/film thickness) during

spin coating. However, due to insolubility in other common spin coating solvents, a low boiling solvent such as MEK was needed to successfully dissolve and spin coat the POM core resists. While creating a more uniform coat, MEK had an issue to be discussed shortly.

MEK was also used to spin coat the trimethyl POSS decamer product (insoluble in PGMEA). Low boiling solvents in general appeared to reduce crystal feature sizes, allow for more rapid acceleration and spin speeds to reduce film thickness, and in some cases, allowed for better POSS resist adherence to the Si substrates. The improved film adherence was likely due to the rapid drying observed during spin coating. With MEK, the decamer resist showed great adhesion to the substrate, while nothing stuck to the substrate when using a solvent such as MIBK.

Mixtures of the POM core and POSS products were also examined using MEK as a solvent. These mixtures included vinyldimethyl POSS/2,6-dimethyl hexamolybdate (2% wt.; 50/50 m/m) and vinyldimethyl-trivinyl POSS/2,6-dimethyl hexamolybdate (2% wt.; 50/50 m/m). Despite a much more uniform looking resist, a vacuum chuck mark appeared (Figure 3.14) on all wafers that used MEK as a resist solvent. Additionally, crystalline features still show up under SEM when using spin coated POSS/POM product mixtures.

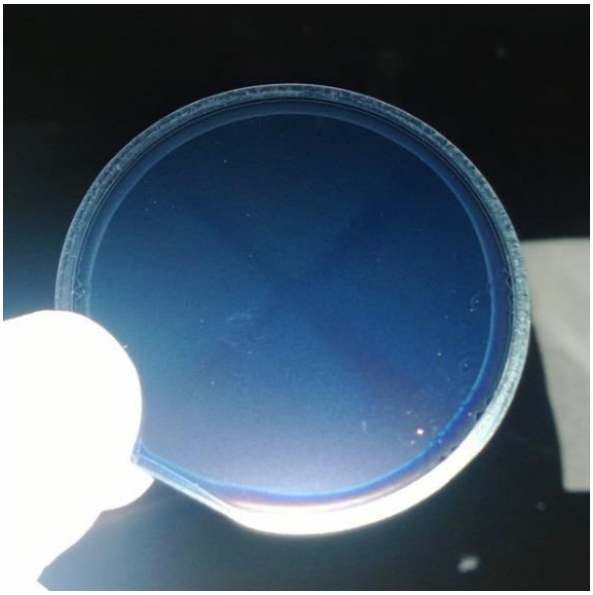

Figure 3.14. Vacuum chuck mark on POSS/POM wafer with MEK solvent.

Lithography

Though the development of these resists was ultimately to be studied with EUVL, E-beam lithography was available and implemented as a proxy during this project. Despite the issue with crystalline POSS resists, studying the lithography side of this project was important in understanding the capabilities of hybrid NBBs with several functional groups. Through E-beam lithography, two important characteristics such as sensitivity and contrast could be determined for the studied POSS films. Sensitivity for a negative photoresist is defined as the dosage that results in more than half of the resist thickness remaining following development (fully developed for positive resists; i.e. no remaining thickness) [41]. Contrast is determined by exposing a resist to a series of exposure doses. Following development, the normalized remaining thicknesses of each exposure are plotted against the exposure doses (logarithmic scale). The resulting plot is called a contrast curve of the photoresist (as seen later in Figure 3.19). The slope of the linear portion of this development curve is defined as the contrast (γ) of a resist, which can also be defined by the following equation.

$$\gamma = \frac{1}{\log(^{D_1}/_{D_0})} \tag{3.1}$$

Where D_0 is the lowest exposure dose at the initial electron/photon-resist interaction and D_1 is the dose required to "fully develop" the photoresist; both based on the determined linear section of the curve. Depending on the resolution of a particular resist and how the linear portion of a contrast curve is interpreted graphically, contrast values can vary slightly. A contrast curve comparing the octamer vinyldimethyl POSS, trivinyl POSS, and a standard SU-8 2010 E-beam resist was obtained and is described later in this section.

Initially, a 5% wt. vinyldimethyl POSS resist was used to test out how this resist would interact with an electron beam. A "test area" on this wafer showed good sensitivity at random doses; another section containing an array of exposures from 1000-3500 μC/cm^2 visually showed full crosslinking when compared to the initial resist.

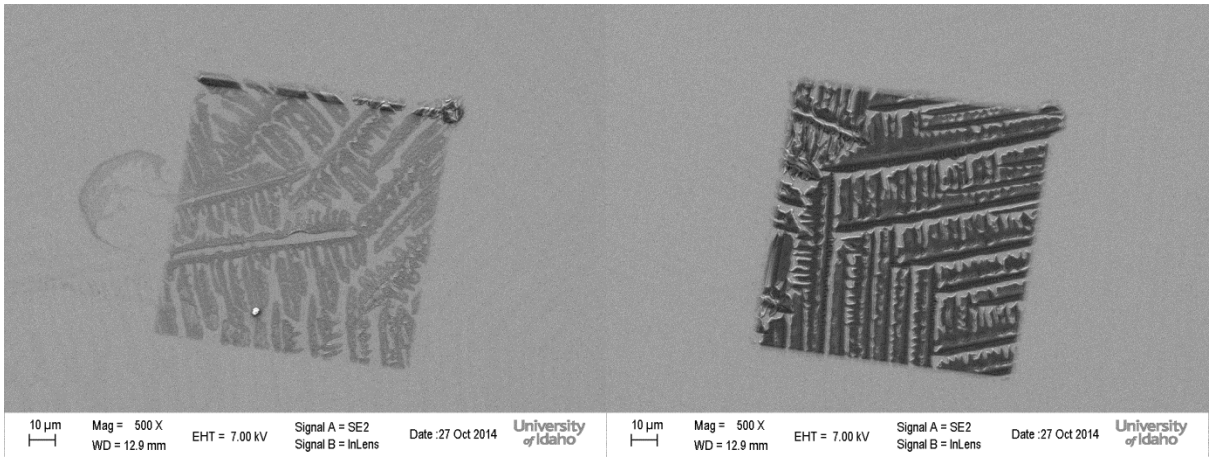

Figure 3.15. 5% wt. vinyldimethyl POSS exposures under SEM (1 and 50µC/cm^2).

The next set of resists exposed were done at doses of 1-2000 µC/cm^2 included vinyldimethyl POSS (5% wt.; Figure 3.15) and trivinyl POSS (4% wt.). Examining these arrays under a light microscope (Figures 3.16, 17) visibly showed a crosslinking progression between 1 and 100 µC/cm^2.

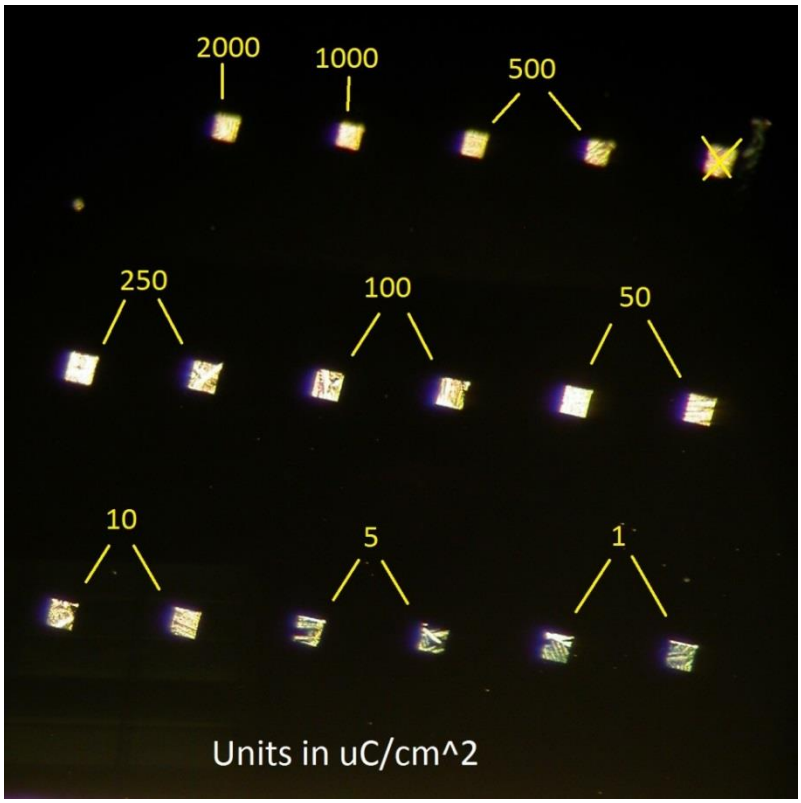

Figure 3.16. Vinyldimethyl POSS (5% wt.) exposures viewed under light microscope.

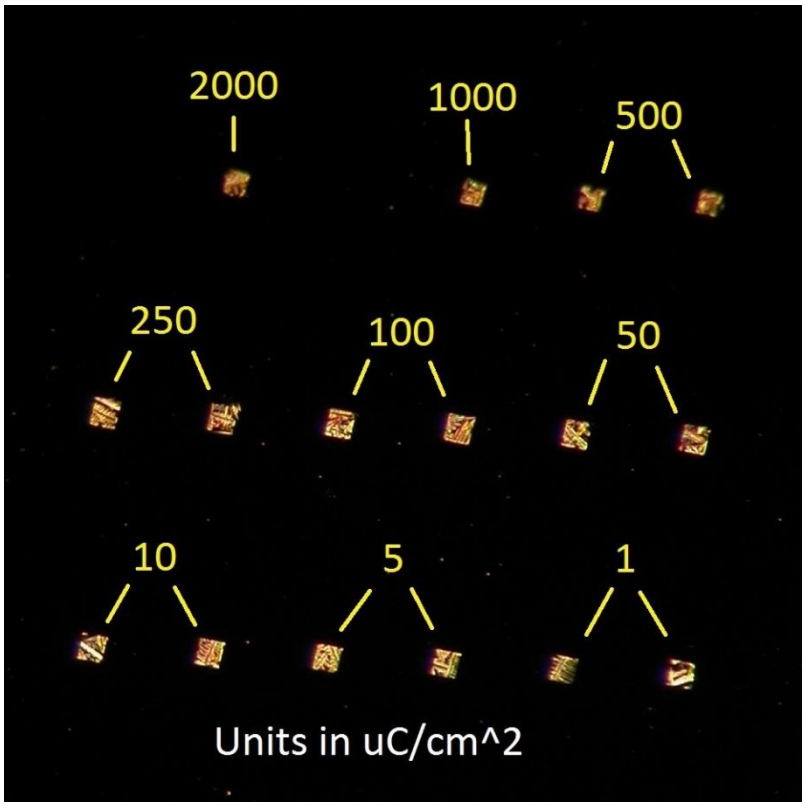

Figure 3.17. Trivinyl POSS (4% wt.) exposures viewed under light microscope.

Following these exposures, E-beam doses were even further fine-tuned. 5% wt. vinyldimethyl POSS (0.01-10 μC/cm^2) and 2% wt. trivinyl POSS (0.1-100 μC/cm^2) were examined (note the decreasing % wt. for trivinyl POSS between resists; this was due limiting supplies of an expensive precursor as research progressed). Additionally, larger areas were exposed to more easily cleave the wafers for cross-sectional imaging. For both of these resists, an exposure dose of 0.5 μC/cm^2 appeared to be the minimum dose that initiated cross-linking in the films. With these films, cross section images were taken under SEM in an effort to form a contrast curve plot. Due to the limited resolution of the SEM, cross sections perpendicular to the electron beam were difficult to completely decipher, therefore, the SEM sample stage was tilted 1° for improved imaging (5° for very low % wt. films). When taking these measurements, it was observed that the vinyldimethyl POSS resist had larger crystalline/ non-uniform clustering and thus, a much poorer resolution when compared to trivinyl POSS resists. Figure 3.18 shows a progression of cross-linking in the trivinyl POSS (2%

wt.) resist as exposure dose is increased. Also to note, while developing these curves, a portion of the wafers was cleaved and an initial, unexposed thickness was measured.

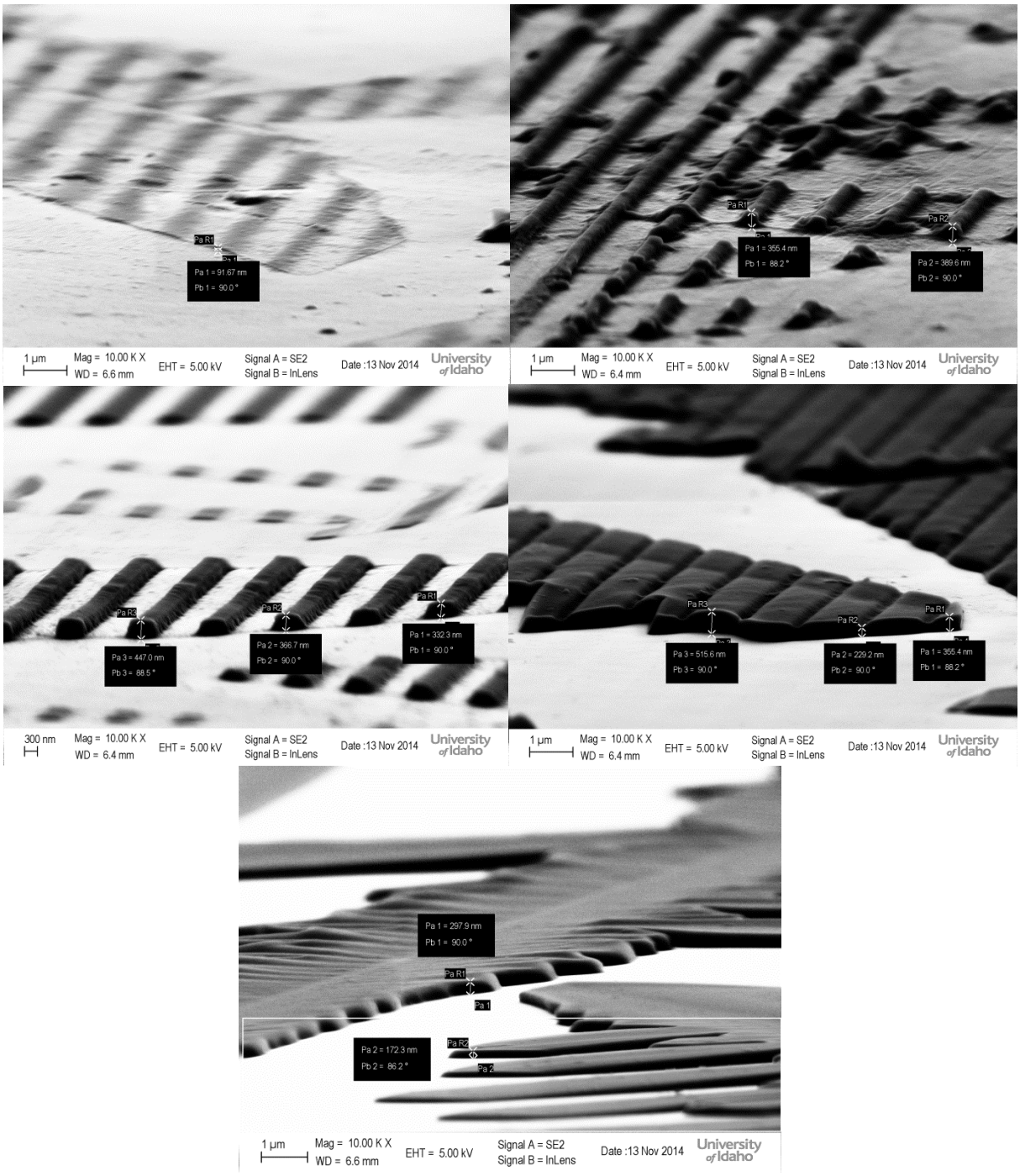

Figure 3.18. Trivinyl POSS (2% wt.) cross-linking progression with increasing exposure dose.

Also measured for contrast curves (0.1-1000 μC/cm^2 doses) was a very thin (0.05% wt.) trivinyl POSS resist (slow spin coat). Due to the low resolution of the SEM and scarcity of measureable material on this wafer, the cross-sectional imaging was done at a stage tilt of 5°. Despite the somewhat lack of material, this very low % wt. film appeared to show the best contrast when compared to more highly solid concentrated resists.

For a comparison, SU-8 2010, a common e-beam resist, was used as a standard reference material. SU-8 is a chemically amplified resist well-known for its durability and high sensitivity [42, 43]. As a more viscous resist than those with a PGMEA solvent, SU-8 2010 gave a much thicker and uniform resist that was easy to identify and image. Exposures were done in the range of 0.1-1000 μC/cm^2. To stay consistent with the POSS resists regarding post-exposure procedures, a post-exposure bake was not done with the first SU-8 wafer. Development revealed optical exposures as low as 0.5 and 1 μC/cm^2, although these exposures did not adhere to the substrate during development. At exposures of 5-1000 μC/cm^2, successful development was achieved. In addition to the non-PEB SU-8 wafer, a PEB wafer was made under the same exposure conditions. Using the same methods as outlined by Microchem [44], however, did not result in what was expected. Rather, the entirety of the photoresist (unexposed regions included) appeared to bake to the substrate and standard development solvent was unable to remove the majority of the unexposed portion of photoresist. This process was repeated and the same issue came about, thus, contrast curved of a PEB SU-8 wafer was not used to compare to POSS resists.

Due to significant non-uniformity exhibited in some of the POSS films, the method of film thickness determination called for several different measurements to be taken at various points on each of these films. An average of these measurements was used in order to develop a rough contrast curve for the given resists. While prone to user error in measurements and potentially not encompassing the entirety of each exposure, this method was preferred to ellipsometry measurements. The main reason for this, again, was the non-uniformity exhibited by films with such crystallinity. Typically, ellipsometry produces optimal results when homogenous films with well-defined layers are observed. Also, to date, no

ellipsometry modelling data appears to have been made for the POSS products studied within this research project. Though the SU-8 2010 resist formed a uniform and well-defined film, the exposures were measured similarly to the POSS materials so as to remain consistent to the measurement techniques used. All thickness measurements were normalized based on the initial thickness measurements of each resist. Once SEM measurement data was compiled, the contrast curve in Figure 3.19 was formed.

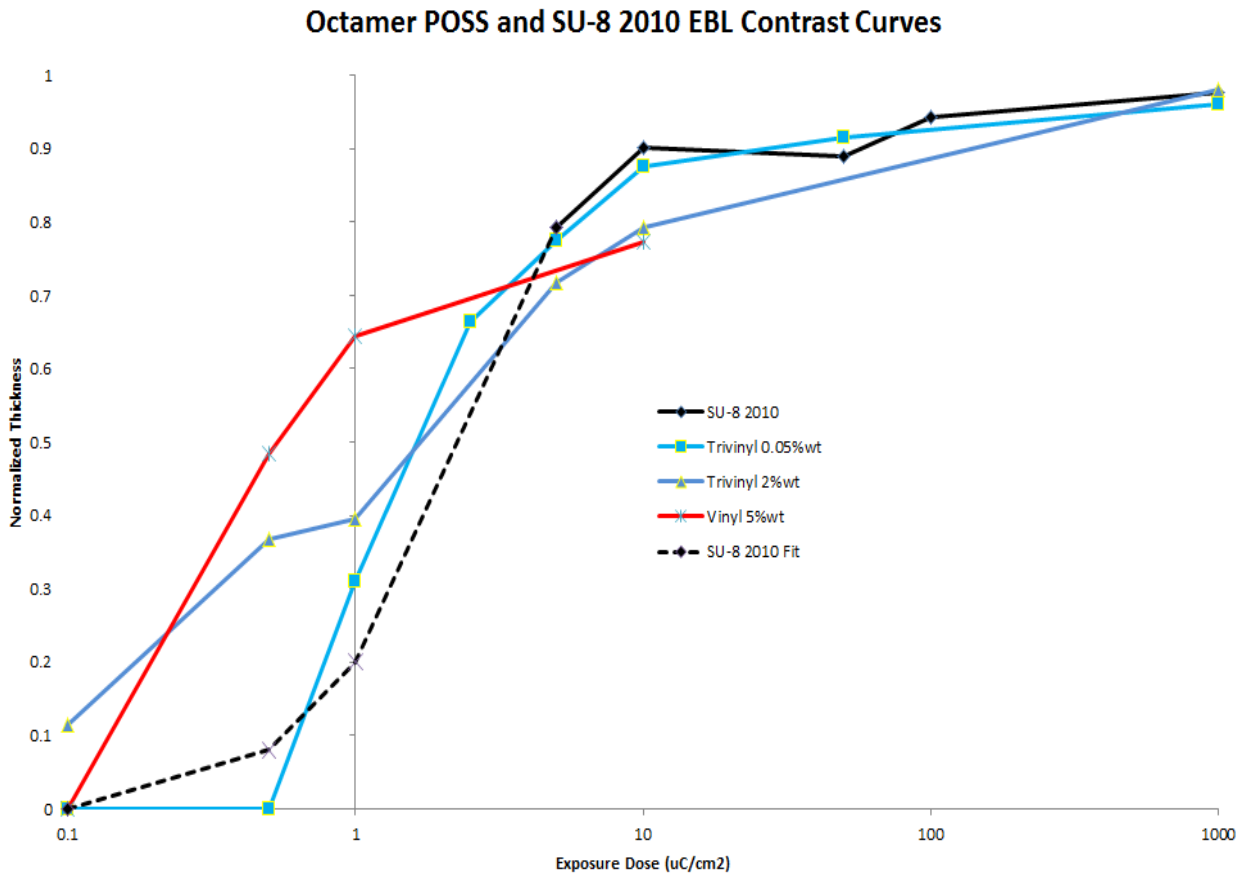

Figure 3.19. Octamer POSS and SU-8 2010 contrast curve.

For the SU-8 standard, note the dotted line between doses of 0.1 and 5 $\mu C/cm^2$. This extrapolation of data was made due to the fact that cross-linking of the resist occurred at 0.5 and 1 $\mu C/cm^2$ and was seen during development, but these exposures did not adhere to the wafer for cross-sectional measurement. Despite the use of an unconventional form of resist thickness measurement, it is clear to see that each of the resists acted as expected as the

exposure doses increased. From this plot and using the definitions described above for sensitivity and contrast of a negative resist, these values were obtained and are as shown in Table 3.5. Because the linear portions on these curves may seem vague in some cases, contrast may differ depending on how this line is determined. The results reported in Table 3.5 are obtained from the "best" calculated contrast. More information on how these values were found is shown in Appendix E.

Table 3.5. Contrast and sensitivity of studied photoresists.

Resist	**Sensitivity [μC/cm^2]**	**Contrast [γ]**
SU-8 2010	2.20	0.876
Trivinyl POSS (0.05%)	1.50	0.975
Trivinyl POSS (2%)	1.60	0.454
Vinyldimethyl POSS (5%)	0.53	0.684

As a chemically amplified resist, SU-8 is meant to have a high sensitivity under e-beam. Because of this, it was encouraging to see that the multiple functional groups for each POSS product acted as expected (heavy amounts of cross-linking) and resulted in a high sensitivity. While backscattering electrons may potentially lead to poor LER and overall resolution for highly sensitive resists within e-beam lithography, a high sensitivity is a characteristic is desirable for translation to EUVL.

Though potentially due to the crystalline nature and/or measurement techniques used, the poor contrast values for a majority of the POSS resists leaves room for much improvement. Despite the fact that many other resists can attain higher contrast values under e-beam, SU-8 has still been noted for its high aspect ratio and vertical sidewall capabilities in thick films. This consideration, when comparing 0.05% wt. trivinyl POSS contrast to SU-8 2010, shows the lone positive result for POSS resist contrast. Figure 3.20 gives a rough schematic of how the sidewalls would theoretically form in both high and low contrast resists.

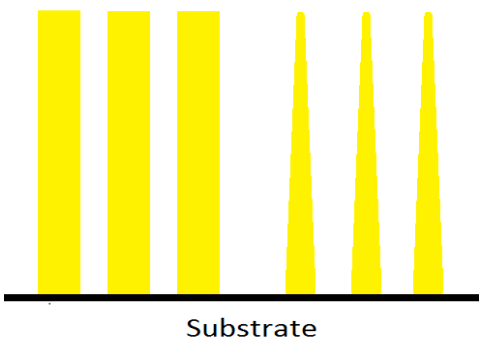

Figure 3.20. High contrast resist (L) vs. low contrast resist (R) sidewalls.

Additionally, Figure 3.21 shows an example SEM image obtained for the SU-8 2010 sidewall, a much more defined wall than what is seen in the POSS exposures.

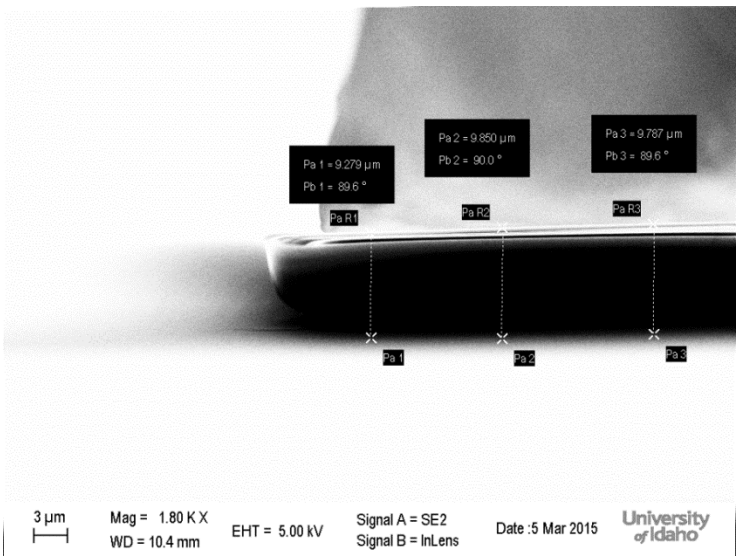

Figure 3.21. SU-8 2010 exposure cross-section.

When compared to the "sidewalls" of the trivinyl POSS development in Figure 3.18, a difference in line edge is observed. In the above SU-8 2010 figure, the sidewall does appear to curve inward near the film/substrate interface. One possible explanation for this is the effect that CAR materials have on final film resolution and LER from photoacid generation. However, more plausible explanations could be the possible lifting of the exposure during the development process or even an effect of the electron beam-sample interaction volume. Though the sidewalls don't appear vertical in Figure 3.18 and the contrast resulted in low

values, the progression during increased exposure doses simply appears to be a “rebuilding” of the crystalline structure. Rather than have a sizeable LER as Figure 3.21 appears to, the POSS products appear to be simply returning to their initial crystalline structures with little noticeable LER effects. Again, these observations were made simply by inspecting SEM images to roughly compare a standard CAR e-beam resist to the stability of novel POSS resists.

In addition to the POSS contrast curves above, mixtures of POSS and POM resists were exposed under e-beam. While unable to polymerize under e-beam as a standalone resist—at its current status in the synthesis stage—all of the studied POM resists were found to be excellent candidates for uniform spin-coating as described in the Spin Coating section above. Though by this time crystalline features were expected for any POSS-containing mixture, POM mixtures were able to bring POSS resists one step closer to a desirable amorphous nature (seen in Figure 3.14). The mixture of 2% wt. (50/50 m/m) vinyldimethyl/trivinyl and monoimide hexamolybdate was exposed under e-beam at doses of 0.1-1000μC/cm^2 (Figure 3.22).

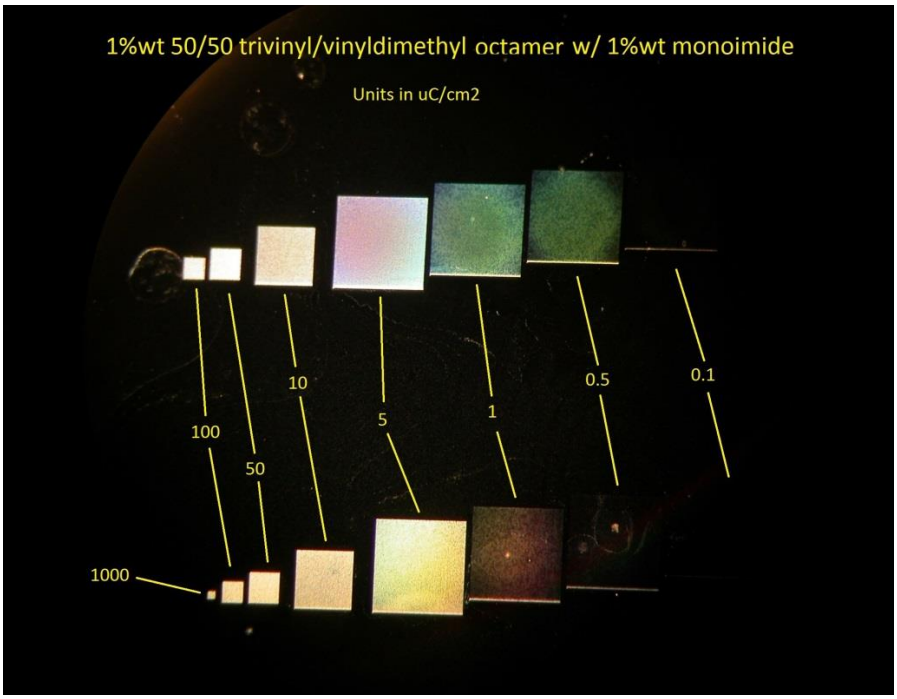

Figure 3.22. POSS/POM mixed resist exposures under light microscope.

Unlike the development “lines” seen at very high magnifications in Figure 3.18, there appeared to be the formation of “crater-like” features that appeared to fill in with increasing dosages, though never completely (Figure 3.23, note the images appear flipped here. This was due to the orientation of the SEM sample stage). These lines do begin to appear at smaller magnifications. In an effort to form a more uniform resist, this wafer was heated to fill in the gaps. Additional observation following this revealed that heating the wafer had no effect on the overall uniformity of the mixed resist.

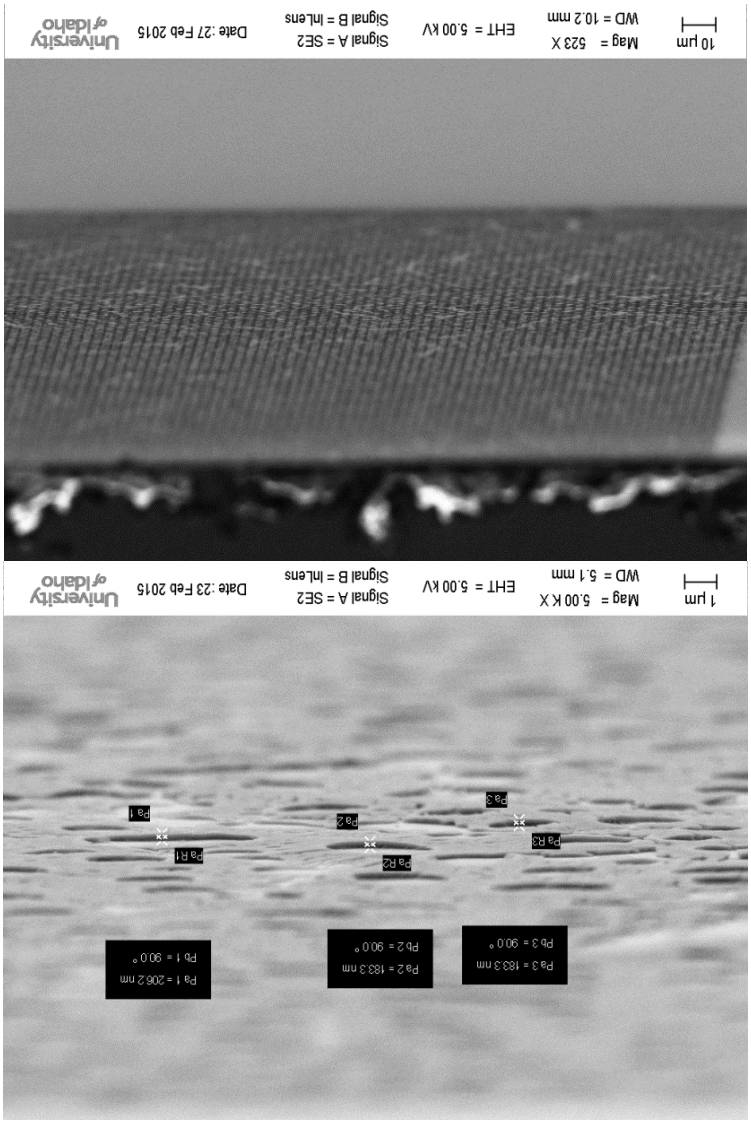

Figure 3.23. Low (top) and high (bottom) magnifications of POSS/POM exposures.

While too crystalline in their current state, POSS resists do show promise in regards to certain characteristics. Whether modifications discovered with further research can make POSS materials viable EUVL resists, or the positive findings can be used as a model for future hybrid materials development, there were many takeaways obtained during this research process. A number of things must still be looked at for future improvement of EUVL technology and photoresists. Chapter 4 discusses a number of options and steps to lead this particular research to the next level.

Chapter 4: Conclusions and Recommendations

SSQ Capabilities

At the start of this research project, there were a few major goals set out to accomplish: synthesize and characterize novel hybrid silsesquioxane materials, develop successful spin coating parameters and e-beam proxy steps, and characterize the novel resists using EUVL facilities of industry partners. POSS hybrid materials with trimethyl and dimethyl corner groups were successfully synthesized according to literature. These procedures were then used to synthesize POSS materials containing corner groups with organic functionality such as vinyldimethyl and trivinyl. These functional POSS products were then spin coated onto Si wafers, where crystalline films proved to be a major issue. When EUVL technology is seeking to push feature sizes to the sub-10 nm level and beyond, micron-sized crystal features in a non-uniform photoresist present a major obstacle. Regardless of this obvious drawback described throughout this paper, these films were then tested to determine the capabilities of crosslinking up to 8 polymerizable corner groups per macromolecule under e-beam. These initial proxies were a good measure of both the limits and capabilities of the studied POSS resists. Results from this—compared to SU-8 2010 (standard e-beam resist)—showed very promising sensitivity for a non-chemically amplified resist.

Because of the crystalline film issue, the POSS resists studied in this research were often compared to hydrogen silsesquioxane (HSQ) due to their somewhat similar structure. HSQ has been heavily studied in literature as a well-known high resolution, high contrast e-beam resist [24-26]. Despite its encouraging properties under e-beam (albeit at a high cost), HSQ has a very low sensitivity and poor long-term stability [45]. Because a highly sensitive resist with superb contrast doesn't exist (due to electron/photon shot noise), tradeoffs often must be made between the varying characteristics. While both HSQ and the novel POSS resists show excellent etch resistance due to a high-Z core, a higher sensitivity is likely a much more desirable trait for high volume manufacturing, given that low power output is one of the top challenges for EUV sources today.

Given its major drawbacks as a resist for EUVL, it was easy to overlook the positive characteristics found in the POSS films, especially the high sensitivity. While actual EUV exposures need to be made to more directly determine certain resist characteristics such as off-gassing, resolution, and etch parameters, e-beam proxies can have a good input on important resist features like contrast and sensitivity when moving forward with novel hybrid materials for EUVL.

E-Beam/EUV Correlation

E-beam data can be very useful and is generally a more widely available research tool for studying photoresists, especially in a University setting. However, e-beam comparisons to other forms of lithography remain important and non-trivial task. Other than obtaining resist characteristics directly from EUVL, a correlation between e-beam lithography and EUVL must be better understood. To start, Table 4.1 [46] provides a quick glance of the energies and wavelengths associated with EUV and e-beam lithography, including the current generation ArF immersion technology.

Table 4.1. Lithography technology energies and wavelengths.

Lithography	Energy (eV)	Wavelength
ArF	6.4	193 nm
EUV	92	13.5 nm
E-beam	20,000 (adjustable)	5.5 pm

While currently under heavy research as another option for next-generation lithography (multi-beam technology), e-beam primarily functions as a single beam of electrons focused by a series of lenses and beam deflectors used as a direct-write method for research in lithography. EUVL systems generally comprise of several mirrors that function as

illumination and projection optics. A reflective photomask is also used for patterning on the photoresist. Figure 4.1 shows some general schematics for each of these systems.

Exposure doses in e-beam lithography are typically measured as a current of electrons interacting with the resist per area ($\mu C/cm^2$), whereas EUV doses are recorded as a measure of the photon energy interaction per area of photoresist (mJ/cm^2). Significant differences can clearly arise when shifting between e-beam to EUVL, both in source and instrumentation setup.

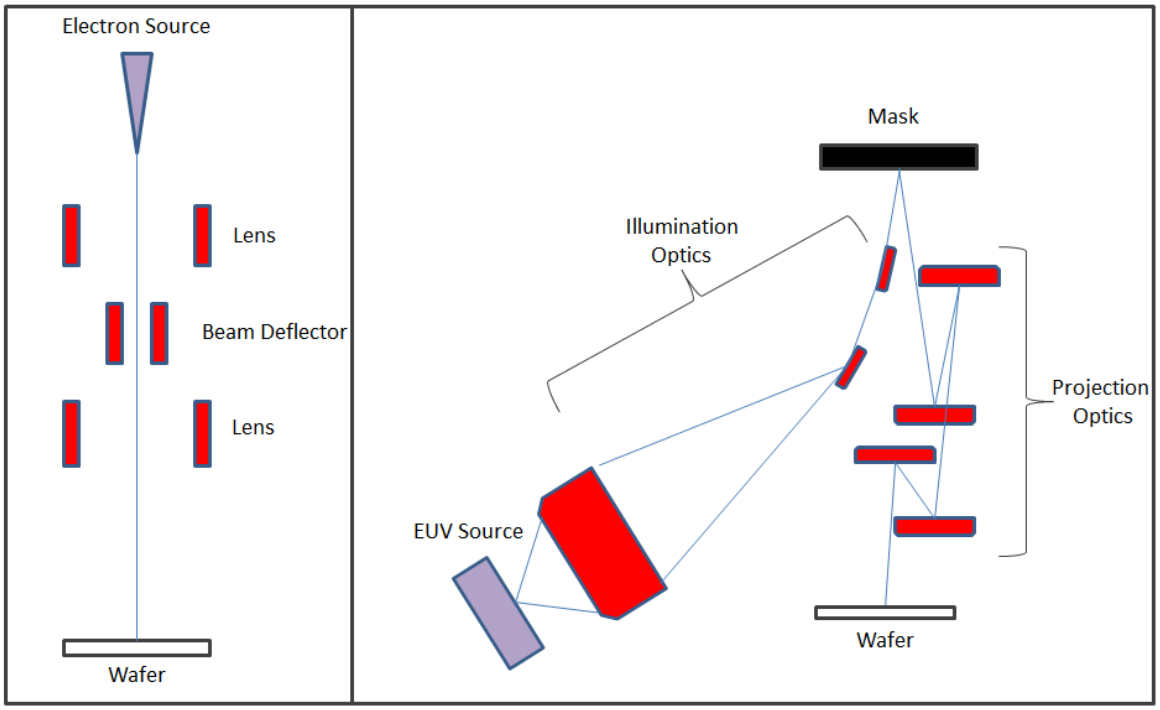

Figure 4.1. E-beam lithography (L) and EUVL (R) system schematics.

Ultimately, a good correlation between e-beam and EUVL is heavily dependent on what resist is used. While some research groups stated very good correlations for doses and outgassing between e-beam and EUVL [47-49], predicting behavior will most often be a non-trivial task. Given a variation of photoacid generating resists, Bozano, et al. [49] found both good correlations (simple multiplication factors; i.e. 1 mJ/cm^2 EUV= 10 $\mu C/cm^2$ e-beam) as well as random behavior prediction showing no correlation whatsoever. To simplify these comparisons and return to a familiar resist, HSQ—as a commonly studied negative resist for

both EUVL and e-beam—can be focused on. Based on the small collection of literature obtained, several factors could affect the outcome of resist sensitivities and contrast. These included resist thickness, resist concentration, development conditions (developer/temperature), accelerating voltage (e-beam), targeted feature size, and instruments/setups used [24, 50-52]. Table 4.2 gives a very simplified idea of how contrast and sensitivity may vary between EUV and e-beam for HSQ resists.

Table 4.2. Contrast and sensitivity for HSQ resists.

Lithography	**Sensitivity**	**Contrast**	**Experimental Adjustment**	**Ref.**
E-beam (10 keV)	750-1250 ($\mu C/cm^2$)	3.0-10.0	Development; Film Thickness	[24]
E-beam (100 keV)	311-637 ($\mu C/cm^2$)	2.7-9.7	Film Thickness	[50]
EUVL	21.0-23.7 (mJ/cm^2)	5.6-15.1	Development	[51]
EUVL	73.8 (mJ/cm^2)	11.8	N/A	[52]

While these references as a whole lack an experimental control between them, they can give some insight for comparisons between HSQ and novel POSS materials due to the structural similarities. There are only roughly 6.8 EUV photons per square nanometer at an exposure energy of 10 mJ/cm^2 (3.4 for 5 mJ/cm^2) [53, 54]. Approximately the same amount of electrons was calculated for an exposure dose of 100 $\mu C/cm^2$ (6.24 e^-/nm^2). Thus, the tradeoff from HSQ to the highly sensitive POSS resists studied seems appealing when shifting to EUVL. The e-beam data obtained through experimentation for the novel POSS materials compared to the above values for HSQ show a vast improvement for resist sensitivity. Because of this, it would be anticipated that novel hybrid materials with multiple functional groups appear to be a likely candidate to meet the targeted sensitivity requirements (<5 mJ/cm^2; [55]) for high volume production.

Future Work

Regarding the continued work in finding a way to make POSS materials a suitable photoresist, the solutions seem to be limited given the research described above. Other than finding the "perfect" mixture of amorphous photoresist with POSS materials or having the ability to trap a POSS resist in a glassy, amorphous state during spin coating, focus must be shifted to other proposed hybrid materials. This brings about the continued research of POM resist synthesis and characterization. It was already shown in this research that POM resists serve as a much better spin coating candidate, especially once a solvent more reliable than MEK is obtained.

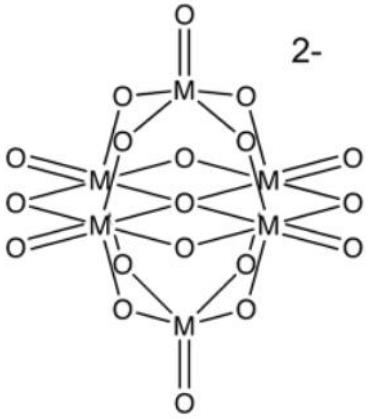

Figure 4.2. Polyoxometalate anion.

In its current state, the POM resists do not have enough attached functional groups for cross-linking under e-beam exposure. Efforts to increase the amount of functional groups to 2+ per macromolecule are in progress until feasible cross-linking is observed under e-beam. Additional functional groups (up to 8 to match the POSS octamer) would be expected to further the sensitivity of the POM resists and allow for a more suitable resist for EUVL technology. Because more uniform resists would be anticipated in these POM materials, more efforts could be devoted to ellipsometry and film modeling for more accurate and consistent film thickness measurements. Finally, characterization at NIST and other industry partners with EUVL facilities can be accomplished. Properties such as off-gassing, resist dissolution, and swelling during development can be obtained. Additionally, line edge

roughness, sensitivity, and contrast can also be found in determining optimum etch parameters for EUVL.

References

1. Thompson, Scott E., and Srivatsan Parthasarathy. “Moore’s Law: The Future of Si Microelectronics. “*Materials Today* 9.6 (2006): 20-25.
2. Willson, Grant, and Bernard J. Roman. "The Future of Lithography: SEMATECH Litho Forum 2008." *ACS Nano* 2.7 (2008): 1323-328.
3. Gatlin, Gregory S.; et al. "Process Development of Electron Beam Lithography in an Academic Environment." *IEEE* (2004): 117-19.
4. Andreas, Erdmann; et al. "Optical and EUV Projection Lithography: A Computational View." *Microelectronic Engineering* 132 (2015): 21-34.
5. Borkar, S. “*Design Challenges for Gigascale Integration.*” 2004.
6. Freund, L. B., and S. Suresh. *Thin Film Materials: Stress, Defect Formation and Surface Evolution*. New York: Cambridge UP, 2003, p. 48-50.
7. Georgia Tech ECE. *“Photolithography.”* 2015.
8. Ronse, Kurt. “Optical Lithography—a Historical Perspective.” *C.R. Physique* 7 (2006): 844-57.
9. Solak, Harun H.; et al. "Photon-beam Lithography Reaches 12.5nm Half-pitch Resolution." *Journal of Vacuum Science and Technology B* 25.1 (2007): 91-95.
10. Wu, Banqiu, and Ajay Kumar. "Extreme Ultraviolet Lithography: A Review." *Journal of Vacuum Science and Technology B* 25.6 (2007): 1743-761.
11. Mertens, B. M.; et al. "Mitigation of Surface Contamination from Resist Outgassing in EUV Lithography." *Microelectronic Engineering* 53 (2000): 659-62.
12. Mertens, Bas; et al. “Progress in EUV Optics Lifetime Expectations.” *Microelectronic Engineering* 73-74 (2004): 16-22.
13. Namatsu, Hideo; et al. "Supercritical Drying for Nanostructure Fabrication without Pattern Collapse." *Microelectronic Engineering* 46 (1999): 129-32.
14. Mortini, Benedicte. “Photosensitive Resists for Optical Lithography.” *C.R. Physique* 7 (2006) 924-30.
15. Ito, Hiroshi, Carlton G. Wilson, and Jean M. Frechet. “Positive- and Negative-working Resist Compositions with Acid Generating Photoinitiator and Polymer with Acid

Labile Groups Pendant from Polymer Backbone.” International Business Machines Corporation, assignee. Patent 4491628, 1985.

16. Meagley, Robert P., Michael D. Goodner, Bob E. Leet, and Michael L. McSwiney. “Pixelated Photoresists.” Intel Corporation, assignee. Patent 8003293 B2, 2011.
17. Van Steenwinckel, David; et al. "Resist Effects at Small Pitches." *Journal of Vacuum Science and Technology B* 24.1 (2006): 316-20.
18. *International Technology Roadmap for Semiconductors*. 2011.
19. Carraro, Mauro, and Silvia Gross. “Hybrid Materials Based on the Embedding of Organically Modified Transition Metal Oxoclusters or Polyoxometalates into Polymers for Functional Applications: A Review.” *Materials* 7 (2014): 3956-3989.
20. Harrison, Philip G. "Silicate Cages: Precursors to New Materials." *Journal of Organometallic Chemistry* 542 (1997): 141-83.
21. Babin, S.; et al. "Comparative Study of the Characteristics of Octavinylsilsesquioxane Dry Resist in Ultraviolet, Electron-beam and X-ray Exposure." *Microelectronic Engineering* 35 (1997): 129-32.
22. Nealey, Paul F.; et al. "Pixelated Chemically Amplified Resists: Investigation of Material Structure on the Spatial Distribution of Photoacids and Line Edge Roughness." *Journal of Vacuum Science and Technology B* 25.6 (2007): 2508-513.
23. Kang, Huiman; et al. "Control of the Critical Dimensions and Line Edge Roughness with Pre-organized Block Copolymer Pixelated Photoresists." *Journal of Vacuum Science and Technology B* 27.6 (2009): 2993-2997.
24. Berggren, Karl K.; et al. "Understanding of Hydrogen Silsesquioxane Electron Resist for Sub-5-nm-half-pitch Lithography." *Journal of Vacuum Science and Technology B* 27.6 (2009): 2622-627.
25. Mollard, L.; et al. "HSQ Hybrid Lithography for 20nm CMOS Devices Development." *Microelectronic Engineering* 61 (2002): 755-61.
26. Georgiev, Y. M.; et al. "Surface Roughness of Hydrogen Silsesquioxane as a Negative Tone Electron Beam Resist." *Vacuum* 77 (2005): 117-23.

27. Fullmer, Gregory R.; et al. "NMR Chemical Shifts of Trace Impurities: Common Laboratory Solvents, Organics, and Gases in Deuterated Solvents Relevant to the Organometallic Chemist." *Organometallics* 29 (2010): 2176-179.
28. Hasegawa, Isao; et al. "An Improved Procedure for Syntheses of Silyl Derivatives of the Cubeoctameric Silicate Anion." *Applied Organometallic Chemistry* 17 (2003): 287-90.
29. Matisons, Jani G.; et al. "Silsesquioxanes: Part I: A Key Intermediate in the Building of Molecular Composite Materials." *Journal of Organometallic Chemistry* 565 (1998): 159-64.
30. Laine, R. M.; et al. "The Selective Dissolution of Rice Hull Ash to Form [OSiO1.5]8[R4N]8 (R=Me, CH2CH2OH) Octasilicates. Basic Nanobuilding Blocks and Possible Models of Intermediates Formed during Biosilification Processes." *Journal of Materials Chemistry* 15 (2005): 2114-121.
31. Groenen, E.J. J.; et al. "Double-ring Silicate Anions in Tetraalkyl-ammonium Hydroxid/silicate Solutions; Their Possible Role in the Synthesis of Silicon-rich Zeolites." *Zeolites* 6 (1986): 403-11.
32. Hoebbel, D.; et al. "Zum Anionenaufbau von Tetra-n-butylammoniumsilicaten und ihren Wäβrigen Lösungen." *Zeitschrift Fur Anorganische Und Allgemeine Chemie* 509 (1984): 85-94.
33. Hoebbel, Von D. "Zur Konstitution des neuen Silicatanions $[Si_{10}O_{25}]^{10-}$." *Zeitschrift Für Anorganische Und Allgemeine Chemie* 418 (1975): 35-44.
34. Scheler, H.; et al. "Untersuchungen Zur Konstitution der Anionen in Trimethyl-(2-hydroxyethyl)ammoniumalumosilicatlösungen und den Daraus Kristallisierenden Verbindungen." *Zeitschrift Für Anorganische Und Allgemeine Chemie* 586 (1990): 194-202.
35. Harrison, Philip G., and Chris Hall. "Preparation and Characterization of Octasilsesquioxane Cage Monomers." *Main Group Metal Chemistry* 20.8 (1997): 515-29.

36. Agaskar, Pradyot A. "Facile, High-Yield Synthesis of Functionalized Spherosilicates: Precursors to Novel Organolithic Macromolecular Materials." *Inorganic Chemistry* 29 (1990): 1603.
37. Wann, Derek A.; et al. “The Gas-Phase Structure of the Decasilsesquioxane $Si_{10}O_{15}H_{10}$.” *Dalton Transactions* (2009): 6843-6848.
38. Hasegawa, Isao, and Sumio Sakka. "Silicate Species with Cagelike Structure in Solutions and Rapid Solidification with Organic Quaternary Ammonium Ions." *Zeolite Synthesis* 398 (1989): 140-51.
39. Reidy, Richard F., and Laura B. Rothman. "Cryogenic Aerosols and Supercritical Fluid Cleaning." Handbook of Silicon Wafer Cleaning Technology. 2nd ed. Norwich: Willam Andrew, 2008. 473.
40. Oizumi, H.; et al. “Development of New Negative-tone Molecular Resists Based on Calixarene for EUV Lithography.” *Journal of Photopolymer Science and Technology* 21 (2008): 443-449.
41. Cui, Zheng. Nanofabrication: Principles, Capabilities, and Limits. N.p.: Springer, 2009.
42. Williamson, Fred, and Eric A. Shields. "SU-8 as an Electron Beam Lithography Resist." *IEEE* (2003): 57-60.
43. Del Campo, A., and C. Greiner. "SU-8: A Photoresist for High-aspect-ratio and 3D Submicron Lithography." *Journal of Micromechanics and Microengineering* 17 (2007): 81-95.
44. SU-8 2000 Processing Guidelines. *Microchem.*
45. Lee, Sung-Il.; et al. "Organosilicate Polymer E-beam Resists with High Resolution, Sensitivity and Stability." *Applied Organometallic Chemistry* 27 (2013): 644-51.
46. SPIE Vol. 7520. (2009).
47. Clift, W. M. "Scaling Studies of Capping Layer Oxidation by Water Exposure with EUV Radiation and Electrons." *Emerging Lithographic Technologies VIII* 5374 (2004): 666. SPIE Proceedings.

48. Oyama, Tomoko G. "Prediction of Resist Sensitivity for 13.5-nm EUV and 6.x-nm EUV Extension from Sensitivity for EBL." *Extreme Ultraviolet (EUV) Lithography IV* 8679 (2013). SPIE Proceedings.
49. Bozano, Luisa D.; et al. “EUV and Electron-beam Lithography Performance Comparison.” IBM Almaden Research Center, 2011.
50. Sidorkin, V.; et al. "Resist Thickness Effects on Ultra Thin HSQ Patterning Capabilities." *Microelectronic Engineering* 86 (2009): 749-51.
51. Ekinci, Yasin.; et al. "20 Nm Line/space Patterns in HSQ Fabricated by EUV Interference Lithography." *Microelectronic Engineering* 84 (2007): 700-04.
52. Mojarad, Nassir; et al. "Beyond EUV Lithography: A Comparative Study of Efficient Photoresists' Performance." *Scientific Reports* 5 (2015): 1-7.
53. Kotera, Masatoshi; et al. “Photoelectron Trajectory in a Resist for EUV Lithography.” *Microprocesses and Nanotechnology* (2007): 94-95.
54. Neisser, M., and KY Cho. “Resist Improvements needed for EUVL Extension.” SEMATECH Litho Forum, 2012.
55. Yueh, Wang; et al. “Patterning Capabilities of EUV Resists.” *Advances in Technology and Processing XXI* 5376 (2004): 434-42. SPIE Proceedings.

Appendix A: ^{1}H NMR Spectra

Trimethyl POSS

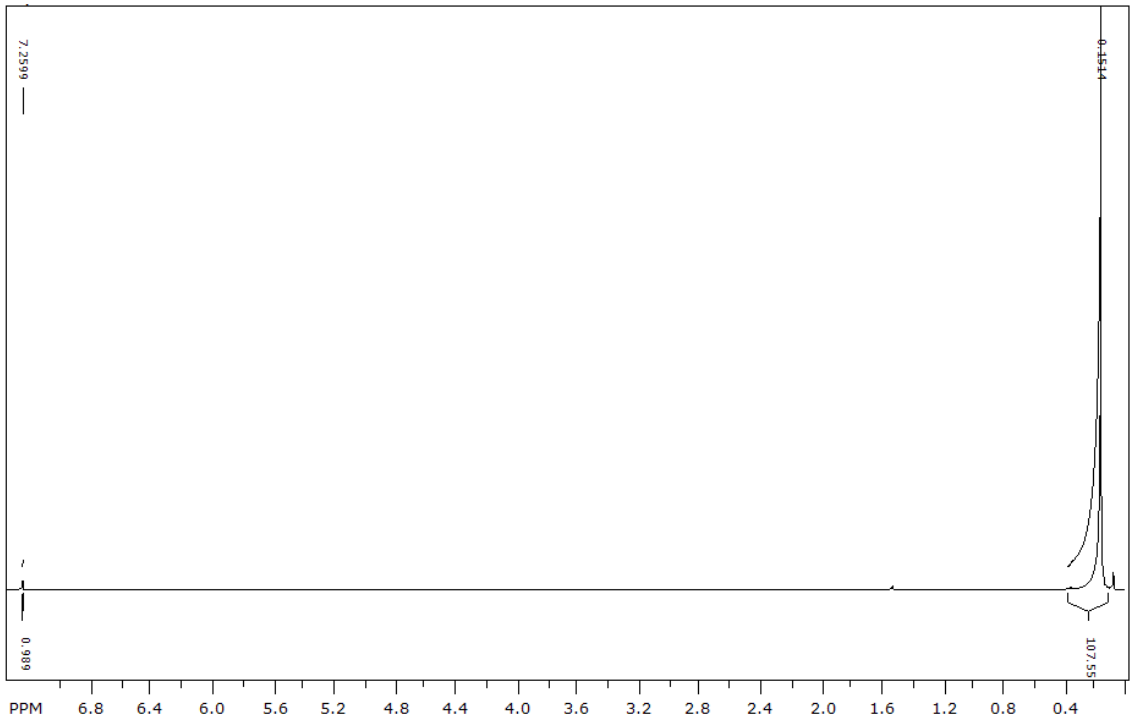

Vinyldimethyl POSS

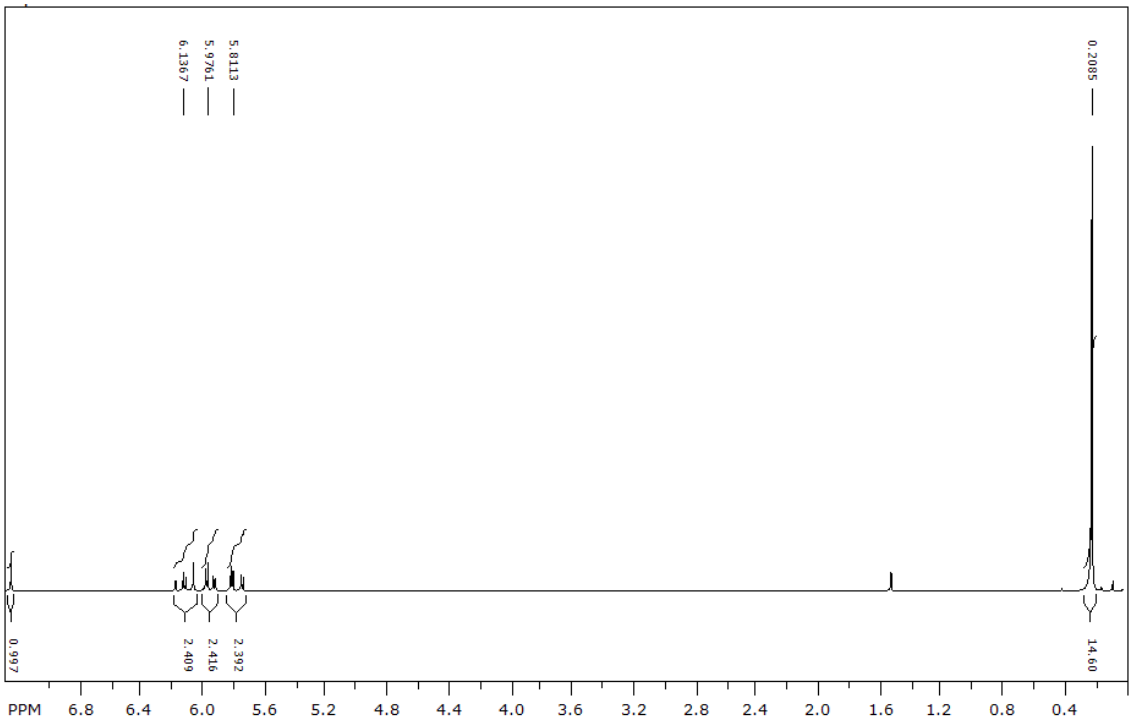

Dimethyl POSS

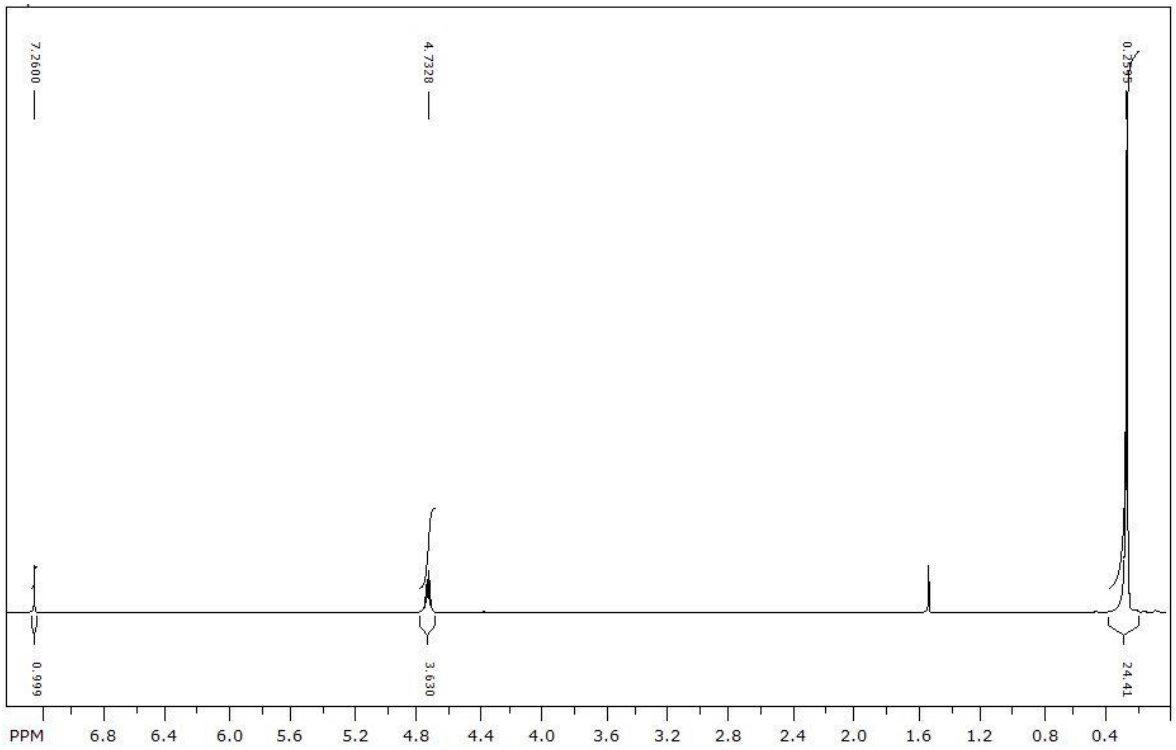

Trivinyl POSS

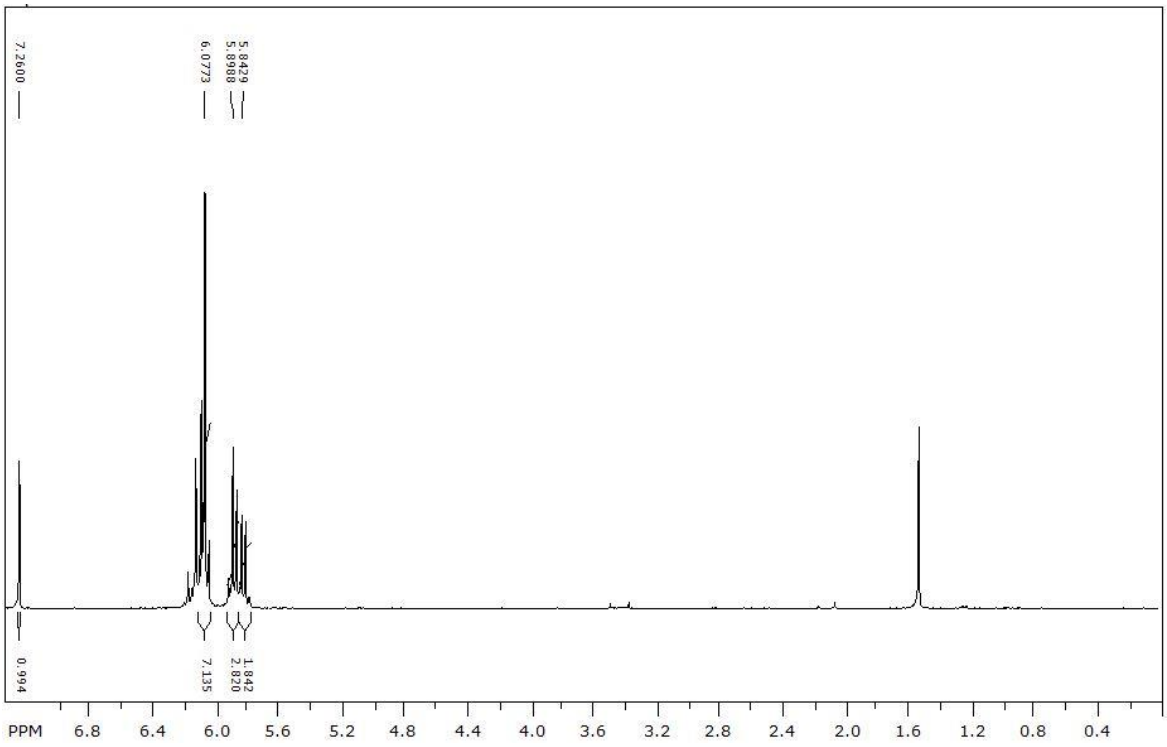

Trimethyl/Vinyldimethyl POSS

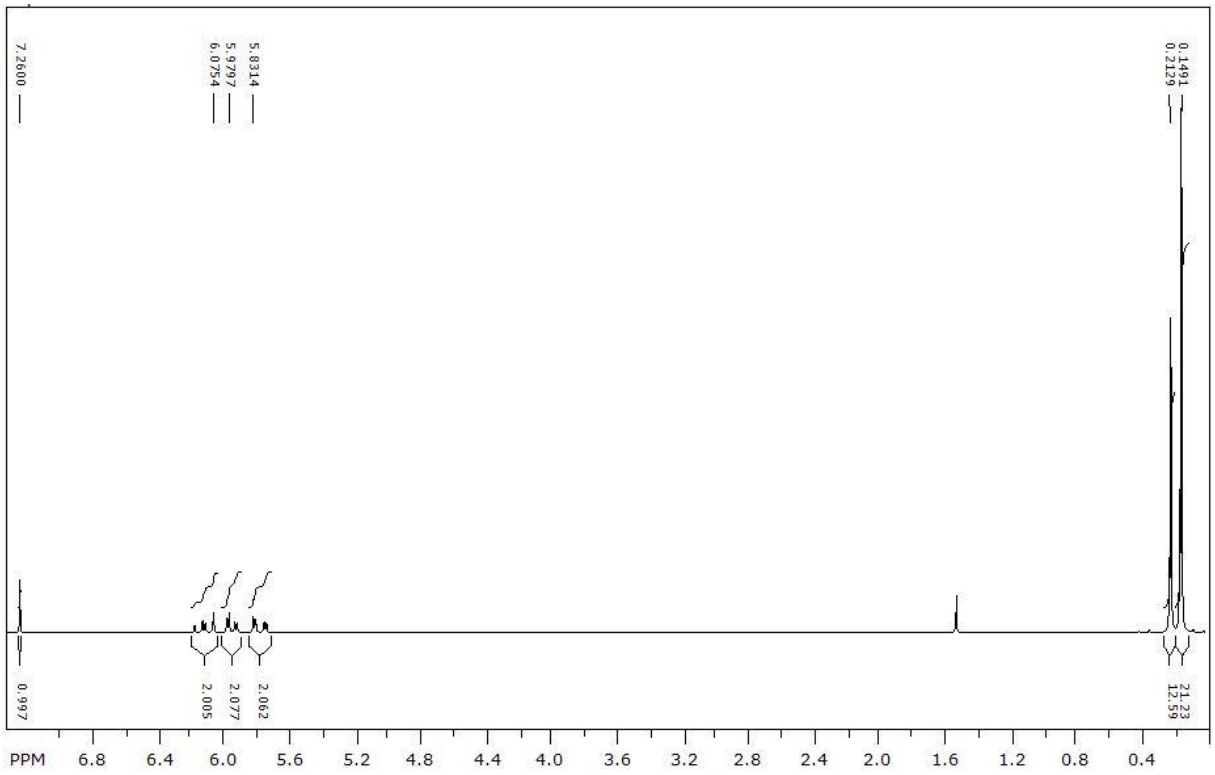

Vinyldimethyl/Trivinyl POSS

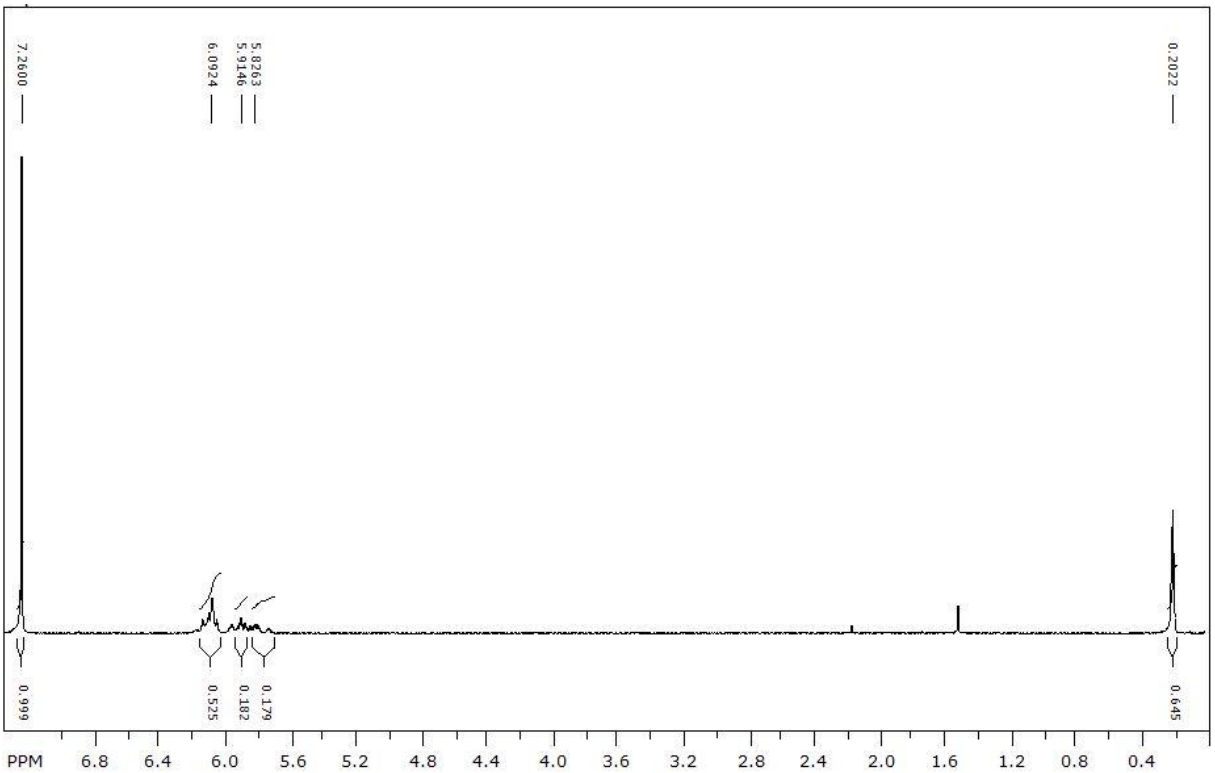

7-Octenyldimethyl POSS

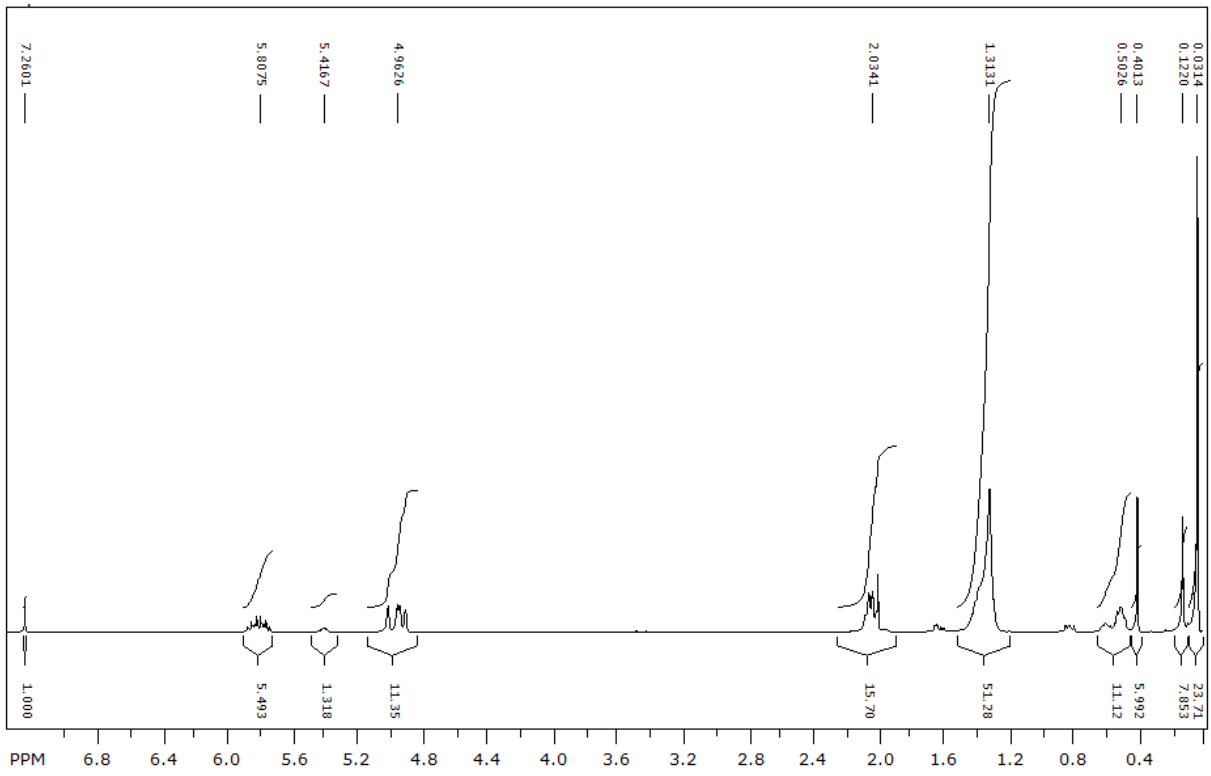

5-Hexenyldimethyl POSS

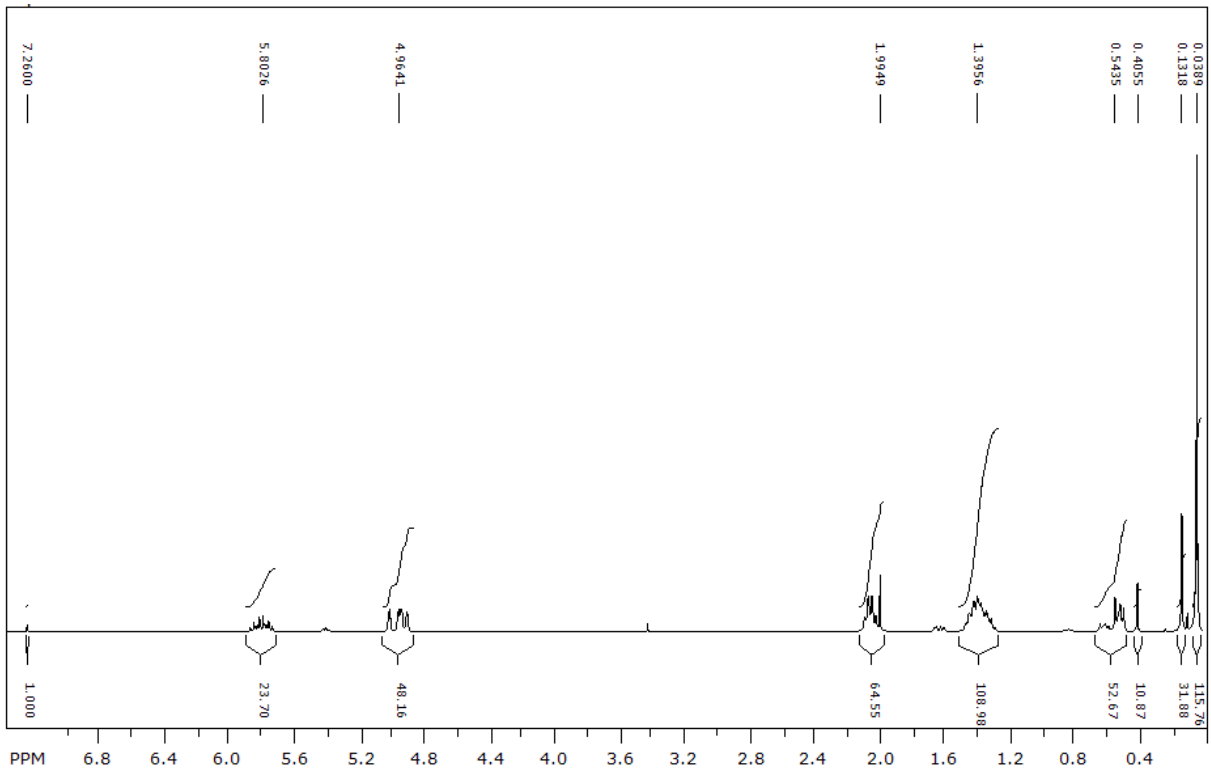

7:1 Vinyldimethyl:5-Hexenyldimethyl POSS

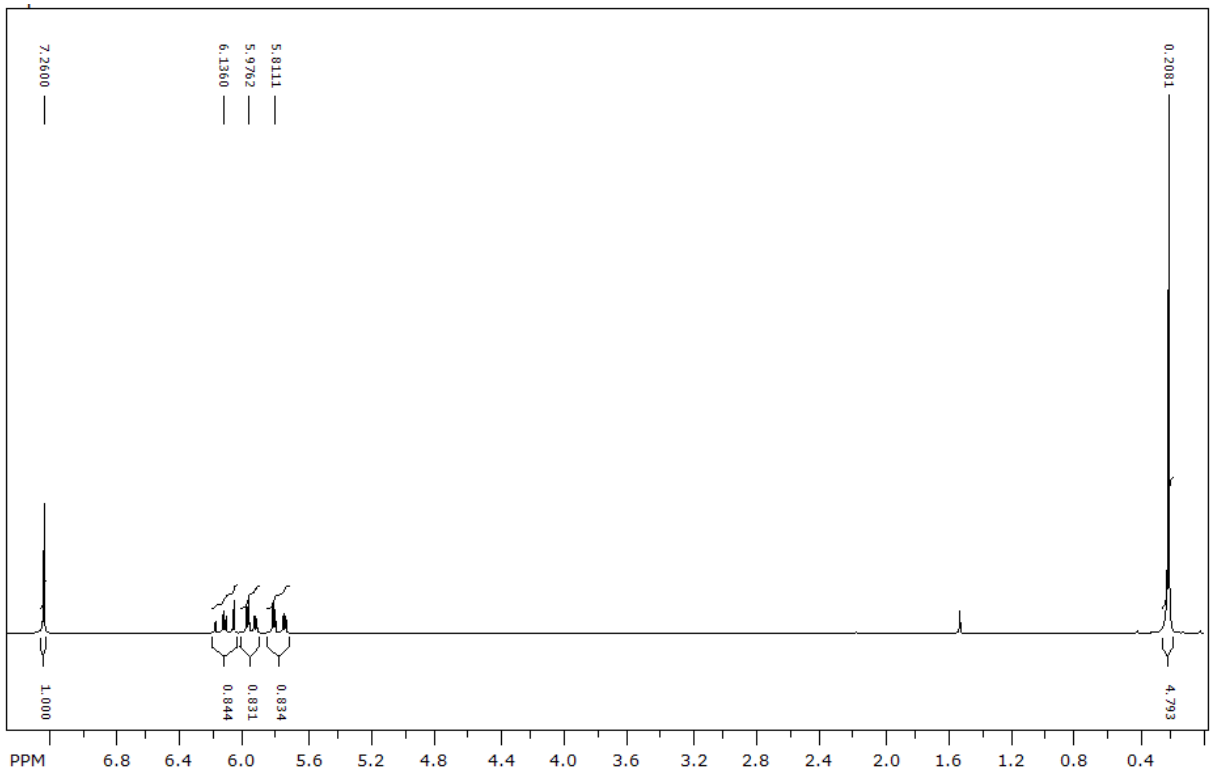

6:2 Vinyldimethyl:5-Hexenyldimethyl POSS

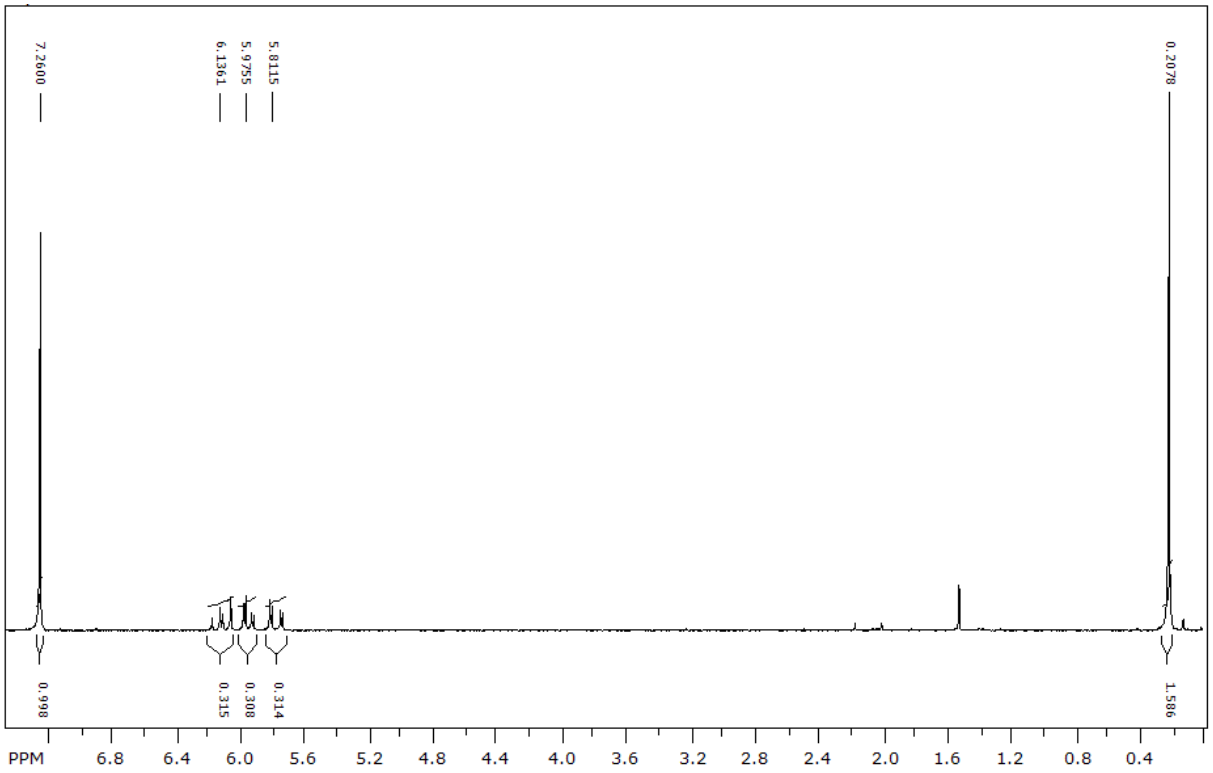

5:3 Vinyldimethyl:5-Hexenyldimethyl POSS

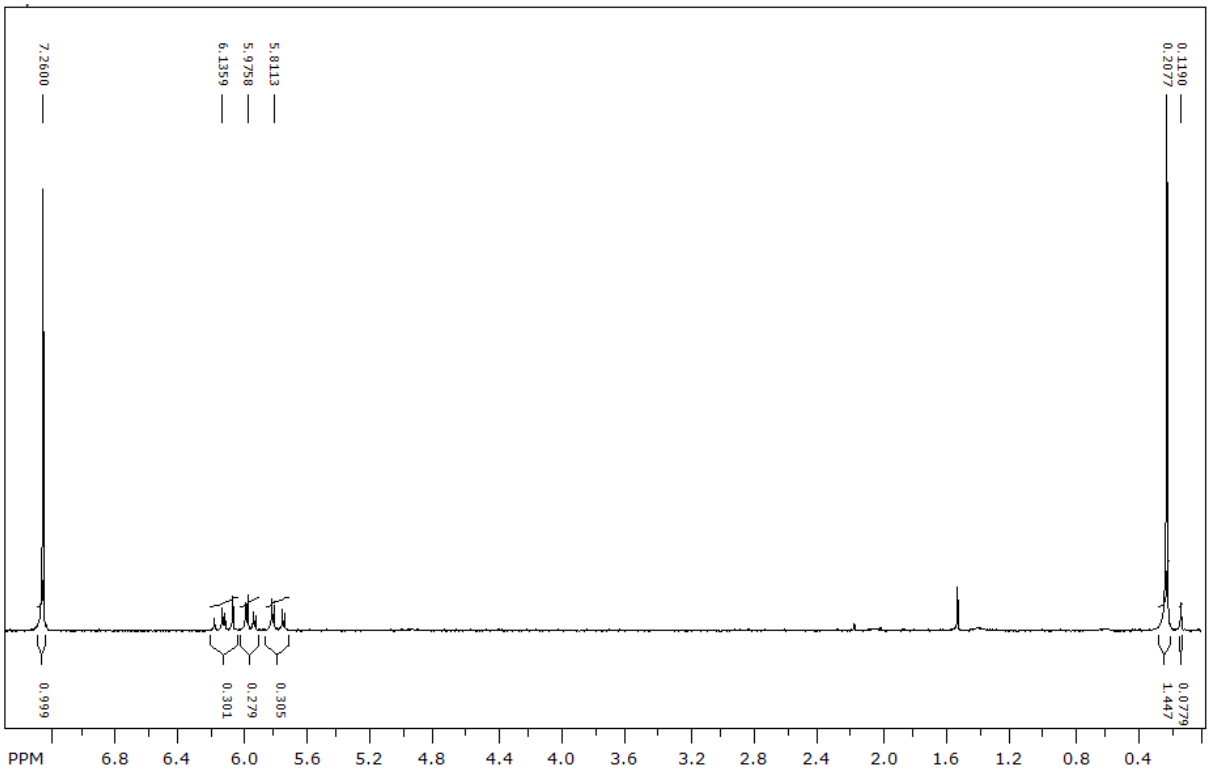

4:4 Vinyldimethyl:5-Hexenyldimethyl POSS

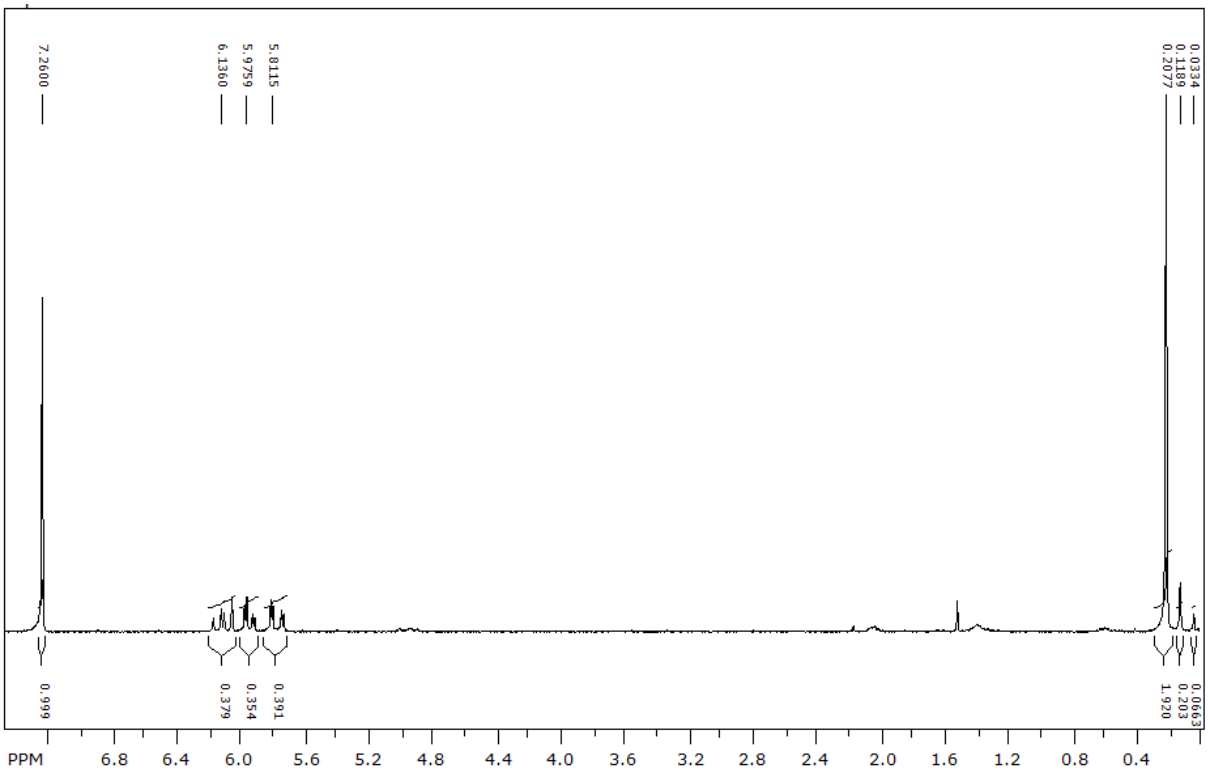

Trimethyl POSS (Decamer)

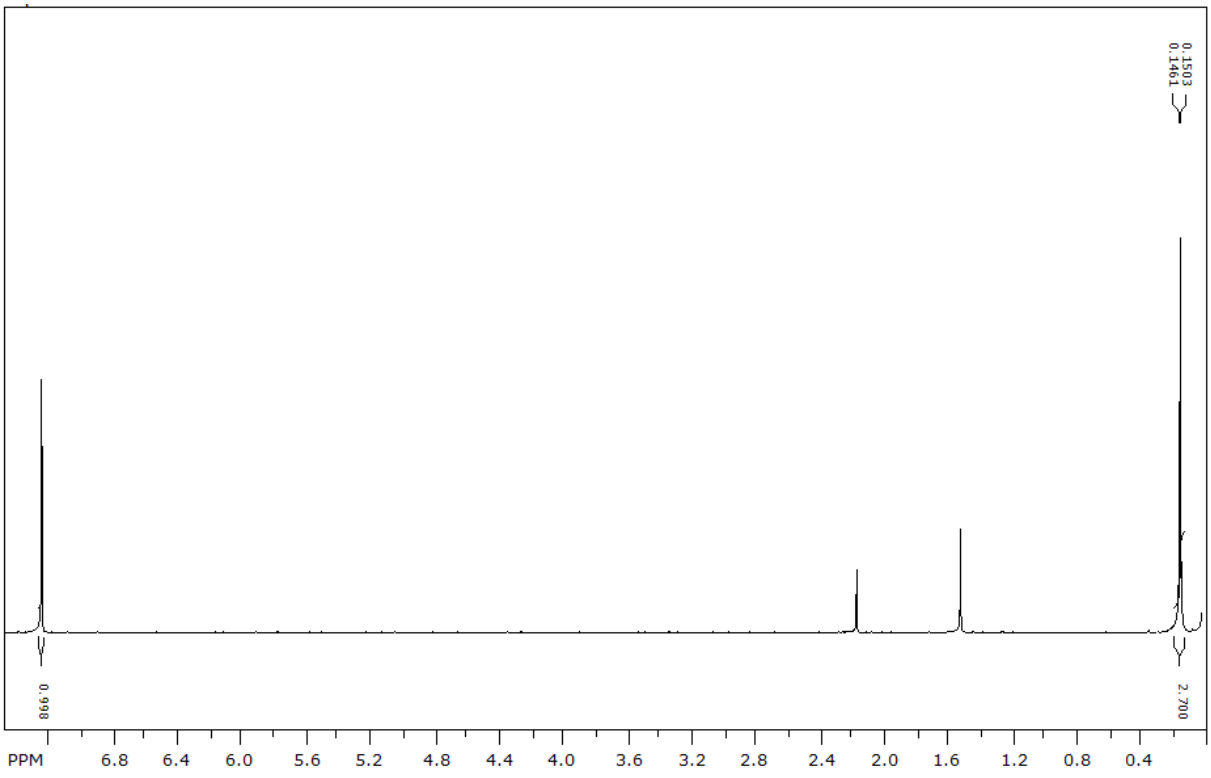

Appendix B: Powder X-ray Diffraction Plots

Trimethyl POSS

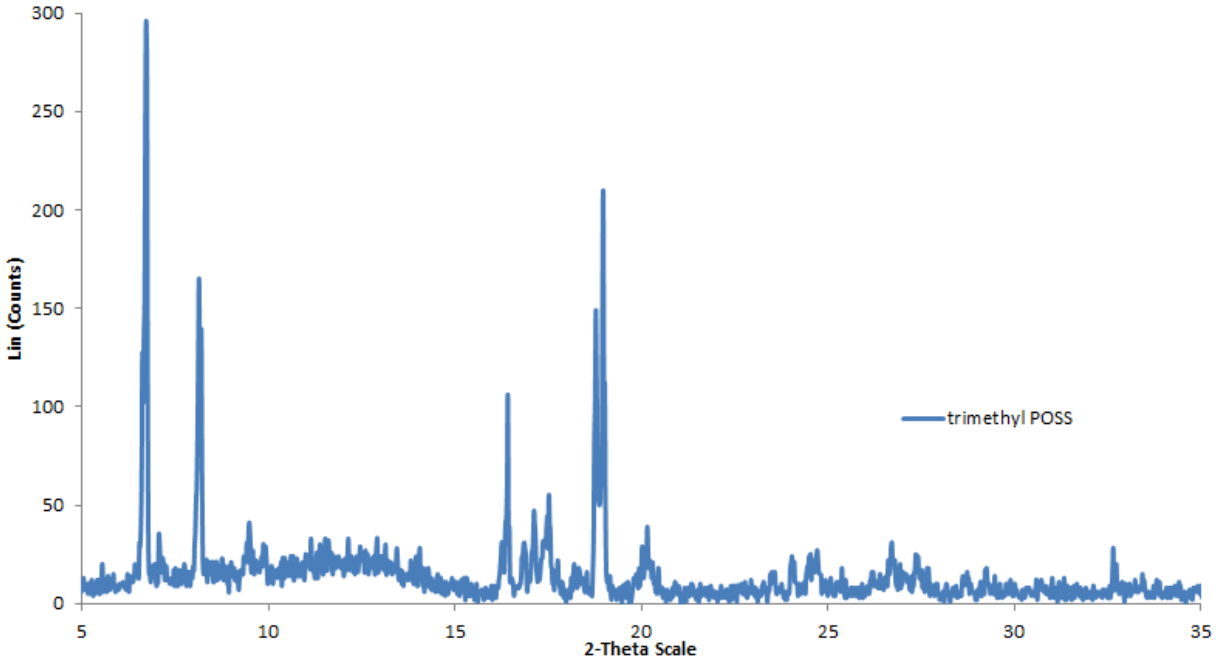

Vinyldimethyl POSS

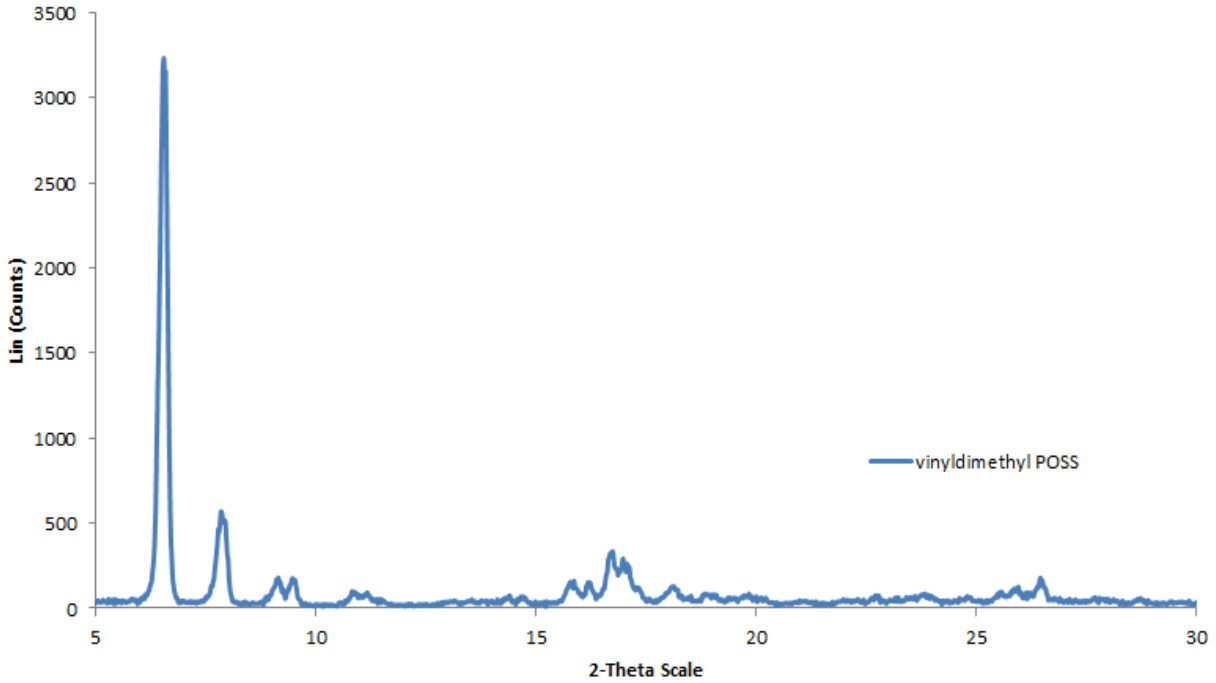

Dimethyl POSS

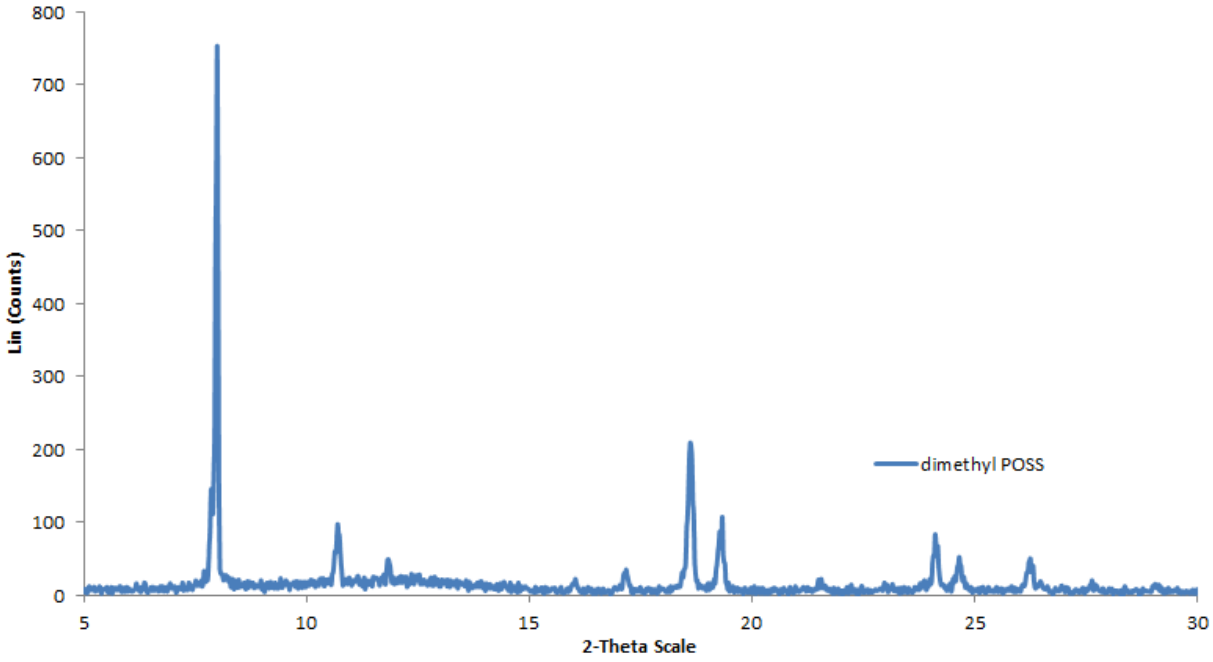

Trimethyl/Vinyldimethyl POSS

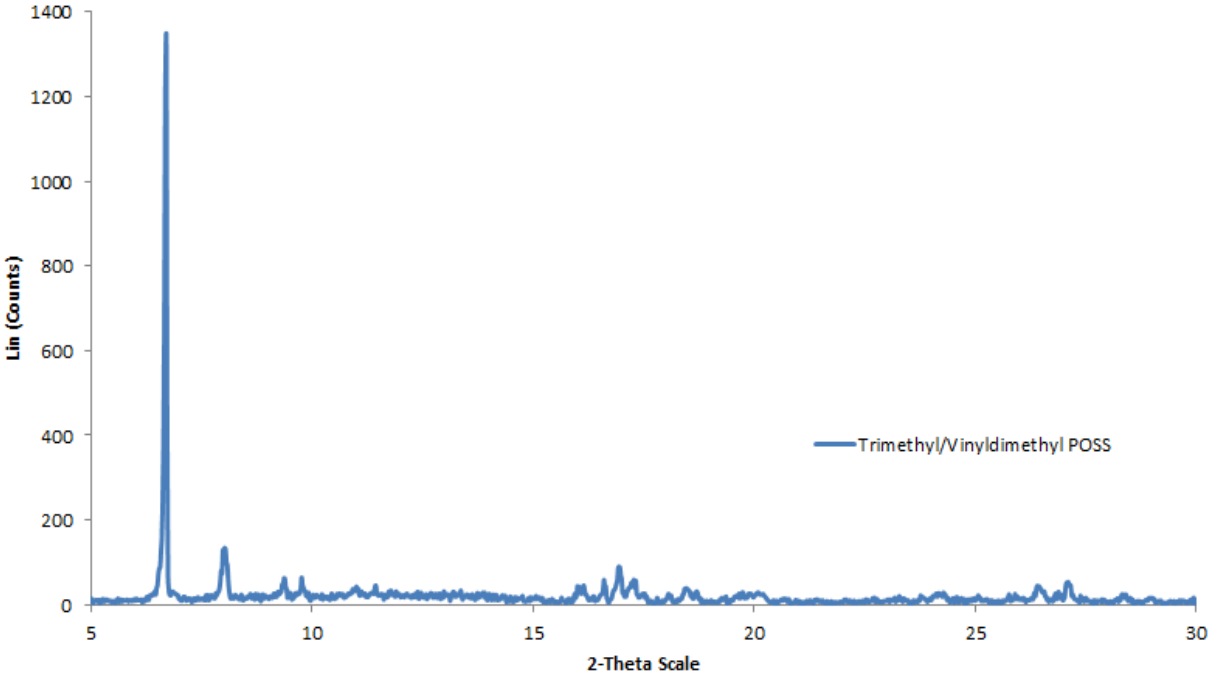

Vinyldimethyl/Trivinyl POSS

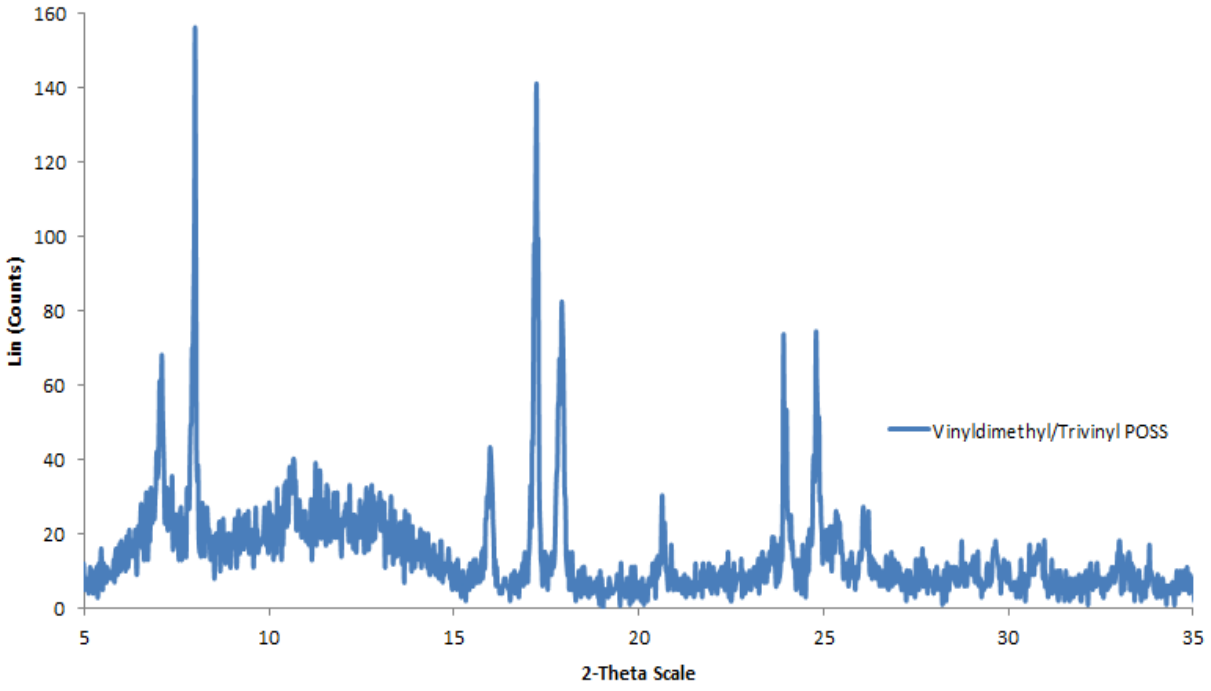

Trimethyl/Vinyldimethyl/Dimethyl/Trivinyl POSS

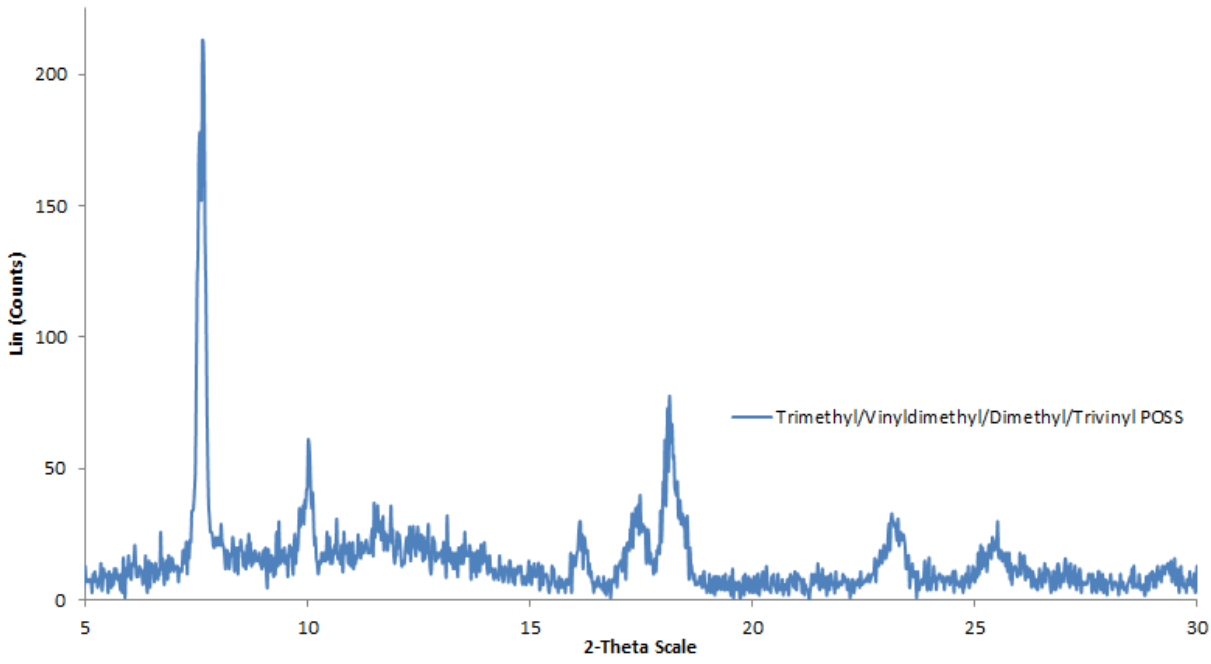

Trimethyl POSS (Decamer)

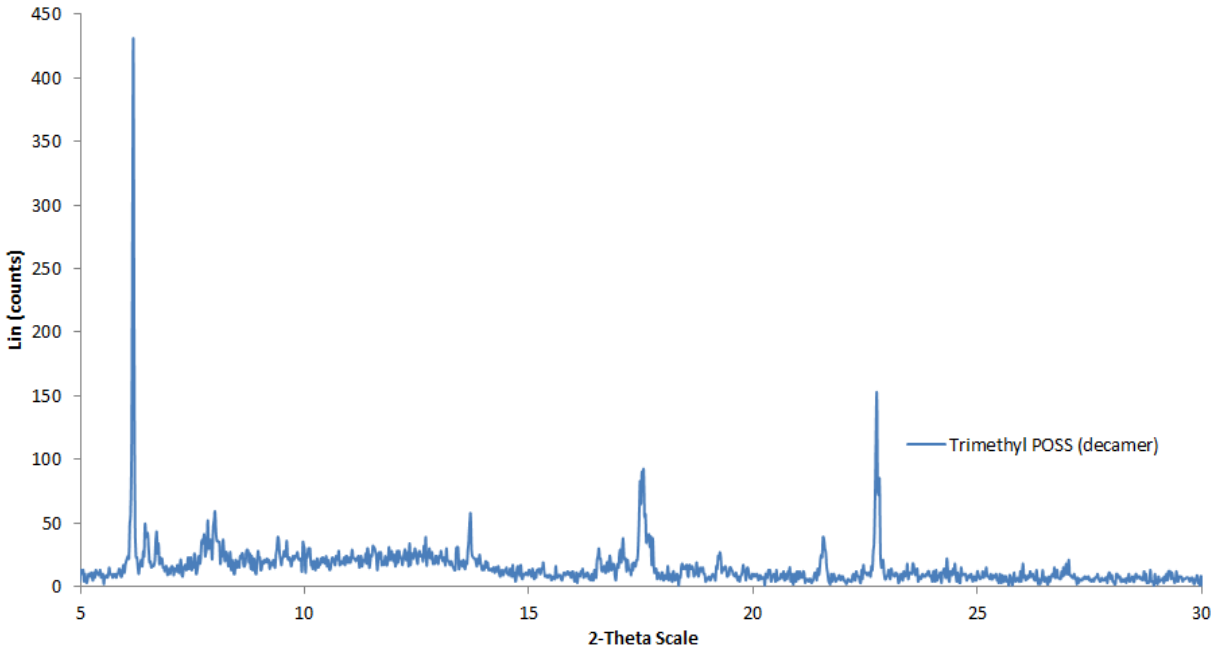

Appendix C: Additional Wafer Images/Micrographs

Vinyldimethyl POSS 1% and 2% wt. in PGMEA

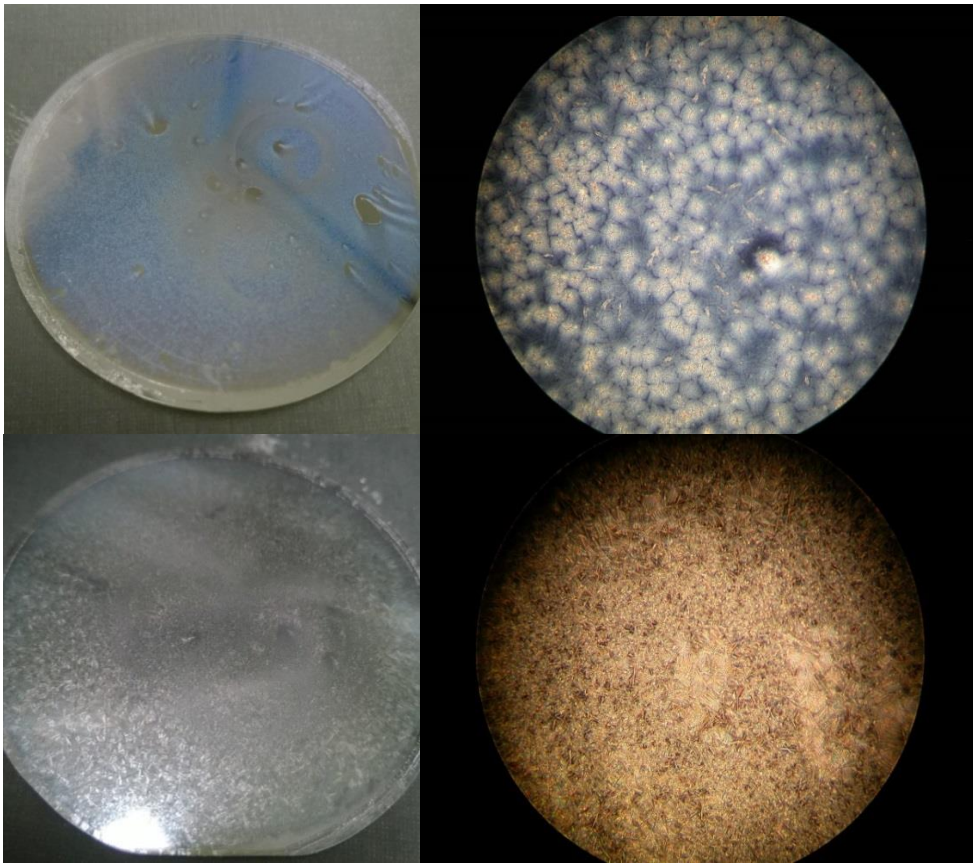

Initial vinyldimethyl (5% wt. in PGMEA) micrograph exposures

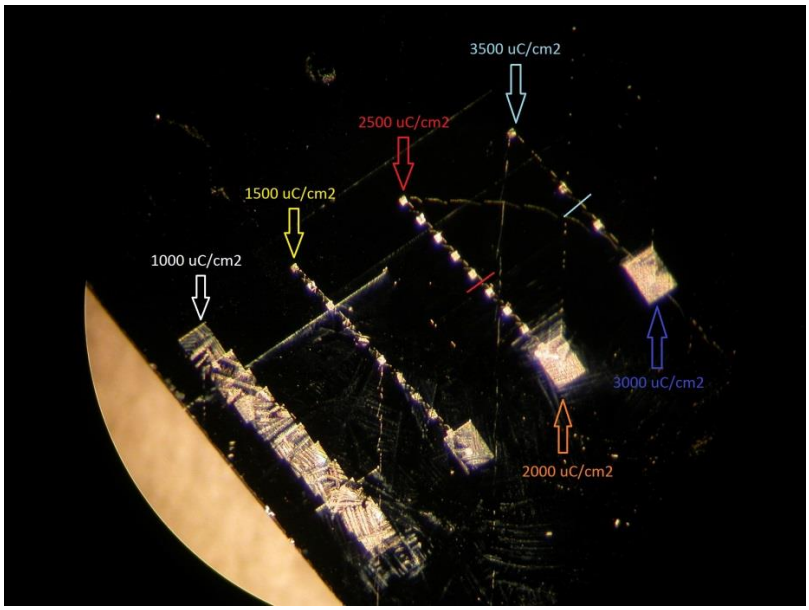

Trivinyl POSS 2% and 4% wt. in PGMEA

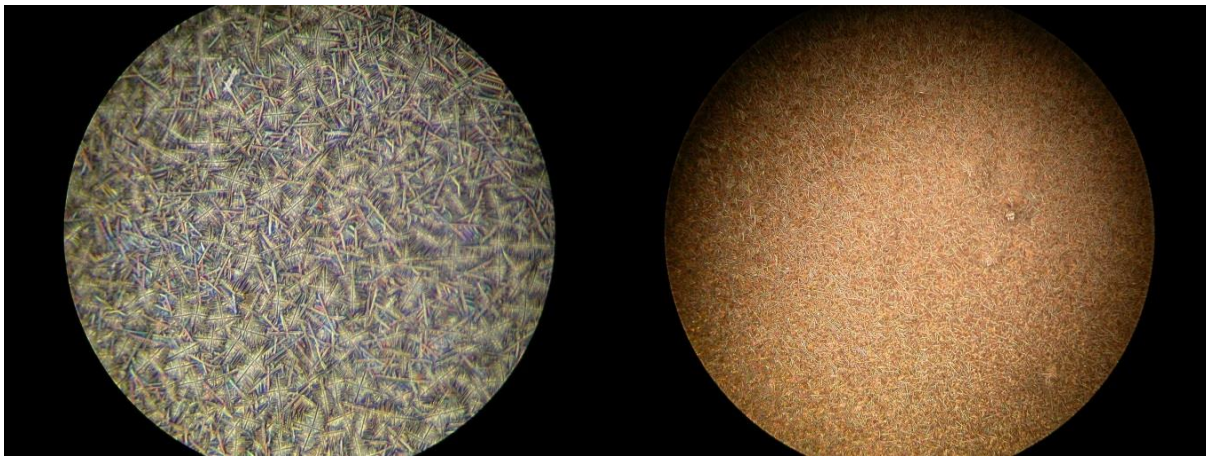

Trivinyl POSS 0.05% and 2% wt. micrograph exposures

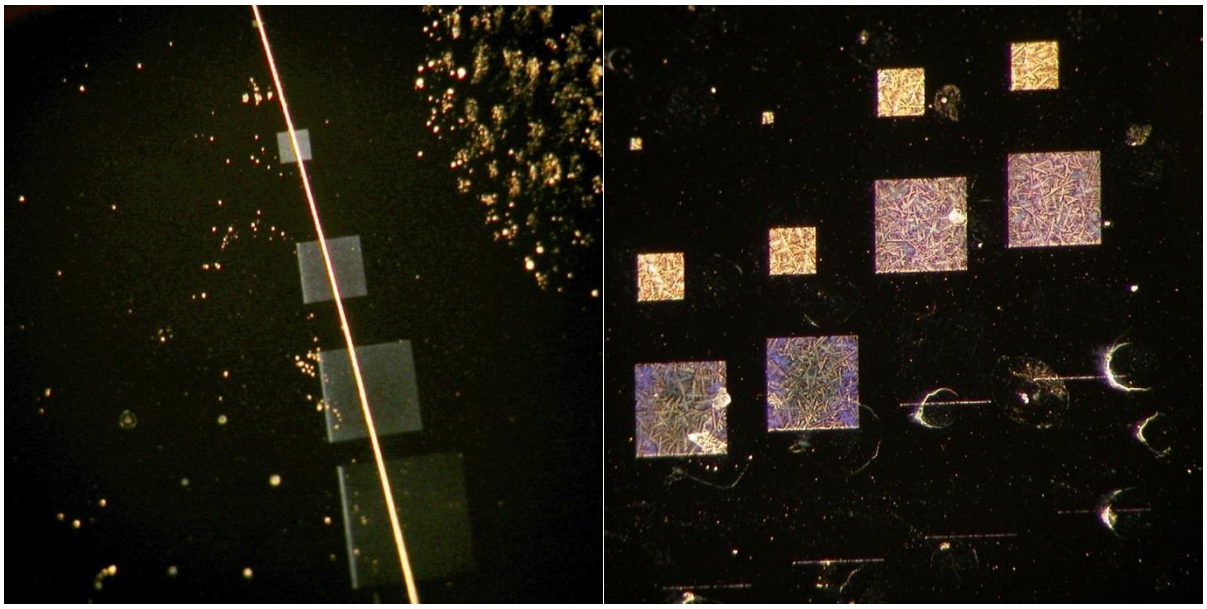

5-Hexenyldimethyl POSS

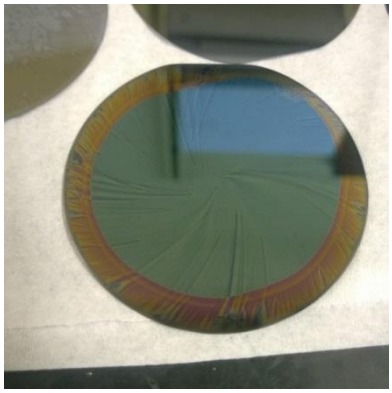

Tri-N-Propyl/Vinyldimethyl POSS drop test in THF

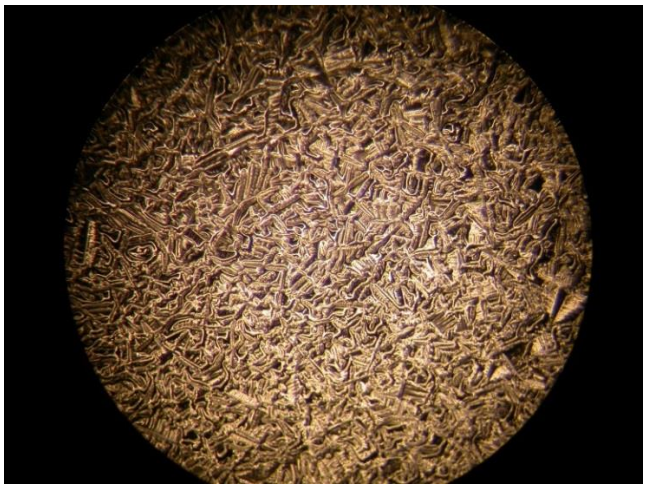

Trimethyl POSS Decamer 1% wt. in MEK

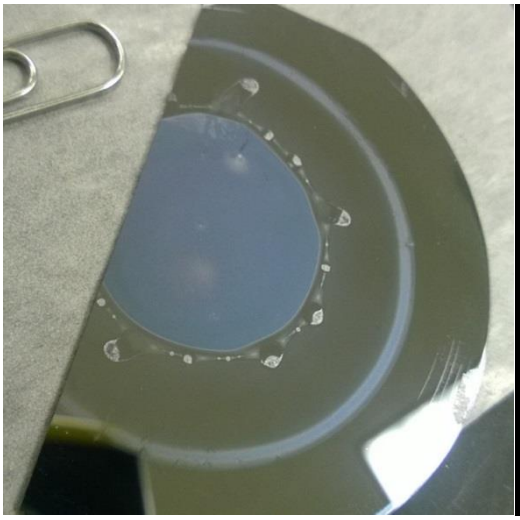

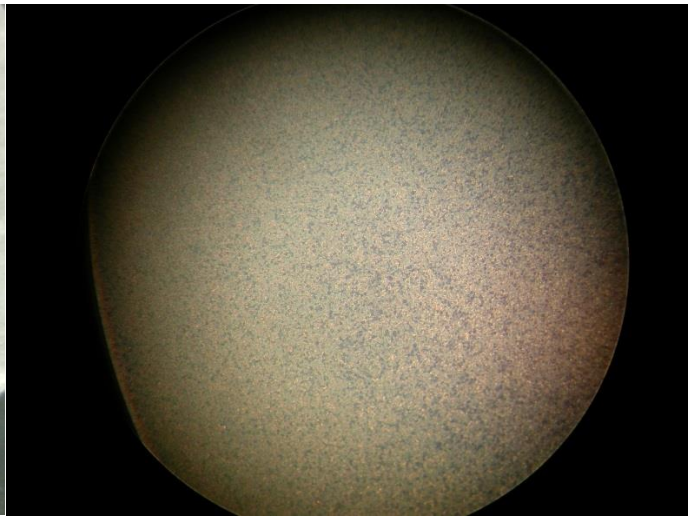

Trivinyl POSS/POM 2% wt. resist

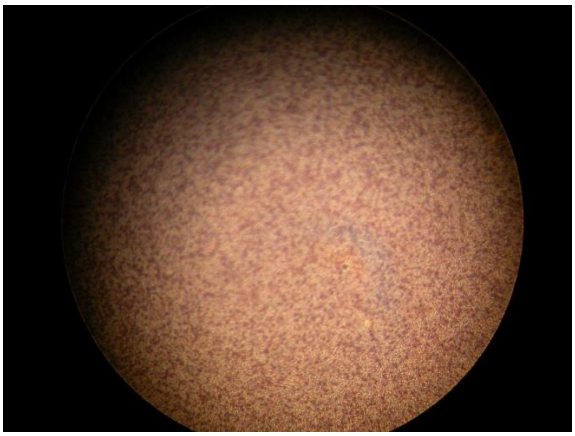

Monoimide POM resist (1% wt. in MEK) low acceleration-low speed and high acceleration-high speed coating

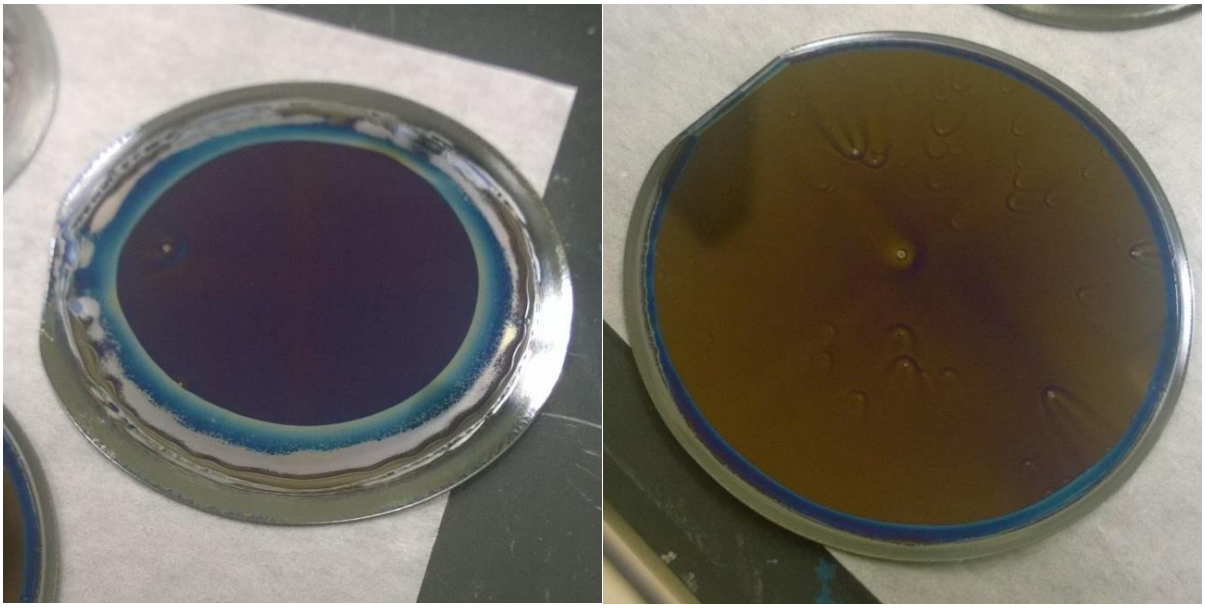

Appendix D: Additional SEM Images

Vinyldimetyl (5% wt.) exposures (1 and 50 µC/cm^2)

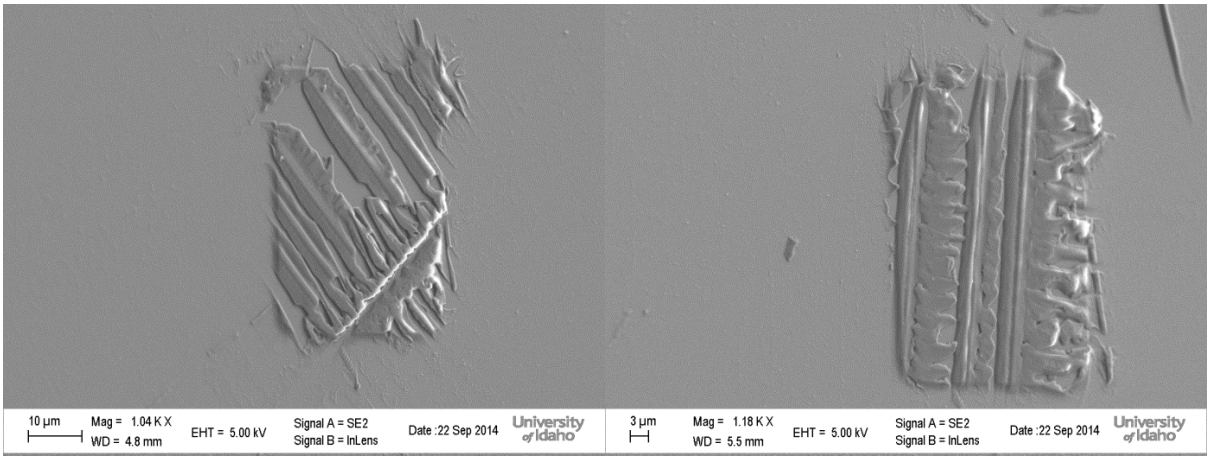

Vinyldimethyl (5% wt.) initial thickness

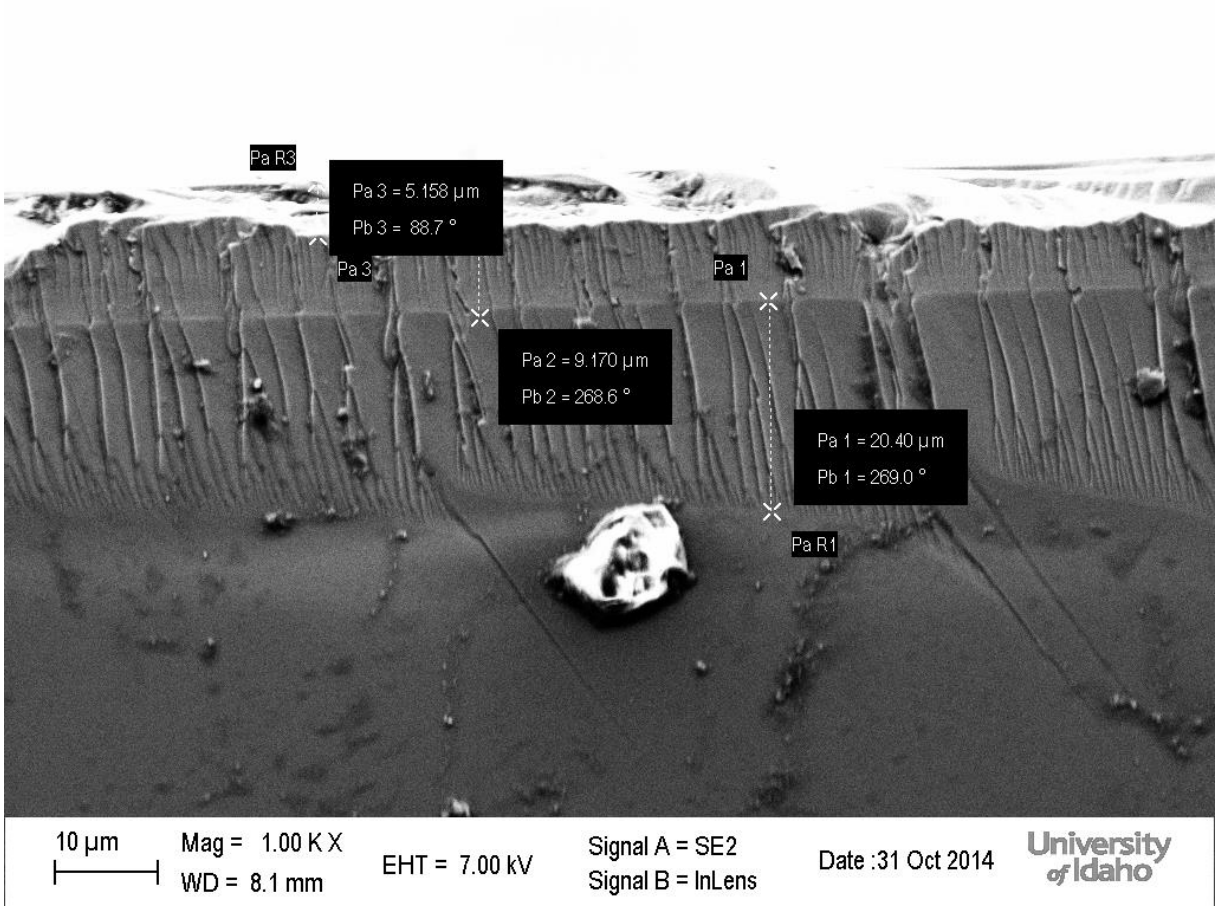

Vinyldimethyl POSS exposure cross section examples (0.5 and 1 μC/cm^2)

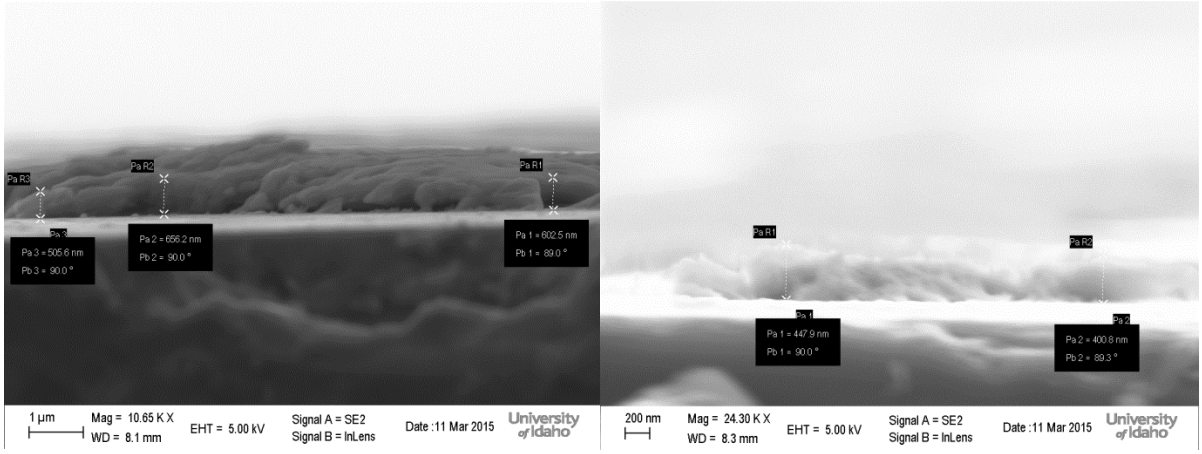

Trivinyl POSS (4% wt.) exposure (10 μC/cm^2)

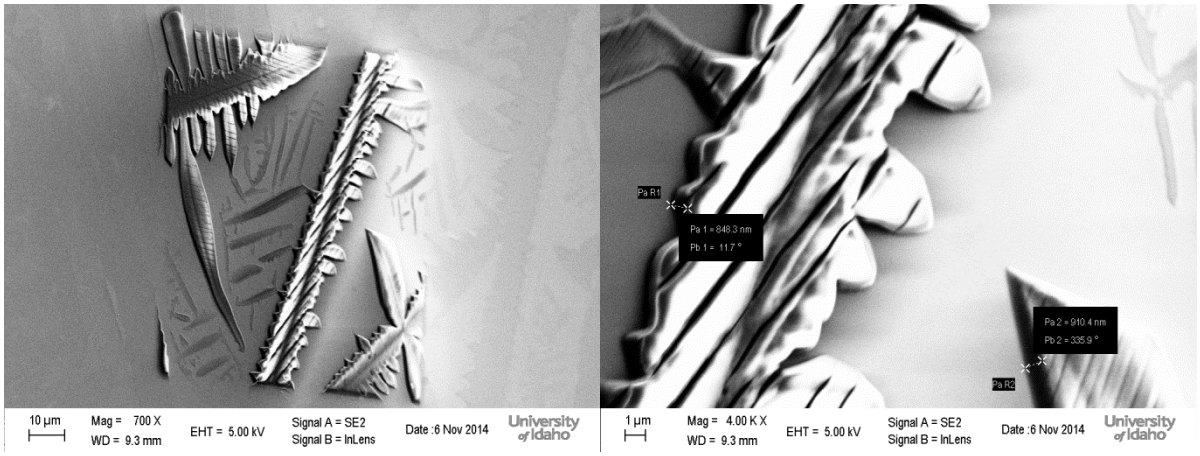

Trivinyl POSS (2% wt.) exposure cross sections (0.5 and 5 μC/cm^2)

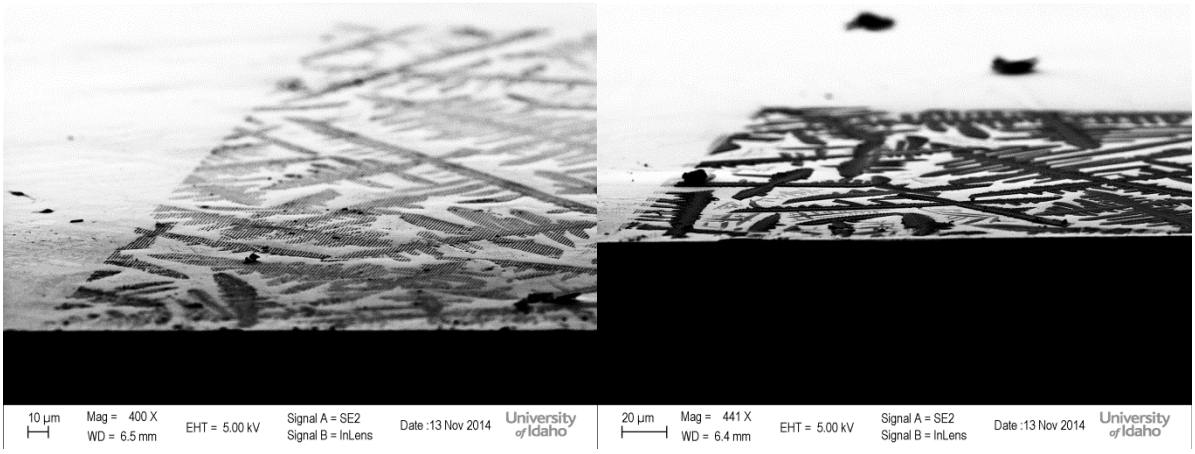

Trivinyl POSS (0.05% wt.) cross section examples (5 and 1000 μC/cm^2)

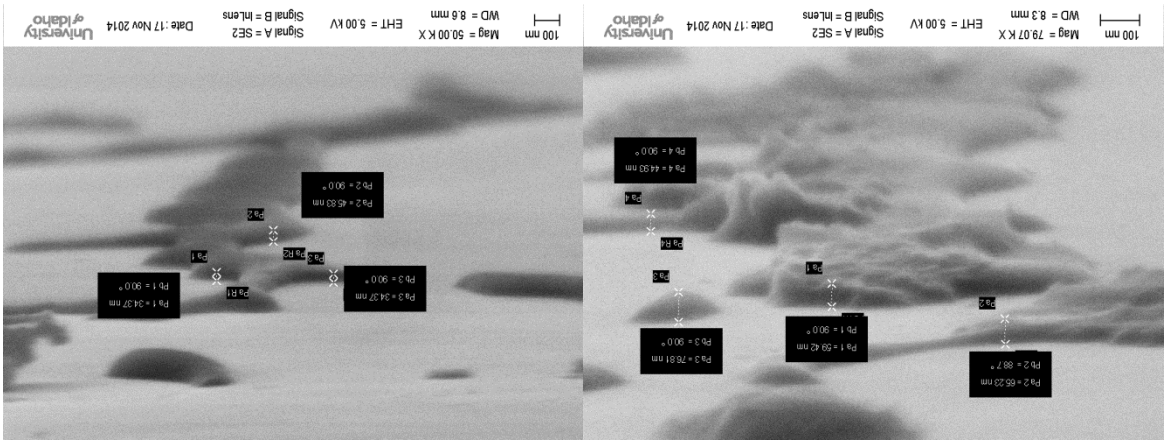

Appendix E: Contrast Curve Measurement Technique

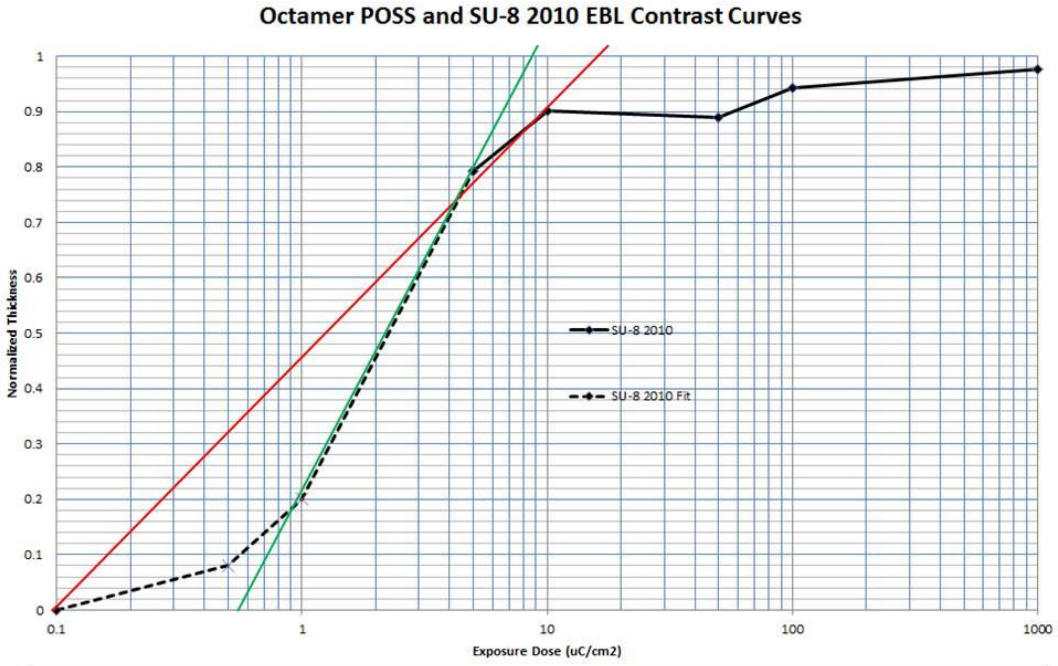

Sensitivity: 2.20
Contrast: 0.496 - 0.876

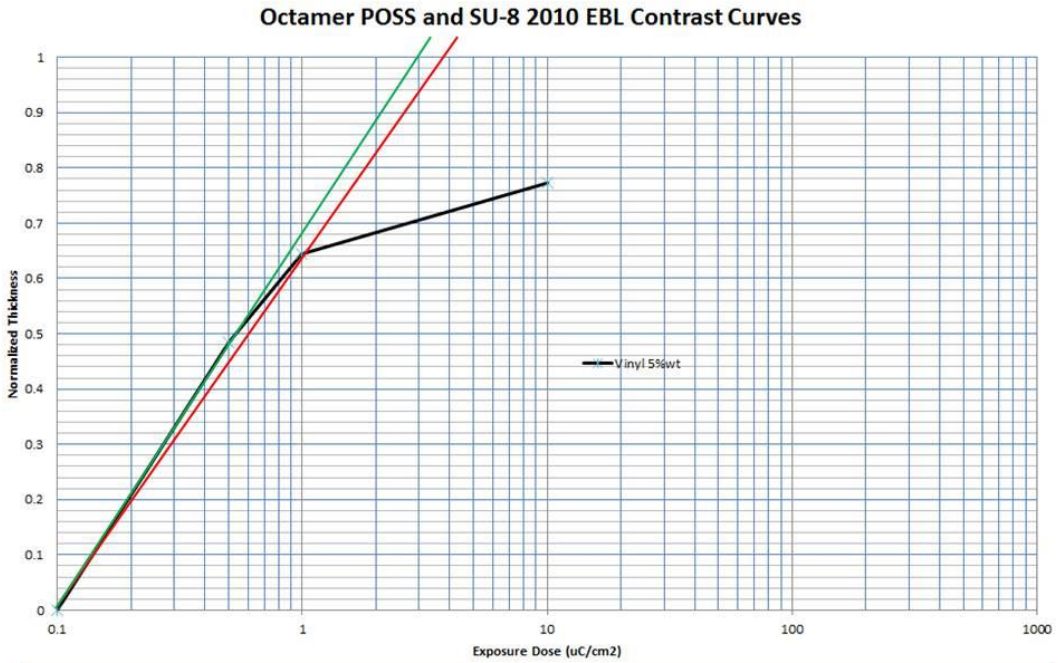

Sensitivity: 0.53
Contrast: 0.629 - 0.684

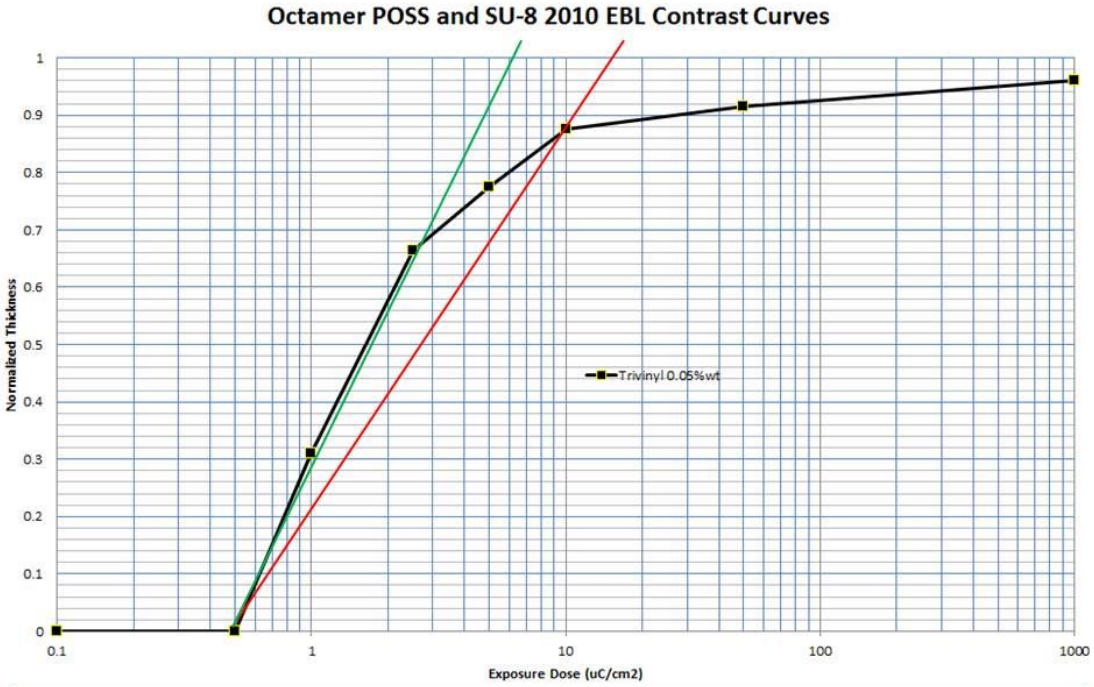

Sensitivity: 1.50
Contrast: 0.759 - 0.975

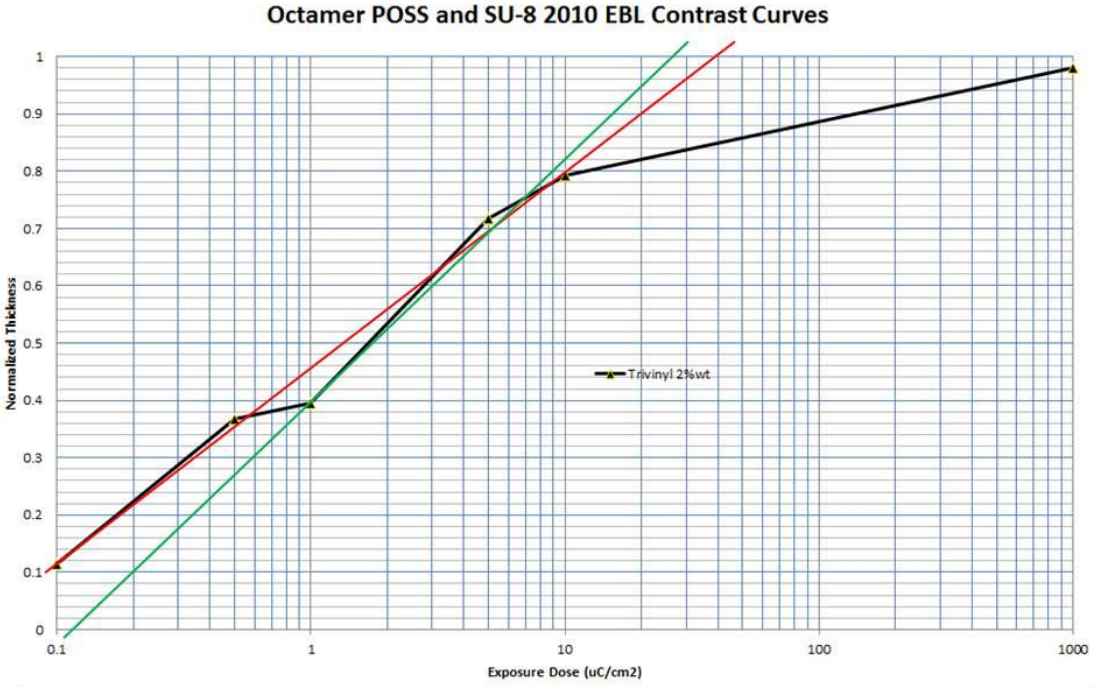

Sensitivity: 1.60
Contrast: 0.346 - 0.454